Final Report of the

Igneous Consequences Peer Review Panel

Prepared for:

Bechtel SAIC Company LLC

Las Vegas, Nevada

Prepared by:

Emmanuel Detournay, Larry G. Mastin, J.R. Anthony Pearson,
Allan M. Rubin and Frank J. Spera

April 2003

The Panel is working under contract to Bechtel SAIC Company LLC,
for the Office of Civilian Radioactive Waste Management of the U.S. Department of Energy

TABLE OF CONTENTS

CHAPTER 1 INTRODUCTION

1.1 BACKGROUND

For several years, the issue of whether volcanic/igneous events are important contributors to overall risk for the U.S. Department of Energy's (DOE) proposed Yucca Mountain Repository (YMR) has been under consideration both within the Yucca Mountain Project ("the Project") itself and within the staff and contractors of the U.S. Nuclear Regulatory Commission (NRC). Other interested parties, such as the State of Nevada and the U.S. Nuclear Waste Technical Review Board, have also given the issue important consideration. Much technical work has been done to examine and evaluate this issue, and more is underway and planned.

In early 2002, at the request of the U.S. Department of Energy's Office of Civilian Radioactive Waste Management, Bechtel SAIC Company LLC (BSC) formed the "Igneous Consequences Peer Review Panel" to review the technical basis used to analyze the consequences of igneous events (IEs) that might impact the repository and to recommend any additional tasks that would significantly strengthen the program. As part of the Panel's initial instruction, BSC charged it with examining a set of eight questions, which are displayed in Table 1-1 (see next page).

The Panel was formed in the spring of 2002. Its membership initially consisted of six individuals selected by the Project's senior management. After presenting the Panel's Interim Report, the then Chair resigned, with the concurrence of the Project's management, as he had accepted a full-time post connected with the Project at DOE, and was replaced by one of the remaining five members. These individuals are working under contractual agreements with the Project, and the Project is also providing administrative support (by setting up meetings and conference calls, for document dissemination, etc.); otherwise, the Panel is working entirely independently of the Yucca Mountain Project.

1.2 PANEL MEMBERSHIP

The Panel's membership has been as follows:

Robert J. Budnitz, Future Resources Associates Inc.
(Chair until September 2002)

Emmanuel Detournay, University of Minnesota

Larry G. Mastin, U.S. Geological Survey

J.R. Anthony Pearson, part-time Scientific Consultant, Schlumberger Cambridge Research, UK (Chair from September 2002)

Allan M. Rubin, Princeton University

Frank J. Spera, University of California at Santa Barbara

Table 1-1 Questions for the Igneous Consequences Peer Review Panel

1. Conceptual Model
   a. Is the conceptual model adequate for framing the analysis?
   b. Does the conceptual model allow for consideration of the key physical processes that are likely to significantly influence magma/drift interactions?
   c. Have any key processes or parameters been omitted that should be accounted for in the model?
2. What level of analysis (e.g., hand calculations versus code calculations) is "sufficient" to capture the nature of magma/drift interactions, given the uncertainties inherent in the input parameters (e.g., magma properties, repository environment)?
3. Quantitative Modeling
   a. Are the software codes chosen for the analysis adequate to model the anticipated physical processes?
   b. Will the modeling adequately account for all significant fluid dynamic processes expected to occur during a transient or sustained magma/drift interaction?
   c. Will the modeling adequately account for rock-mechanics processes that may affect magma/drift interactions and subsequent magma pathways and eruption characteristics?
   d. Are the physical parameters necessary to model magma/drift interactions likely to be sufficiently constrained to produce results with a "reasonable" level of confidence?
   e. Are the assumptions underlying the models appropriate?
4. What alternatives to the modeling approach are feasible, including experimental alternatives?
5. What is the appropriate role of analog studies for understanding magma/drift interactions (e.g., literature review of historic volcanoes to understand analogous magmatic processes or examples of magmatic intrusions that have interacted with geologic or human-engineered structures)?
6. Will the planned modeling provide results that reasonably and realistically represent magma/drift interaction in terms of drift temperature, pressure, and magma inflow and outflow?
7. Will the uncertainties of the models be readily quantifiable? Will it be possible to easily discriminate uncertainties resulting from uncertainties in input parameters versus uncertainties in understanding of complexities of physical processes? To what extent should the uncertainties be quantified, given the intended use of the model outputs to constrain issues such as waste package damage and the possibility that the presence of the repository will influence magma pathways to the surface?
8. Are the methods proposed for use in validating the model adequate?

1.3 TERMS OF REFERENCE AND GENERAL APPROACH

The Panel began its work with a public meeting held in Las Vegas on May 21-22, 2002. The objective of that kick-off meeting was strictly information gathering; the agenda included presentations by several experts working for the Project as well as by experts working for the NRC. The agenda was established through discussions between the Panel's chairman and members of the Yucca Mountain Project staff. A list of the documents provided beforehand and the overheads used in the presentations is given in Chapter 8. During the meeting, opportunities to speak were also afforded to the public. In addition, a general public appeal was made to send the Panel any relevant information, in the form of reports or memoranda, from anywhere worldwide. (Subsequently, numerous pieces of information in the form of reports, memoranda and telephone calls were in fact received from experts and from members of the public, and this information has assisted the Panel greatly.)

It soon became clear to the Panel that the technical arguments used to analyze processes governing interactions between the most likely igneous events and the repository were neither clear-cut nor satisfactorily quantifiable. This meant that we would not be able to answer the questions posed in Table 1-1 simply by reviewing existing documents and recollected oral statements.

We also felt that our combined expertise was inadequate to cover some important issues. Thus, we could not hope to cover (1) any detailed mechanical or chemical issues concerned with the integrity of waste canisters subject to magma flows (whether pyroclastic or lava) within the repository drifts, or (2) the subsequent fate of radionuclides transferring, from damaged canisters, to groundwater by dissolution or colloidal suspension.

These difficulties led us to the conclusion that the best way for us to give helpful answers to the questions posed in Table 1-1 was to attempt some key modeling tasks ourselves. (Our Interim Report gave an indication of the way we were headed, while commenting on those aspects of previous work that we used as our starting point.) This we have done, and much of this report stems from this work.

Throughout this early phase, we kept BSC aware of our thinking, and it was agreed that our Final Report should concentrate on all aspects of modeling the mechanics of interaction of volcanic flow processes with repository drifts. This would include the uncertainties involved and, hence, a need to consider several scenarios. In particular, we should address the possibility of having dog-leg conduits for eruptive flows, in which long sections of one or more drifts could become part of the main channel for pyroclastic or lava flows, as suggested by earlier NRC-contracted research. BSC confirmed their support for our approach immediately following presentation of our Interim Report on September 5 in Las Vegas, and provided financial support for software modification and exploratory numerical calculations into the behavior of dikes rising below and through the repository.

In preparing our report, all members of the Panel have been active in seeking information from colleagues and experts throughout the world and have interacted with many of them. We have made two field trips to the Yucca Mountain area. Having decided to split up responsibility for writing the separate chapters of this report, we have kept in regular contact by e-mail, telephone- and video-conferencing so as to present a view as comprehensive, connected and collectively agreed upon as possible.

1.4 PRINCIPAL ISSUES AND SCOPE OF REPORT

The consequences of any IE (igneous event, to include intrusions and eruptions) obviously depend upon the nature of the igneous event itself. It has repeatedly been remarked by volcanologists that no two such events are wholly alike, and there will be considerable uncertainty over any assumptions that are made regarding the event to be considered. Nevertheless, if consideration is restricted to events similar to those that have taken place in recent times in the neighborhood of the Yucca Mountain repository site, the range of possible events is narrowed significantly.

By reference to available analogs at Crater Flat and Lathrop Wells, consideration has been restricted to basaltic eruptions of total volume between 0.01 km^3 and 1 km^3, thought to be initially rising to the surface as tabular dikes from source regions many km below the surface. A significant feature of the magma will be the magmatic volatiles (mostly water, carbon dioxide and sulfur-bearing gases, ~ 2% to 4% in total, henceforth termed just "gas") held in solution at depth, leading to exsolution that takes place as the magma rises to the surface and decompresses.

The volume of exsolved gas at atmospheric pressure far exceeds the residual melt volume, and Strombolian eruptions are to be expected at some stage of the IE. Examination of neighboring sites of past volcanic events shows that most consisted of a sequence of separate phases, corresponding to different flow regimes, which, taken together, constitute a single IE. (This may be spread over weeks, months or years.) The phases include dikes reaching the surface, formation of Strombolian cones involving pyroclastic flow in conduits carrying tephra and larger molten lava or solid rock lumps into the atmosphere, and lava flows over the surface. Much of the volcanic material erupted settles back on the ground near the cone. Stratigraphic and mapping studies give information about the sequencing of such events.

Bearing in mind that the repository drifts containing waste canisters will be 200 m to 300 m below the surface, the interaction between the IE and the repository will be determined by flow processes well below the surface and by the sequence of phases followed during the complete event. Both of these (i.e., the flows and the sequence followed) may be significantly affected by the presence of the repository. We have regarded an analysis of this issue as a significant part of our task and therefore been led to consider the processes involved in the absence of the repository.

All approaches to the predictive problem have started with a rising dike. The repository drifts will be neither parallel nor orthogonal to the direction of the principal horizontal earth stress at the site. The excavation of drifts and their subsequent filling with high-level waste (HLW) will change the earth stress pattern locally in a time-dependent fashion and thus will alter, to a greater or lesser extent, the geometry of the rising dike. It has been assumed that the propagating dike will break through into one or more drifts. Quite obviously, this will lead to flow (eruption) into the drifts intersected, because they will contain air at atmospheric pressure. It has also been assumed that the deep magmatic material rising in the primary dike will subsequently reach the surface and there erupt in Strombolian or effusive fashion.

A crucial question concerns the path taken by the exsolving magma when it enters its pyroclastic phase: Will the main conduit for the eruption intersect any drifts and, more seriously, will it conceivably follow a drift for a substantial distance? Equally, if, at any stage, largely degassed magma rises to the surface as a lava flow, will this flow follow any drifts for a substantial distance? These are key questions that we have regarded as central to our task, and much of this report is devoted to seeking ways of answering them.

The final and decisive criteria for assessing the consequences of an IE are the amount of radioactive material released into the biosphere and, more specifically, the probable radiation dose that would be sustained by a person living, as such a person would live today, at a specified location some 19 km south of the repository. It has been judged that the location chosen is that most liable to radiation hazard for currently inhabited areas.

Clearly, the latter specific criterion must depend upon the former general criterion through movement of waste radionuclides in the atmosphere or in groundwater from the repository to the chosen location. The general criterion will depend upon the interaction between flowing melt or exsolved gases and the canisters in place during and after periods of flow into and through the drifts. Unless the canisters are damaged and their integrity is lost, there will be no immediate release into the biosphere. If they are damaged and possibly carried to the surface or erupted in shattered form, then they will leak some or all of their radioactive contents into the biosphere.

It has been agreed that this Panel shall not be responsible for analyzing in any detail the questions of mechanical or chemical damage to canisters, nor the processes by which radionuclides released would be transported by aerial, surface or subsurface processes following the eruptions. However, we have been mindful throughout of the need to present our conclusions on the likely magmatic flow processes associated with an IE in such a way as to enable those experts considering the above damage and transport issues to be given realistic starting conditions.

One important and associated issue is the question of damage to the drifts themselves. Proposed designs include various shields to prevent descending water from contacting canisters, backfill of drifts and sealing of the repository at some stated time after filling. The Panel recognizes that such design choices may determine the number of canisters

that would be affected and the degree to which their integrity would be compromised in an IE.

Finally, the uncertainty surrounding any assumptions about the nature and progress of any IE means that several scenarios have had to be considered. We have concentrated on those phases that are the most likely to lead to destruction of the integrity of canisters and subsequent release of radionuclides to the biosphere.

This does not mean that we believe the potentially most hazardous scenarios to be the most likely: they are simply the scenarios that are of greatest importance to the Total System Performance Assessment (TSPA) probabilistic estimates. Where we can, we have sought to introduce and analyze those factors most likely to help define and quantify probabilities. Both the Panel and several of our correspondents have felt that the current assumptions about release of radionuclides, both into the atmosphere and into groundwater, are realistic or conservative (in some cases, overly conservative) given the models used for the interactions considered. Only if significant probability were to be realistically attached to the "dog-leg" scenario would TSPA averages be other than conservative (i.e., overestimate radiation dosages).

This evident need for quantification and reduction of uncertainty has led us to concentrate on giving mathematical form to such physical models as command the greatest acceptance within the community of volcanologists. This has required an interdisciplinary approach, involving expertise in fluid and solid mechanics, thermodynamics, physical chemistry and rheology. At the repository level, the rock is porous, permeable and unsaturated by ground water — features that we have found to play a significant part in expected dike propagation and drift flows. It has led us into original work, and much of this report discusses ideas, presents results and leads to conclusions that are far from standard.

1.5 NATURE AND CONTENT OF THE REPORT

Succeeding chapters of this report present and extend current understanding of the principal issues given in Section 1.4.

Chapter 2 provides a general description of the IEs to be considered, based largely on analog events observable at Crater Flat and Lathrop Wells, previously studied by BSC and others, but also drawing upon information and experience from a much wider range of volcanic events. It sets out the current view of the sequential phases to be anticipated. Volcanologists will not be surprised to read that the Panel regards the predictive problem as an extremely difficult one: the most that can be expected is to place as tight bounds as possible on the inputs to modeling exercises.

Chapter 2 also sets out and discusses the ranges of relevant values available for the full set of parameters needed to prescribe the properties of the magma: chemical composition, volatility of dissolved vapors and gases, thermal conductivity and heat capacity, density and viscosity as a function of pressure and temperature.

This and other information on

(1) the properties of the tuff rocks above and below the repository (modulus, strength, porosity, permeability, fracture toughness, thermal conductivity and heat capacity), and

(2) representative examples of the state of stress in the rocks below the repository

are summarized in Table 1-2. All of this information is used in later chapters.

Chapter 3 covers the central issue: the interaction of a rising dike with repository drifts. Section 3.2 provides a detailed discussion of dike propagation of the type to be expected at the site in the absence of repository drifts. Various mathematical models are presented (there or in associated appendices) to cover a range of magmas: incompressible (i.e., with no volatiles), and compressible (i.e., bubbly, treated as single-phase). They draw extensively on past work but introduce many difficult issues that often are avoided.

A significant feature of these analyses is that a cavity containing gas, at a pressure considerably less than the dike-normal stress, is thought to be present near the tip. At depths where the dike-normal stress in the host rock would otherwise prevent exsolution of gases, the cavity is short, and the propagation velocity is slowly varying and of the order of 1 m/s. At shallower depths, two processes can interfere with this "quasi-steady" scenario and perhaps cause decompression of magma into the gas cavity to become explosive. First, as the difference between the dike-normal stress and the cavity gas pressure decreases, the cavity becomes larger and the tip propagation velocity increases dramatically (apparently unstably) with time. Second, above the water table the permeability of the host rock is so large that the pressure in the cavity would drop far below the fragmentation pressure of a water-rich magma, even if instability of the tip had not yet occurred. Cavity length and pressure play important roles in the interaction with the proposed repository discussed next.

Section 3.3 begins the discussion of interaction with the repository, and covers both the possibility of changes in dike propagation direction and tip speed as the repository is approached (as a result of the additional horizontal earth-stresses induced by waste-generated heat), and the flow of the dike contents into the drifts. The latter is a key issue, and our discussion draws heavily on the mechanical aspects of dike propagation and the tip cavity discussed in Section 3.2. The possibilities of explosive pyroclastic flows, or largely degassed magma flows, are considered separately. Section 3.4 investigates the possibility that flow in a drift might vent to the surface along a fracture distant from the parent dike; this is the dog-leg scenario hinted at by earlier authors. This discussion requires consideration of both the likely normal stresses acting across potential dog-leg fractures, and the pressures that exist within the magmatic flow in the drift (the latter must exceed the former for a dog-leg to occur). The drift pressure in turn depends

Table 1-2 Representative magma and host rock properties

Property	***Range***	***Typical Value***	***Reference***
magma heat capacity	900-1300 J/kg K	1100 J/kg K	Spera(2000)
crystallization enthalpy	250-550 kJ/kg	350 kJ/kg	Spera (2000)
magma thermal conductivity	0.2-1 W/m K	0.5 W/m K	Spera (2000)
magma thermal diffusivity	0.1-1 $x10^{-6}$ m^2/s	$2x10^{-7}$ m^2/s	Spera (2000)
magma viscosity	1-500 Pa s	50 Pa s	Spera (2000)
host rock Young's modulus	13-17 GPa	15 GPa	Project literature
host Poisson's ratio*	.2-.25	.21	Project literature
host rock fracture toughness*	0.2-0.4 MPa $m^{1/2}$	0.3 MPa $m^{1/2}$	Project literature
host rock thermal conductivity*	0.5-1 W/m K	0.8 W/m K	Project literature
host rock density*	1500-2500 kg/m^3	2000 kg/m^3	Project literature
host rock permeability	10^{-12}-10^{-13} m^2	5x 10^{-13} m^2	Project literature
host rock heat capacity	900-1100 J/kg K	1000 J/kg K	Project literature
horizontal stress (S_h) at 646 m	not applicable	4.2 MPa	Stock et al., 1985
horizontal stress (S_h) at 1288 m	not applicable	14.8 MPa	Stock et al., 1985
host rock matrix porosity	0.10-0.16	0.13	Project literature
host rock lithophysal porosity	0.03-0.12	0.06	Project literature
volume fraction gas in magma with 2 wt % H_2O at 1150 °C and 4.2 MPa	not applicable	0.84	Appendix 2
volume fraction gas in magma with 2 wt % H_2O at 14.8 MPa	not applicable	0.43	Appendix 2
volume fraction gas in magma with 4 wt % H_2O at 4.2 MPa	not applicable	0.94	Appendix 2
volume fraction gas in magma with 4 wt % H_2O at 14.8 MPa	not applicable	0.74	Appendix 2

*****values at laboratory scale.

upon whether the flow is one of lava or pyroclastic material, and again each possibility is considered in turn. The impact of the different scenarios on the TSPA, based on crudely estimated probabilities, is explained.

Chapter 4 is concerned with eruption itself and the processes associated with eruption that control canister entrainment and transport of waste. Those processes include engulfment of canisters into a widening conduit, movement and lifting of canisters, and dispersal of waste through the atmosphere during an eruption. This chapter specifically critiques TSPA assumptions regarding the number of canisters that might be incorporated into an erupting conduit and the area over which waste might be dispersed.

The final chapter consists of a set of conclusions and recommendations based on the arguments and results presented in Chapters 2 to 4.

1.6 ACKNOWLEDGEMENTS

The Panel wishes to thank Jean Younker and Thomas Rodgers of Bechtel SAIC Company for their unstinted assistance in expediting the Panel's work. Their prompt resolution of many issues, both technical and administrative, has been accomplished with both insight and courtesy. The Panel also wishes to acknowledge the outstanding support of Mark Board of BSC, Frank Perry of Los Alamos National Laboratory, and particularly the work done under great pressure by Alexei Savitski at the University of Minnesota.

CHAPTER 2 VOLCANOLOGICAL SETTING, ERUPTION CHRONOLOGY, AND MAGMA AND HOST ROCK PROPERTIES

2.1 INTRODUCTION

The probability of igneous disruption at the proposed Yucca Mountain Repository (YMR) is estimated to be approximately 1 chance in 6250 over 10,000 years. This exceeds the NRC criterion of 1 chance in 10,000 over 10,000 years. Thus, igneous disruption is deemed a credible risk, and its consequences must be explored fully. The purpose of this chapter is to provide prefatory information and includes:

(1) a review of the history and volcanological setting of the Crater Flat region;

(2) a summary of eruption chronologies of volcanic centers comparable to possible future igneous activity at the Yucca Mountain Repository (YMR);

(3) determination of the thermodynamic and transport properties of magma most relevant to potential dike-drift interactions at YMR; and

(4) a brief review of the salient thermophysical properties and state of stress in the shallow crust beneath the YMR.

2.1.1 The Past Is the Key to the Future

The principle guiding the structure and content of this chapter is that the history of volcanism and eruptive styles of Pliocene to Quaternary volcanoes in the Crater Flat Volcanic Zone (CFVZ) represents the best guide to possible future activity at the YMR. Meaningful evaluation of the igneous consequences of magmatism at the proposed YMR demands examination of a number of critical issues including:

(1) the volume of magma involved in an igneous (intrusive or extrusive) event;

(2) the composition (including volatile content) and material properties (thermodynamic and transport) of intruded or erupted magma and of the host rock (Miocene volcanic tuff);

(3) the eruptive style and chronology or sequence of events unfolding on a time scale of hours to days to weeks to months to years; and

(4) the relation between magma pressure and depth beneath the YMR (i.e., the state of stress beneath Yucca Mountain and the properties of the Miocene tuff host rock) and its bearing on magma transport.

Before an analysis of the dynamics of magma-drift interaction can be made (see Chapter 3 in this report), specific attributes of the magma — its probable composition, volume, rheological and dynamical states — must be prescribed or at least bounded by reference to the previous volcanological history of the region and state-of-the-art petrologic methods. Similarly, the state of stress beneath Yucca Mountain must be understood, because the propagation of a magma-filled crack (i.e., a dike) depends markedly on the stress field and properties of the repository host rock.

2.1.2 Scope of the Problem

At the outset, it is important to emphasize the difficulty of the problem. One wishes to predict the quantitative characteristics of a low-probability igneous event at a restricted site (Yucca Mountain) over the next 10,000 years. Even without the perturbing effects of the repository drifts, the precise course the eruption follows (its style, duration, temporal variability, volume and dynamics) cannot be predicted precisely. The task of the Panel has been to provide a technical basis for, or indicate what research needs to be accomplished in order to put bounds on, the behavior expected during possible magma-drift interaction.

We have found an epistemological approach useful in conceptualizing this complex sequence of problems. Information relevant to magma-drift interaction and ultimately relevant to the Total System Performance Assessment (TSPA), especially our confidence in the TSPA process, can be categorized according to the following scheme:

(a) information that is known currently (e.g., thermophysical properties of the shallow crust beneath Yucca Mountain);

(b) information that is knowable but presently unknown (e.g., over what period of time were the ~ 1-Ma-old Quaternary Crater Flat basalts erupted?); and

(c) information essentially unknowable and likely to remain so except within broad order-of-magnitude bounds (e.g., likely volume of a future eruption).

2.1.3 Chapter Organization

The remainder of this chapter is organized as follows. In Section 2.2, the volcanological history of Crater Flat and environs is reviewed. The main purpose is to establish the volcanological history of the region as a guide to possible future magmatic events. Sections 2.3 and 2.4 address the issue of magmatic volatiles. In Section 2.5, an analysis of representative eruption chronologies is presented to indicate the range of variation expected and to discern trends or tendencies important to incorporate into magma-drift interaction scenarios. Outstanding issues that bear on the TSPA and the analysis of magma-drift interaction are highlighted in Section 2.6. An important aspect of possible disruptive volcanic activity at the proposed YMR is the chronological sequence of eruption phases or

dynamical states. This is sometimes given the appellation "eruption chronology." It has been said (Wohletz and Heiken, 1992) that "Ash particles are like snowflakes in that no two are alike." In fact, this quote is equally valid for entire eruptions: each follows a volcano-specific sequence of events that collectively define the eruption chronology. What general trends can be extracted by examining the volcanological record of eruptions comparable to previous ones at Crater Flat? In Section 2.7, we summarize the composition and properties (thermodynamic and transport) of magma considered most likely disruptive at YMR. Extensive documentation of phase relations and properties of possible disruptive Yucca Mountain basalt is presented in Appendix 2. These provide an internally consistent set of properties useful in dynamic modeling studies that may be carried out by the Project or other agencies in the future. A table of nomenclature may be found in Appendix 2 (Table 2B). Section 2.8 summarizes the properties of the host Tuff and provides background on the current state of stress at YMR.

2.2 SYNOPSIS OF VOLCANIC HISTORY OF CRATER FLAT

The following summary of the volcanic history of the Yucca Mountain area is provided for geological context and to establish the likely composition and crystallinity of magma relevant to potential igneous disruption at the proposed YMR. Details of this summary are drawn from Perry et al., 1988, with additional information from Project scientists, the relevant peer-reviewed international literature and other geoscientists who have responded to Panel requests for information following the May 2002 and August 2002 meetings in Las Vegas and at other times during the period of Panel review. Discussions in the field during a two-day field trip in November 2002 involving approximately 20 participants were especially useful to the Panel. The level of cooperation of Project scientists and other informed individuals for information or clarification has been exemplary.

2.2.1 Pre-Pliocene History of Yucca Mountain Region

Miocene (23.7- 5.3 Ma) silicic volcanism in the Yucca Mountain region is succeeded by late Miocene-Quaternary basaltic volcanic activity. The basaltic activity can be divided into two major episodes: basalt of the silicic episode (BSE) that occurred during the waning stage of silicic volcanism (> 8 Ma); and Postcaldera Basalt (PB) from ~ 9 million years (Ma) to the Quaternary. The postcaldera episode can be further subdivided into the Older Post-caldera Basalts (OPB), which outcrop north and northeast of Yucca Mountain, and the Younger Post-caldera Basalts (YPB), which outcrop west, southwest and south of Yucca mountain. The OPB ages range from ~ 9 Ma (basalt of Pahute Mesa) to ~ 6.3 Ma (basalt of Nye Canyon); a rough estimate of the total eruptive volume of the OPB cycle is ~ 1 km^3. There is an apparent volcanic hiatus of about 2.5 Ma (from 7.2 Ma to 4.7 Ma) in the Yucca Mountain region that separates the Older Post-caldera Basalts (OPB) from the Younger Post-caldera Basalts (YPB). The YPB have been studied in more detail than the older BSE and OPB volcanic rocks by the Project because, as argued by the Project,

the YPB post-caldera magmatic record provides the temporally proximate — and hence more critical — basis for forecasting future magmatic activity at the YMR. The Panel agrees with this assessment. Basaltic, rather than silicic, magmatism represents the most likely igneous event in the Yucca Mountain region in the next 10 ka, and the record of the Pliocene-Quaternary volcanic history of the Crater Flat Volcanic Zone (CFVZ) is most relevant to possible activity in the future. From a geologic perspective, it is impossible to definitively rule out other types of magmatism. However, the "recent" past is the best guide to the future.

2.2.2 Pliocene-Quaternary Volcanic History of Yucca Mountain Region

In order of decreasing age, the basalts of the YPB include the basalt of Thirsty Mesa, the basalt of Amargosa Valley, the Pliocene basalt of southeast Crater Flat, the basaltic andesite of Buckboard Mesa, the Quaternary basalt of Crater Flat, the basalt of Sleeping Butte and the Lathrop Wells basalt. Except for the basaltic andesite of Buckboard Mesa, all YPB products lie within a narrow northwest-trending zone located west and south of Yucca Mountain termed the Crater Flat Volcanic Zone (CFVZ) by Crowe and Perry (1989). Information on the age, petrographic characteristics, volume and composition of the Younger Post-caldera Basalts of the CFVZ are summarized in Table 2-1.

The integrated volumetric eruption rate averaged over the past 4.78 Ma is 1.22 km^3 Ma^{-1} or 0.012 km^3 per 10,000 years. The integrated rate over the past 1 Ma is 0.43 km^3 Ma^{-1} or 0.004 km^3 per 10,000 years. The integrated rate over the past 100 ka is 0.6 km^3 Ma^{-1} or 0.006 km^3 per 10,000 years. A plot of cumulative eruptive volume versus time for post-Miocene volcanic activity in the CFVZ is presented in Appendix 2 (Figure 2A). The information presented in Table 2-1 does not take account of possible additional basaltic volcanic rocks buried by alluvium. Aeromagnetic data (see below) suggests that recently identified magnetic anomalies may represent buried basaltic volcanic rocks in the CFVZ. The age and volume of these putative volcanic rocks are presently unknown, although potentially knowable. Additional information on the age and volumes of these volcanic rocks could impact estimates of the eruption frequency at Crater Flat and environs.

2.2.3 Summary of Salient Petrologic Features of CFVZ Activity

Based on observed characteristics of Pliocene to Quaternary volcanism in the CFVZ, the following conclusions are drawn.

- The most likely magma composition in the CFVZ is potassic trachybasalt (IUGS classification). A representative devolatilized composition used in further property and dynamic calculations is given in Table 2A (Appendix 2).

Table 2-1 Abbreviated volcanological history of CFVZ

YPB Unit	Age ± 2σ (Ma)	Volume (km^3)	Phenocrysts	Composition
Thirsty Mesa	4.88 ± 0.04 4.68 ± 0.03	3	sparse olivine	potassic trachybasalt
Amargosa Valley	3.85 ± 0.05	~ 0.8 (buried in alluvium)		basaltic
Pliocene basalt of southeast Crater Flat	3.75 ± 0.04 3.69 ± 0.06 3.65 ± 0.06	0.68	olivine >plag >cpx (Σ ~ 15 vol %)	basaltic
Buckboard Mesa	3.15 ± 0.08 3.08 ± 0.04	1	olivine & sparse amphibole	trachyandesite
Quaternary basalts of Crater Flat (Little Cones, Red Cone, Black Cone and Makani Cone)	Little Cones 0.77 ± 0.02 0.83 ± 0.16 1.02 ± 0.10	0.002	olivine & sparse amphibole at Red Cone & Little Cones	potassic trachybasalt
	Red Cones 0.92 ± 0.06 1.05 ± 0.14 1.08 ± 0.04	0.105		
	Black Cone 0.94 ± 0.05 0.96 ± 0.15 1.05 ± 0.08 1.05 ± 0.14 1.10 ± 0.05	0.105		
	Makani Cone 1.16 ± 0.10 1.17 ± 0.06	0.006		
Sleeping Butte	Hidden Cone 0.56 ± 0.10 0.32 ± 0.03	0.03	sparse amphibole	potassic trachybasalt
	Little Black Peak 0.39 ± 0.03 0.36 ± 0.04	0.03 0.03		
Lathrop Wells	~ 0.075 ± 0.01	lava ≈ 0.03 tephra ≈ 0.025 TOTAL ≈ 0.06	sparse olivine and plagioclase	potassic trachybasalt to subalkaline basalt

- The phenocryst content of magma relevant to igneous disruption at the YMR is likely to be low (~ a few modal percent). The presence of sparse olivine phenocrysts (with or without spinel inclusions) suggests that the Quaternary eruptive products at CFVZ were not multiply phase-saturated at depth before eruption. Coexistence of groundmass olivine, plagioclase, clinopyroxene and magnetite suggests that the Quaternary basalts of Crater Flat and the Lathrop Wells basalt did reach multiple saturation (cotectic crystallization), associated with loss of magmatic volatiles and cooling upon decompression, in the very near surface. Magma viscosity values based on aphyric melts of Lathrop Wells composition (extensively provided in Tables 2C, Appendix 2) are appropriate below the depth of volatile saturation.
- The presence of significant basaltic tephra at Lathrop Wells (tephra/lava ratio ≈ 1) and at other CFVZ eruptive sites indicates that the volume fraction vapor (θ) in the magmatic mixture (melt plus vapor) exceeded the critical volume fraction ($\theta_{crit} \approx 0.7$) associated with the rheological transition from homogeneous bubbly flow to pyroclastic flow for at least some eruptive phases of individual eruptions. A critical parameter for igneous consequences of magma-drift interaction is the depth at which this rheological transition, the so-called fragmentation depth, occurs and how this depth may vary temporally during a single eruption made up of one or more eruptive phases. The volatile abundance (mainly H_2O, CO_2 and S-bearing gas species) is the most important parameter affecting magma fragmentation depth.

2.3 VOLATILE CONTENT OF POSSIBLE DISRUPTIVE MAGMA AT YMR

Determination of the pre-eruptive volatile content of disruptive YMR magma is critical input for an informed evaluation of the thermal and dynamic consequences of magma-drift interaction. The abundance of magmatic volatiles can be estimated within certain bounds. Such bounds may then be used to quantify the thermodynamic and transport properties of potentially disruptive magma. H_2O is by far the most abundant volatile species in basaltic magmas; consequently, attention is focused upon estimating the dissolved H_2O content of pre-eruptive basalts, although the abundance of dissolved CO_2 is also considered. Three approaches can be used to estimate the volatile content of Crater Flat basaltic magma:

(1) presence of amphibole, a hydroxyl-bearing phenocryst in some CFVZ basalts that puts limits on the dissolved H_2O content of parental magma;

(2) study of dissolved volatiles in melt (glass) inclusions trapped in phenocrysts from CFVZ basalt; and

(3) comparison of the petrographically observed sequence of crystallization with experimental phase equilibration studies.

Each of these approaches has been applied to put bounds on the pre-eruptive volatile content of CFVZ basaltic volcanic rocks. Section A2-3 of Appendix 2 (“Estimating Magmatic Volatiles in CFVZ Basalts”) provides details of these methods. In summary,

the presence of sparse phenocrysts of amphibole in some of the Quaternary basalts of Crater Flat and at Hidden Cone (basalt of Sleeping Butte), measurements of volatile abundance in melt (glass) and fluid inclusions from Lathrop Wells and the observed sequence of crystallization in phenocrysts and groundmass constrains the pre-eruptive dissolved H_2O content of recent CFVZ magmas. **H_2O concentrations in the range 2.5 wt % to 4 wt % with bulk mass H_2O/CO_2 ratios around 6-20 are representative.** Although the vapor phase is rich in O, H and C, other components, such as S (species H_2S, SO_2, H_2SO_4) and the Halogens F and Cl (species HCl and HF), are present and chemically reactive at magmatic temperatures.

2.4 CORROSIVE PROPERTIES OF MAGMATIC VOLATILES

The concentration of magmatic gas species (i.e., mole fractions of H_2O, CO_2, SO_2, CO, CH_4, H_2, H_2S, HCl, HF) is a predictable function of temperature, pressure, bulk vapor phase composition and oxygen fugacity (f_{O2}). The speciation of the magmatic gas phase has implications for the corrosion of waste canisters. It is beyond the scope of this Panel to address the chemical reactivity of waste packages — specifically, Stainless Steel Type 316NG and Ni-based Alloy 22 with magmatic vapors steel (e.g., CWRMS, 2001, Fig. 3-6). Although H_2O is the dominant volatile species, the reactivity of magmatic vapor will depend on its specific composition and temperature. **If magmatic gas-corrosion studies are carried out by the Project, the effects of pressure and temperature changes should be considered in evaluating the speciation of the magmatic multi-component vapor.**

2.5 ERUPTION CHRONOLOGY

The consequences of a basaltic eruption through the YMR cannot be anticipated theoretically in the absence of descriptions of comparable eruptions elsewhere. Observational information has been derived for the TSPA from two primary sources:

(1) stratigraphic and petrologic analyses of ancient basaltic eruptive centers in the nearby Basin and Range; and

(2) historical observations of basaltic eruptions presumed analogous to possible future events at Yucca Mountain.

Among the historical examples considered by the Project or the NRC, the 1975-76 Tolbachik Fissure Eruption (Fedotov and Markhinin, 1983), the 1943-1952 eruption of Parícutin (Luhr and Simkin, 1993), several eruptions since 1850 at Cerro Negro (Viramonte and DiScala, 1970; Hill et al., 1998) and the 1973 Heimaey, Iceland eruption (Self et al., 1974) have figured prominently. Historical analogs provide important information on eruptive style, duration, intensity and extent of tephra dispersal and underscore the complex variability of individual eruptions. Single eruptions can often be broken into distinct eruptive phases; an awareness of the intrinsic variability of eruptive phases is im

portant to keep in mind. Studies of the prehistoric vents at Crater Flat, reviewed above, provide information on magma composition, petrology, volatile content and eruptive volume, but limited information on tephra dispersal due to age and extensive erosion of the tephra blankets. Knowledgeable volcanologists have disagreed on the degree to which tephra may be dispersed during a future eruption at Yucca Mountain. In particular, have violent Strombolian phases taken place during Crater Flat eruptions, and could they take place during a future Yucca Mountain event?

2.5.1 Analog Volcanic Systems

Yucca Mountain volcano-hazard studies have focused on eruptions of Cerro Negro (Nicaragua), Parícutin (Mexico), Tolbachik (Kamchatka) and Heimaey (Iceland) as analogs of potential future Yucca Mountain activity. The Panel recognizes that no analog volcanic system makes a perfect fit for the "ideal" monogenetic alkali-basalt cinder cone in a continental setting with eruptive volume in the range 0.01 km^3 to 1 km^3. Volcanic eruptions are unique events: like snowflakes, no two are alike. The Igneous Consequences Panel decided to survey independently a small part of the vast volcanological literature on eruption narratives to seek further insights regarding duration, style, and processes that might directly impact radioactive waste release. In Appendix 2 (Table 2D and Section A2.5.2), details are summarized for a few basaltic eruptions approximately analogous to possible future activity at Yucca Mountain. These illustrative examples were chosen based on available documentation and to provide a hint of the variability (within bounds) of Strombolian eruptions most relevant to past (Pliocene-Quaternary) and possible future volcanic activity at the YMR.

2.5.2 Eruptive Chronology of Lonquimay Volcano, Chile and Capulin Mountain, New Mexico, USA

In Appendix 2 (Section A2.5.2), detailed eruption narratives are presented for two Strombolian-style eruptions. These particular examples were chosen to illustrate typical patterns of behavior. The first is from a subduction-zone polygenetic volcano in southern Chile (Lonquimay) that has erupted five times in the past 150 years. The second example is Capulin volcano, a ~ 8 ka monogenetic cinder cone from the Raton-Clayton Volcanic Field in northeastern New Mexico.

2.5.3 Eruption Chronology Narratives: Critical Points for the YMR

Among basaltic eruptions in general (see Appendix 2, Table 2D and Section A2.5.2), a few points are especially relevant to radioactive waste release at Yucca Mountain. The implications of these points are discussed further in Chapter 4 with respect to the transition from dike flow to conduit flow during violent Strombolian eruptions.

- The duration of short-lived basaltic eruptions ranges from less than a day (e.g., Cerro Negro, 1992) to tens of months. For violent Strombolian eruptions, mass flows of ~ 10^6 kg/s are realizable. A sustained violent Strombolian eruption could produce ~1 km^3 of tephra in about two weeks, or 0.1 km^3 (e.g., Lathrop Wells volume) in about one day at this mass flow rate. This is extreme behavior. For the more typical Strombolian eruption rate of ~ 10^4 kg/s to 10^5 kg/s, eruption durations are 100 to 10 times longer, of the order of months to years. Eruptions that produce of the order of 0.1 km^3 to1 km^3 (Appendix 2, Section A2.5.2 and Table 2D) typically last one to several years. The volumes of eruptions in the CFVZ within the last ~5 Ma vary between 0.005 km^3 and 1 km^3, which suggests eruptive durations in the range of weeks to years assuming a typical normal Strombolian rate of 10^4 kg/s averaged over the entire eruptive episode. If Lathrop Wells (V ~ 0.06 km^3) is indeed a monogenetic volcano, then the eruption may have lasted ~ 5 months. It is important to keep in mind that the rates cited here are peak rates — that is, if periods of normal Strombolian activity are interspersed with eruption of mildly effusive lavas, then average mass flow rates (~ 10^3 kg/s) are more representative, and eruption durations are proportionally longer.

- Eruptions originating as basaltic fissure eruptions ("curtain of fire") evolve to central vents within hours or days.

- Scoria cones often develop to near their maximum height within days or weeks of the eruption onset (e.g., Parícutin, Heimaey, and Lonquimay). Thereafter, cone construction alternates with cone destruction when lava pressure within the cone pushes one flank out in a small sector collapse. The collapse of the cone flank may mark the onset of an eruptive phase that is dominated by emission of lava flows, such as at Parícutin in June 1943. At Surtsey and at Capulin Mountain, lava intruded through the earlier-built cinder cone or scoria pile to exit at a vent low on the flank of the cone (Thorarinsson, 1967). These effects cause changes in lava elevation of hundreds of meters, probably resulting in subsurface pressure fluctuations of a few to several MPa.

- Vent locations may change throughout the course of eruption; multiple vents may be active simultaneously, producing either tephra or lava or both.

- The greatest magma discharge, and the most violent, tephra-producing magmatic activity (excluding hydromagmatism), tends to occur early in the eruptive sequence. For example, at Parícutin, both magma discharge and the tephra:lava ratio both decreased systematically from 1943 to 1950 (Luhr and Simkin, 1993, p. 5). At Laki (Iceland) in 1783 to 1785, 90% of the erupted lava was emplaced during the first five months of the nine-month eruption (Thordarson and Self, 1993). At Heimaey, the eruption began with an effusion rate of 10^2 m^3/s, dropped to 60 m^3/s after two weeks, 10 m^3/s after two months, and 6 m^3/s after three months, finally ending after six months (Williams and Moore, 1983). At Kilauea, although the eruption that began in 1983 is continuing, violent lava fountains were generated only during the first three

years. There are exceptions to this tendency: at Tolbachik, the eruption began in September 1975, and periods of rejuvenation in April (associated with a change in magma composition) and July 1976 increased both the magma-discharge rate and the number and height of explosive ejections (Fedotov et al., 1983). Violent phases near the end of basaltic eruptions have tended to be associated with hydromagmatism, as at Tolbachik in 1976 (Doubik and Hill, 1999). Tephra production for the 1995 Cerro Negro eruption reached a peak about ten days after the start of the eruption. Although there is a tendency for the initial phase of an eruption to be more explosive than later phases, exceptions are uncommon but not rare.

- The ratio of tephra to lava emitted can vary during the course of a single eruptive phase lasting for days, weeks, months or years. Both tephra and lava can be emitted simultaneously, sometimes from the same vent and sometimes from multiply active vents. The tephra/lava ratio usually decreases as the eruption progresses.

- The ratio of lava to tephra emitted during different eruptions (discrete in time) or different eruptive phases of the same eruption can be different. For example, at Lonquimay, eruptions separated by a century were distinct. The 19-month eruption, beginning in June 1887, produced 0.1 km^3 of lava but very little tephra, whereas the lava/tephra ratio was ~ 2 for the 1988-1990 eruption.

2.6 UNRESOLVED VOLCANOLOGICAL ISSUES AT THE CFVZ

2.6.1 Eruptive Volumes

Eruptive volumes reported in Table 2-1 (plotted in Figure 2A of Appendix 2) for Crater Flat volcanism are likely minimum values. A number (at least a dozen) of aeromagnetic anomalies believed to represent basaltic lava flows buried by alluvial deposits have been located in the Crater Flat region. The Panel has not been presented with an analysis of the estimated volumes or ages of the buried geophysical anomalies (interpreted as buried basaltic volcanic rocks) identified to date. For the purposes of establishing a working framework, the Panel offers the following provisional analysis. There are ten known unburied eruptive vents in the Yucca Mountain region younger than 5 Ma, and seven buried volcanoes were identified in aeromagnetic surveys up to 1995. This gives a sum of 17 volcanic events over the past 5 Ma, assuming, for illustrative purposes, each anomaly represents an independent volcanic event. If the magnetic anomalies recently identified (Blakeley et al., 2000; O'Leary et al., 2002) represent buried basalt flows or tephra deposits that are less than 5-M-yr old, then the total number of post-Miocene vents is ~30, roughly double previous estimates. If all of the most recently identified aeromagnetic anomalies are relatively young (e.g., ~ 0.5 Ma to 1 Ma) with eruptive volumes ~ 0.05 km^3, then eruption probabilities would increase significantly. Alternatively, if the buried volcanics are at the opposite end of the age spectrum (e.g., 2 Ma to 4 Ma), the probability picture changes — although not dramatically, provided volumes associated with individual anomalies are ~ 0.05 km^3 or less. Finally, if all buried volcanics (magnetic anomalies) are pre-Pliocene, eruption probabilities change little. **A preliminary**

conclusion is that until better information regarding the number, volume and the age distribution of buried basaltic lavas and tephra is available, it will be difficult to know how to adjust estimates of volcanism rate and recurrence interval most relevant to disruptive igneous activity at the proposed YMR. One of the recommendations of this Panel is that further attempts be made to define the ages and volumes of the buried magnetic anomalies.

2.6.2 Crater Flat Volcanism: Monogenetic or Polygenetic?

Large polygenetic composite or shield volcanoes, such as Mount Saint Helens and Mauna Loa (Hawaii), respectively, are built on time scales of 10^5 yr to 10^6 yr by episodic eruption from a single vent or series of vents in close proximity at repose intervals of 1 yr to 10^2 yr. In contrast, Quaternary volcanic eruptions at Crater Flat are most likely monogenetic. These eruptions consist of only a single episode, lasting weeks to months to years, after which activity ceases at a particular vent. Monogenetic activity typically forms small topographically simple volcanic constructs characterized by cinder cones and associated lava flows. Although an eruption from a particular monogenetic vent is not protracted, activity in a multiple-vent monogenetic basalt field can be protracted over Ma time periods. Geochronological data made available to the Panel, as summarized in Table 2-1, does not allow unequivocal determination of the period of time over which volcanism was active for the Pliocene basalts of Southeast Crater Flat, the Quaternary Basalts of Crater Flat or at Lathrop Wells, although the evidence leans toward (short-duration) monogenetic activity at Lathrop Wells. There are a number of geochronological laboratories capable of making high-resolution age determinations on basaltic compositions. For ages around 1 Ma, high-precision Argon 39/40 measurements with uncertainties as small as several thousand years can be obtained if samples are suitable (holocrystalline groundmass). More typical uncertainties lie in the 10 ka to 30 ka range. **High-precision geochronological information would enable better estimates of volcanic recurrence rates at Crater Flat relevant to igneous consequences at the proposed YMR at relatively modest cost. This issue could be clarified, or at least significantly better constrained, by an intensive high-resolution geochronological program.**

2.6.3 Hydromagmatism at Crater Flat?

The term “hydromagmatism” encompasses all processes, subsurface or surficial, involving the interaction of magma or magmatic heat with meteoric or connate (formation) water in the Earth (Wohletz and Heiken, 1992; Fisher and Schmincke, 1984). Of particular concern at the YMR is a possible phreatomagmatic eruption. A phreatomagmatic (or hydrovolcanic) eruption is an explosive volcanic eruption resulting from the interaction of rising magma with groundwater or shallow surface water. The explosivity of a phreatomagmatic eruption is due the expansion of non-magmatic (initially cool) groundwater due to magmatic heating. Phreatomagmatic ash forms by thermal contraction and shattering of glass and can be differentiated from ash formed by the release of magmatic

volatiles by examination. A characteristic type of volcanic deposit known as *base surge* typically forms during phreatomagmatic activity. At the 100 m to km scale, unique volcanic structures known as *maars* can form during phreatomagmatic eruptions. A *maar*, or phreatomagmatic explosion structure, is a small volcano characterized by a crater that is wide (~100 m to 1000 m) relative to its height, with a crater floor that generally lies below the local level of surrounding topography.

In summary, phreatomagmatism produces unique readily identified textures and structures across a variety of scales — from the sub-millimeter (ash size and shape) to the meter (bed forms of pyroclastic surge deposits) and finally to the map scale of kilometers (e.g., maars). What is the relevance of phreatomagmatism to potential volcanic activity at the proposed YMR site? No evidence of phreatomagmatic activity has been discovered in either the Pliocene basalts of southeast Crater Flat or in the Pleistocene (~ 1Ma) potassic trachybasalts of Crater Flat. However, at Lathrop Wells, the youngest of the Crater Flat volcanoes, Project geologists interpret a ~ 1 m thick deposit as being of phreatomagmatic origin. This deposit sits on a scoria layer about 1 m in thickness, which suggests that a phreatomagmatic phase of activity took place early in the eruptive sequence at Lathrop Wells — although not at the very beginning. The total volume of the deposit interpreted as hydrovolcanic is small compared to the entire (lava plus tephra) volume of the Lathrop Wells deposit. Predictions regarding the propensity of hydrovolcanism in the next 10,000 years at the YMR necessarily involve geohydrological and climate considerations beyond the scope of the Igneous Consequences Review Panel. **Based primarily on the Pliocene to Pleistocene volcanic history of Crater Flat, there is no overriding reason to believe that phreatomagmatism would play a pivotal role in any potential volcanic activity at the proposed YMR site in the next 10,000 years. Nevertheless, efforts to better comprehend the volume, timing, dynamics and significance of hydrovolcanism at Lathrop Wells should continue. These efforts may involve trenching in order to develop stratigraphic and spatial distribution as well as examination by SEM and other instrumental methods of putative phreatomagmatic ash.**

2.7 MAGMA PROPERTIES

Once bulk composition and volatile content are established for possible disruptive magma, its thermodynamic and transport properties may be estimated and utilized in dynamic and thermomechanical models relevant to magma-drift interaction. Magma is defined as a multiphase mixture of silicate liquid (synonymous with melt), coexisting vapor (mainly H_2O + CO_2) and entrained solid particles (e.g., phenocrysts, xenocrysts or lithic inclusions). In Appendix 2 (Tables 2C), some important thermodynamic and transport properties are presented in tabular form as a function of pressure for potassic trachybasaltic magma (major element composition is reported in Appendix 2, Table 2A) with varying amounts of H_2O and CO_2 added. At equilibrium conditions, volatile species partition between coexisting melt and vapor depending on pressure, temperature and oxygen fugacity. If vapor components other than H, C and O are ignored, then, at the prevailing conditions of oxygen fugacity, the dominant species are H_2O and CO_2.

2.7.1 Use of the Magma Property Tables

Properties have been computed for magma at temperatures 1050 °C, 1150 °C and 1220 °C for H_2O/CO_2 mass ratios ($\equiv Z_{H2O}/Z_{CO2}$) equal to 2, 4, 6, 10 and 20 and total volatile content ($Z_{H2O} + Z_{CO2}$) equal to 1, 2, 3 and 4 wt %. For each permuted triplet of temperature, Z_{H2O}/Z_{CO2} ratio and total volatile content ($Z_{H2O} + Z_{CO2}$) properties are calculated at 100 MPa, 90 MPa, 80 MPa, 70 MPa, 60 MPa, 50 MPa, 40 MPa, 30 MPa, 20 MPa, 17 MPa, 14 MPa, 11 MPa, 8 MPa, 5 MPa, 2 MPa and 0.10133 MPa (1 atmosphere). Additional tables for pure H_2O and pure CO_2 with Z_{H2O} or Z_{CO2} equal to 4 wt % and 8 wt %, respectively, are provided for reference. Fifty-four Excel tables are presented as Tables 2C in Appendix 2. The model of Papale (1999) has been used to compute dissolved H_2O and CO_2 and vapor phase compositions of potential disruptive magma. Other algorithms (Spera, 2000) were used to compute additional properties, including density of melt, vapor, magma, pure CO_2, pure H_2O and pure SO_2, the mass fraction, volume fraction and composition of vapor, the shear viscosity of volatile-saturated melt, the fugacity of H_2O and CO_2, the isobaric and isochoric heat capacity of H_2O and CO_2 and sound speeds (sonic velocity) of melt, vapor and magma. Details are provided in the description of Tables 2C in Appendix 2.

2.7.2 Representative Example of Magma Properties

As an example, representative magma properties are portrayed graphically in Figures 2-1(a-g) for 4 wt % total volatiles, Z_{H2O}/Z_{CO2} = 20 (bulk mass ratio of water to carbon dioxide = 20) and T= 1150 °C as a function of pressure. Note the strong dependence of most properties on pressure.

2.7.3 Magma Fragmentation Depth: Variation with Volatile Abundance

There is a strong dependence of magma properties on pressure (depth) and on the bulk volatile content of magma as revealed in Appendix 2, Tables 2C, and in Figure 2-1(a-g). This arises due to exsolution of dissolved volatiles and attendant magma (melt plus vapor) expansion accompanying decompression. For a homogeneous magmatic mixture, decompression associated with ascent is a quasi-equilibrium process. The magma temperature varies by less than a few tens of degrees (Mastin and Ghiorso, 2001) during quasi-isentropic expansion, because the mass fraction of melt ($1-\phi$) is large compared to vapor mass fraction (ϕ) — even at low pressure, when θ (volume fraction of vapor) may be large. The melt phase acts as a heat reservoir during magma expansion. The sensitivity of properties with pressure depends on the initial (pre-eruptive) abundance of magmatic volatiles, $Z_{H2O} + Z_{CO2}$. The volume fraction of vapor (θ) in the magmatic mixture plays a critical role in magma eruptive dynamics. As an illustration, imagine the following contrasting set of possible magma thermodynamic states at the moment a repository drift is breached by a dike:

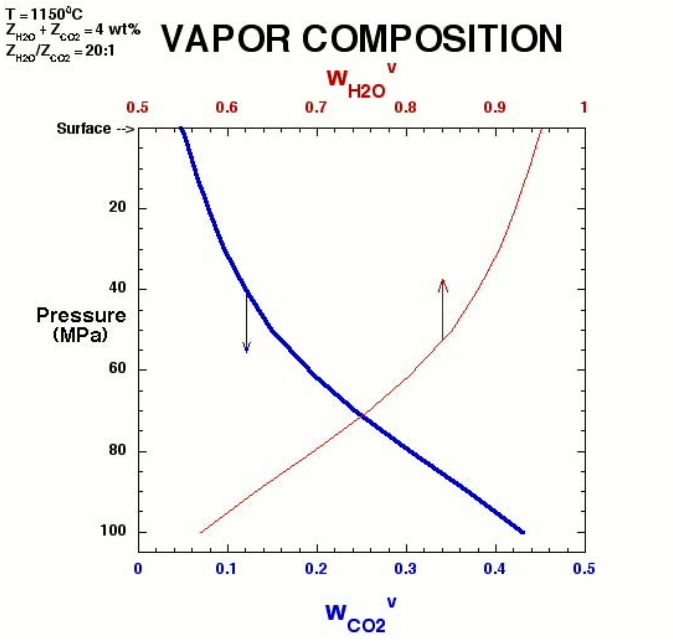

Figure 2-1a *Mass fraction of H_2O (w_{H2O}^{v}) and CO_2 (w_{CO2}^{v}) in vapor phase versus pressure for disruptive Yucca Mountain Basalt for total water (Z_{H2O}) and carbon dioxide (Z_{CO2}) content of 3.8 wt % and 0.2 wt %, respectively, at 1150 °C*

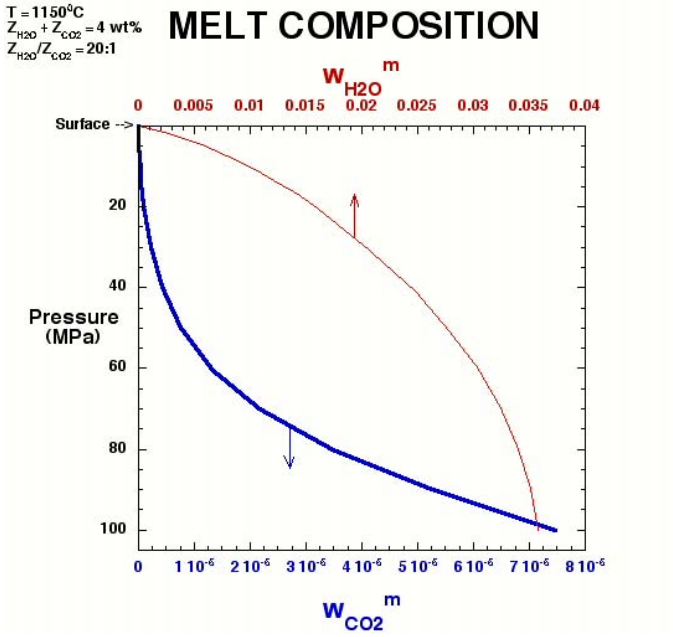

Figure 2-1b *Mass fraction of dissolved H_2O (w_{H2O}^{m}) and CO_2 (w_{CO2}^{m}) in melt phase versus pressure for disruptive Yucca Mountain Basalt for total water (Z_{H2O}) and carbon dioxide (Z_{CO2}) content of 3.8 wt % and 0.2 wt %, respectively, at 1150 °C*

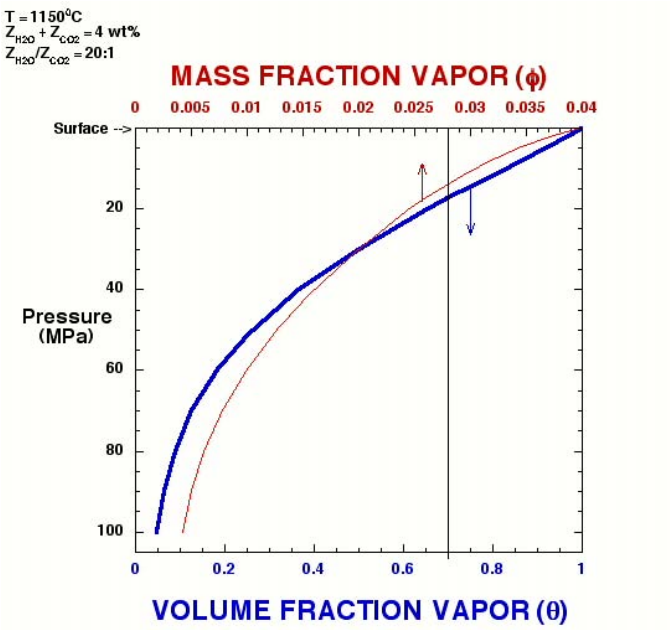

Figure 2-1c *Mass fraction (ϕ) and volume fraction of vapor (θ) in disruptive Yucca Mountain. Basalt for total water (Z_{H2O}) and carbon dioxide (Z_{CO2}) content of 3.8 wt % and 0.2 wt %, respectively, at 1150 °C (The volume fraction of vapor (θ) at which vapor is the continuous phase (i.e., the magma fragmentation condition) is approximately θ_{crit} = 0.7. In this example, the fragmentation pressure is about 20 MPa, which corresponds to a depth of 1.6 km beneath Yucca Mountain.)*

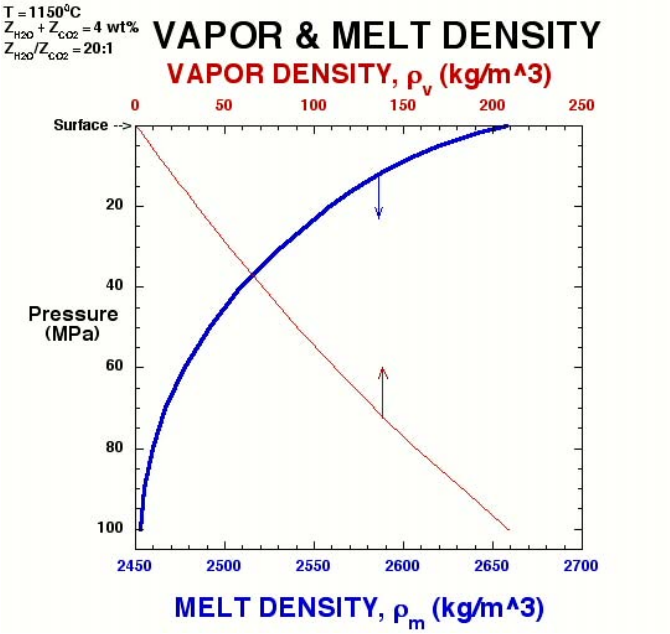

Figure 2-1d *Density of vapor (ρ_v) and volatile-saturated melt (ρ_m) versus pressure for Disruptive Yucca Mountain Basalt for total water (Z_{H2O}) and carbon dioxide (Z_{CO2}) concentrations of 3.8 wt % and 0.2 wt %, respectively, at 1150 °C. (Melt density increases upon decompression because the dissolved volatile content drops sharply along the 1150 °C isotherm.)*

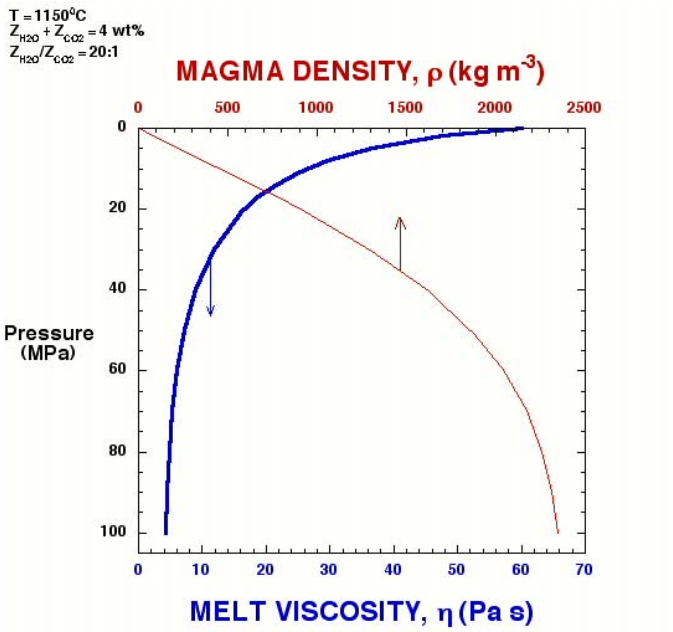

Figure 2-1e ***Density of magma (ρ) (i.e., two-phase mixture) and shear viscosity of melt (η_m) versus pressure for disruptive Yucca Mountain Basalt for total water (Z_{H2O}) and carbon dioxide (Z_{CO2}) content of 3.8 wt % and 0.2 wt %, respectively, at 1150 °C. (Note that density of magma decreases rapidly upon decompression due to exsolution of volatiles from coexisting melt.)***

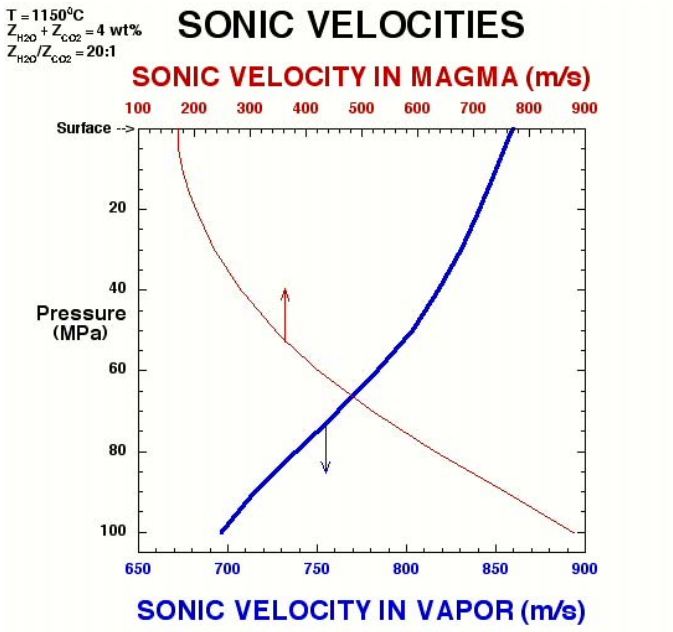

Figure 2-1f ***Sonic velocity of magma (i.e., two-phase mixture) and coexisting vapor for disruptive Yucca Mountain Basalt for total water (Z_{H2O}) and carbon dioxide (Z_{CO2}) content of 3.8 wt % and 0.2 wt %, respectively, at 1150 °C. (Sonic velocity for magma is computed assuming magma is homogeneous bubble- (volatile-saturated) melt mixture. This assumption breaks down close to θ_{crit}. More complex separated flow models become increasing important as $\theta \rightarrow$ unity.)***

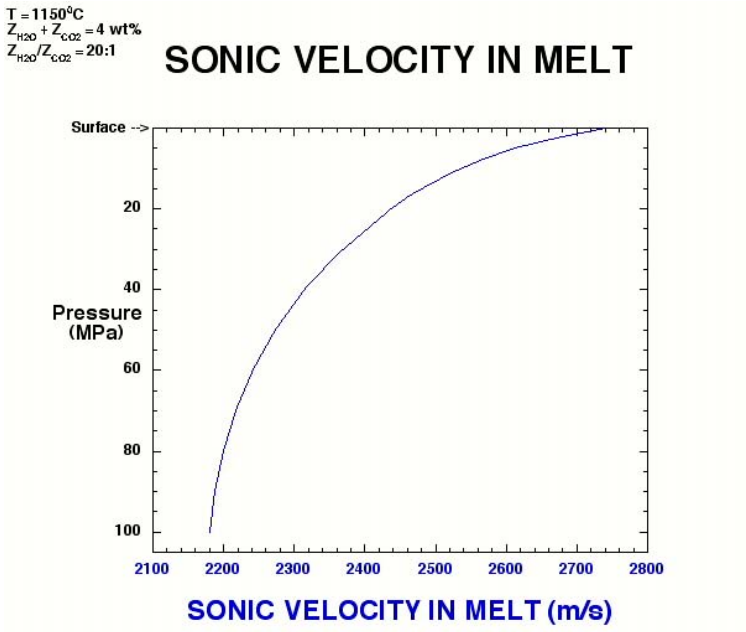

Figure 2-1g ***Sonic velocity of volatile-saturated melt for disruptive Yucca Mountain Basalt for total water (Z_{H2O}) and carbon dioxide (Z_{CO2}) content of 3.8 wt % and 0.2 wt %, respectively, at 1150 ℃***

(1) melt-dominated (low-volatile content) essentially incompressible viscous magma ($\eta_m \sim 100$ Pa s) at Reynolds number ($Re \equiv \rho Uw/\eta \approx 55$) corresponding to laminar flow ($w = 2$ m , $U = 1$ m/s , $\rho = 2700$ kg/m^3);

(2) homogeneous bubbly-flow (melt plus vapor) of "just-compressible'" magma with a fraction of bubbles (θ) < 40 volume per cent at Mach number ($Ma \equiv U/c \approx 0.3$) and $Re \approx 10^{3\text{-}4}$ (At these conditions, the flow straddles the boundary between laminar and turbulent flow and the effects of compressibility are non-negligible — but not dominant. Typical scale values are: magma sonic velocity of 230 m/s, magma velocity, density and viscosity of 70 m/s,1500 kg/m^3 and 10 Pa s, respectively.) ;

(3) two-phase fragmented ($\theta > 0.7$) and separated flow with melt and vapor moving at different speeds in a "fully compressible", choked, highly turbulent ($Re > 10^4$) regime. (Under choked conditions, the vapor may be supersonic and the melt subsonic at the dike-drift. throat. Typical scales for magma velocity and density are 230 m/s, 500 kg/m^3, respectively.

These disparate thermodynamic initial states leading to rather distinct magma-drift interaction scenarios are differentiated on the basis of the local volume fraction of vapor (θ) in the magmatic mixture. The volume fraction of vapor can, and often does, vary during the course of a single volcanic eruption, generally made up of a sequence of eruptive phases from a single or several simultaneously active vents perhaps overlapping in time. A common pattern, for example, is for an eruption to start as a fissure eruption that quickly localizes to a single conduit. An explosive phase characterized by relatively high rates of

tephra production (e.g., cinder cone development and dispersal of volcanic ash over a wide area) often initiates an eruption. As the explosive eruptive phase wanes, one or more lava flows may occur and spread out around the cinder cone. Alternatively, some eruptions begin with a more mildly effusive phase that intensifies to a Strombolian phase. The stratigraphic record of the deposit can sometimes be deciphered to construct an eruption chronology.

2.7.4 Magma Fragmentation Depth: Limitations and Assumptions

A lower-bound estimate of the fragmentation depth can be found by equating the (thermodynamic) pressure of magma, corresponding to the critical value $\theta_{crit} \approx 0.7$ of the volume fraction of vapor, to the horizontal stress, $S_h(z)$. Extensive tables are presented in Appendix 2 (Tables 2C) to facilitate this calculation. Roughly, $S_h(z) \approx 2/3\ S_v(z)$ beneath Yucca Mountain, with $S_v(z) \approx \rho g h$, where ρ is the mean density of the overburden repository host rock, and h is depth. Results of such calculations are summarized in Figure 2-2, which shows the variation of fragmentation pressure with volatile abundance. Although strictly valid for a volatile mass ratio $Z_{H2O}/Z_{CO2} = 6$, the fragmentation pressure varies little (less than 1 MPa) for Z_{H2O}/Z_{CO2} ratios in the range 2 to 20. Therefore, this plot is a good approximation as long as H_2O is the dominant volatile species, which is almost certainly the case for CFVZ eruptions. The fragmentation pressure varies from 4 MPa to 17 MPa at 1150 °C as total volatile concentrations increase from 1 wt % to 4 wt %. These pressures correspond to contemporary values of the least compressive stress in the host rock at depths of ~ 500 m and ~ 1400 m, respectively.

Results presented in Figure 2-2 and in Tables 2C (Appendix 2) ignore bleed-off of gas in the country rock from the tip cavity, which separates the magma front from the tip. In addition, equating the magma pressure (in a rough sense) with S_h ignores the steep pressure gradient below the ascending magma front. Inclusion of these effects are discussed in Chapter 3.

2.7.5 Transport Properties

The magma transport properties considered here include the shear viscosity of both melt (η_m) and magma (η) and the thermal conductivity (k). In heat transport calculations, the thermal diffusivity, $\kappa \equiv k/\rho C_p$, is the quantity needed and can be computed from thermal conductivity using values of the density and isobaric specific heat capacity from Tables 2C (Appendix 2).

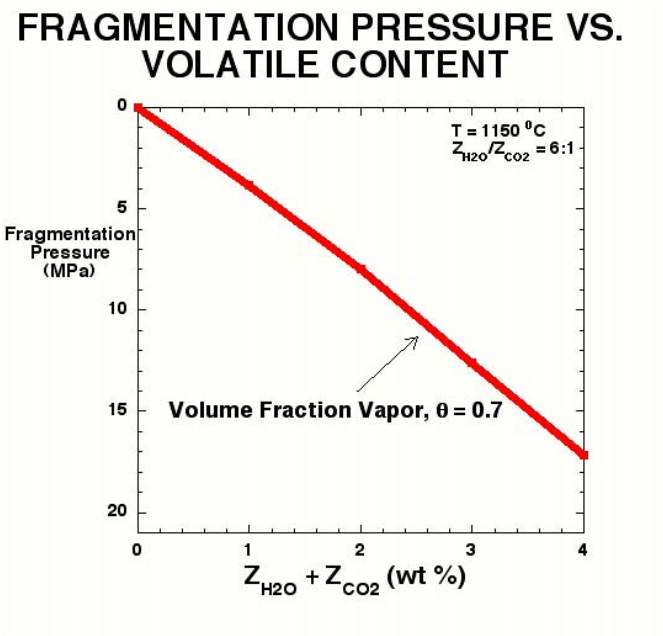

Figure 2-2 ***Fragmentation pressure or pressure at which the volume fraction of vapor reaches θ_{crit} = 0.7 for disruptive Yucca Mountain Basalt as a function of the total volatile content of magma treated as a closed system at 1150 °C (The fragmentation pressure is very weakly dependent on Z_{H2O}/Z_{CO2} for values > 6; hence, this plot is valid for essentially all reasonable water/carbon dioxide ratios.)***

2.7.6 Shear Viscosity

Melt viscosity is sensitive to temperature and dissolved H_2O. The variation of melt viscosity is given for a range of temperatures and dissolved water contents in Appendix 2 (Table 2C). In addition to changes in the melt viscosity, the effects of vapor bubbles in two-phase magma must also be considered. Bubbles can alter the magma shear viscosity by an order of magnitude (either increase or decrease) relative to bubble-free melt at otherwise similar pressure-temperature conditions depending on the local rate of shear in the (homogeneous) magmatic mixture. Bubbles also impart significant non-Newtonian behavior to magma, and this can affect the dynamics and heat transfer characteristics of magma-drift and magma-canister interactions. A discussion of the rheological properties of bubbly magma, treated as a homogeneous mixture, is given in Appendix 2, Section 2.6.1, "Rheology of Bubbly Magma". Also in Appendix 2, Figure 2B, the relative shear viscosity of magma is shown as a function of volume fraction vapor (θ) and Capillary number (*Ca*) (see also Appendix 2, Section A2.6.1). **The conclusion is that for conditions of flow at Yucca Mountain, it is important to take into account the shear rate dependence of the shear viscosity.** At high shear rate in a bubbly mixture, magma viscosity is up to an order of magnitude less than that of single phase melt at identical temperature, pressure and shear rate. It is relatively straightforward to incorporate this effect into future magma-drift dynamic calculations performed by Project scientists by parameterization of results presented in Figure 2B (Appendix 2).

2.7.7 Thermal Conductivity

For analysis of heat transport of magma-drift and magma-canister interaction, the total thermal conductivity (k_T) of magma is needed. The total thermal conductivity represents the sum of two terms: the lattice or phonon conductivity (k_P), and the radiative conductivity (k_R). The relative magnitude of the phonon and radiative contributions to the melt thermal conductivity, as well as its absolute value, is uncertain by about a factor of ten (Spera, 2000). One major issue involves the variation of magma opacity with the concentration of transition metals and dissolved water. When opacity is large, the radiative contribution is small, and the phonon conductivity (k_P) is the appropriate thermal property. From measurements on Hawaiian basaltic melts, there is a factor-of-two decrease in k_P as temperature increases in the range 1150 °C to 1350 °C. Based on values reported in the literature (Buttner et al., 2000; Snyder et al., 1994), it is estimated that the phonon thermal conductivity at 1100 °C is in the range 0.7 W/m K to 1.1 W/m K for potassic trachybasalt melt. For magma, values can be calculated based on mixture theory and the properties of melt and coexisting vapor, although this has not been done here. Thermal conductivity is one of the most poorly known physical properties of silicate melts and magmatic mixtures. For the purpose of modeling thermal magma-drift interaction, a value in the range 0.3 W/M K to 1.0 W/m K may be used as a first approximation.

2.8 HOST ROCK PROPERTIES AND STATE OF STRESS

2.8.1 Host Rock Properties

The thermophysical properties and state of stress of the repository host rock (Miocene-age silicic volcanic tuffs) have been studied exhaustively by the Project. Critical properties include isobaric specific heat, density, thermal conductivity, porosity and pore pressure, permeability, fracture toughness and elastic moduli. Ranges and representative values for these parameters are presented in Table 1-2 in Chapter 1 of this report. It is important to note that propagation of a magma-filled crack (i.e., a dike) depends on host rock properties —not simply the properties and volatile content of the magma. For example, in Chapter 3, the significance of the tip cavity, the region ahead of the magma front, is discussed in detail. The permeability of the host rock plays an important role in defining the gas pressure in the crack tip, which, in turn, affects the flow of magma and the nature of dike-drift interaction.

In addition to thermophysical parameters, the state of stress (i.e., the magnitude and orientation of the principal stresses and their variation in space and time throughout the repository region) plays a prominent role in the coupled fluid dynamic-fracture mechanical problem of magma ascent.

2.8.2 State of Stress at Yucca Mountain

Yucca Mountain lies within the southern Basin and Range stress province, which is undergoing active ESE-WNW extension (Zoback, 1989). The state of stress in the Yucca Mountain region has been investigated using hydraulic fracturing stress measurements, breakouts, drilling-induced fractures, earthquake focal mechanisms and fault-slip orientations (e.g., Carr, 1974; Springer et al., 1984; Stock et al., 1985; Rogers et al., 1983; Warren and Smith, 1985; Harmsen and Rogers, 1986; Frizzel and Zoback, 1987; Sandia National Laboratories, 1997). A comprehensive review of these data is given in Stock and Healy (1988).

Most studies give the orientation of the most compressive horizontal stress (S_H) as ~N30E$\pm$15°. Uncertainty in this orientation results from both inaccuracies in measurement and real variations in stress with depth and location, as observed, for example, in breakout and drilling-induced fracture orientations, which vary by up to 40° in Yucca Mountain boreholes (Stock et al., 1985). Stress measurements at < 1.5 km depth give $\Phi = (S_H\text{-}S_h)/(S_v\text{-}S_h) = 0.5\text{-}0.7$, and $S_h/S_v = \sim 0.32\text{-}0.63$, where S_h represents the least compressive horizontal stress. Magma-filled fractures will tend to open orthogonal to the direction of the least principal stress (S_h) along the direction of S_H. The magnitude of S_h at Yucca Mountain lies close to the point of failure for optimally oriented normal faults having friction coefficients of ~ 0.6 (Stock et al., 1985; Zoback and Healy, 1984). However, the faults in this area have moved little during the last few million years (Stewart, 1988), and Yucca Mountain is less active seismically than surrounding areas (Rogers et al., 1983). Earthquake focal mechanisms at 3 km to 12 km depth for the region give normal, strike-slip, and oblique solutions that are inferred to result from slip on pre-existing faults in a stress regime where $S_v \approx S_H$, or $\Phi = \sim 1$ (Harmsen and Rogers, 1987; Zoback, 1989). The shallow in-situ stress measurements and deeper focal mechanisms suggest an increase in Φ with depth from ~ 0.5 in the uppermost kilometer to ~ 1 below 3 km, implying an increase in the anisotropy of the stress field in the horizontal plane.

The anisotropy in the horizontal stress field controls the maximum angle from S_H at which a dike may intrude pre-existing fractures. Specifically, a dike may intrude a fracture only if the magma pressure (p_m) exceeds the normal stress resolved on the dike σ_{11}^d plane. This condition is met when

$$-\cos(2\alpha) > \frac{(p_m - S_H) + (p_m - S_h)}{(S_H - S_h)} \qquad (2\text{-}1)$$

where α is the angle between S_H and the dike plane (Delaney et al., 1986). Values of p_m - S_h for basaltic dikes are typically several MPa (Pollard, 1987; Rubin, 1995a).

Assuming that the state of stress is controlled by a coefficient of friction on optimally oriented faults, the ratio of principal stresses in a normal faulting regime is limited by the following relation (Brace and Kohlstedt, 1980; Zoback and Healy, 1984):

$$\frac{S_v - p_p}{S_h - p_p} < \left[\mu + \sqrt{\mu^2 + 1} \right] \qquad (2\text{-}2)$$

where μ is the coefficient of friction, and p_p is pore pressure. In places where the water table is shallow and p_p follows the hydrostat (p_p = ~ 0.4 S_v), this relation implies a ratio S_h/S_v close to 0.6.

Figure 2-3 shows the degree to which a dike could deviate from the S_H orientation at Yucca Mountain as a function of depth. This plot is based on the following assumptions.

1. The state of stress is controlled by a coefficient of friction of 0.6 on optimally oriented faults.
2. p_p follows a normal hydrostatic gradient (10 MPa/km) below the water table.
3. $S_v \approx S_H$ at depths greater than a few kilometers.

The figure suggests that a dike could deviate significantly from the orientation of S_H if directed by pre-existing fractures. Televiewer logs from Yucca Mountain boreholes indicate that most steeply dipping fractures strike N30-60E, roughly in the same range as orientations of S_H (Stock et al., 1985). By comparison, PVHA analyses (CWRMS M&O, 2000b, p. 102) suggest that the dike that intersects the repository will be oriented between about N10E and N60E, within the 10% and 90% CDF. This range is reasonable given our knowledge of the state of stress at Yucca Mountain and the uncertainty associated with it.

Finally, it should be noted that although a dike can open and follow a pre-existing fracture if the condition in Eq. (2-1) is met, it will not propagate in its own plane beyond the end of that fracture. Instead, it will open a tail-crack that abruptly turns away from the fracture orientation and (in pristine rock) eventually aligns with S_H. Alternatively, if the fracture is one of a parallel set, the dike may step over to the next pre-existing fracture and follow it. Sequential stepping of this type may form a stair-step dike whose overall orientation is closer to that of S_H than the fracture orientation.

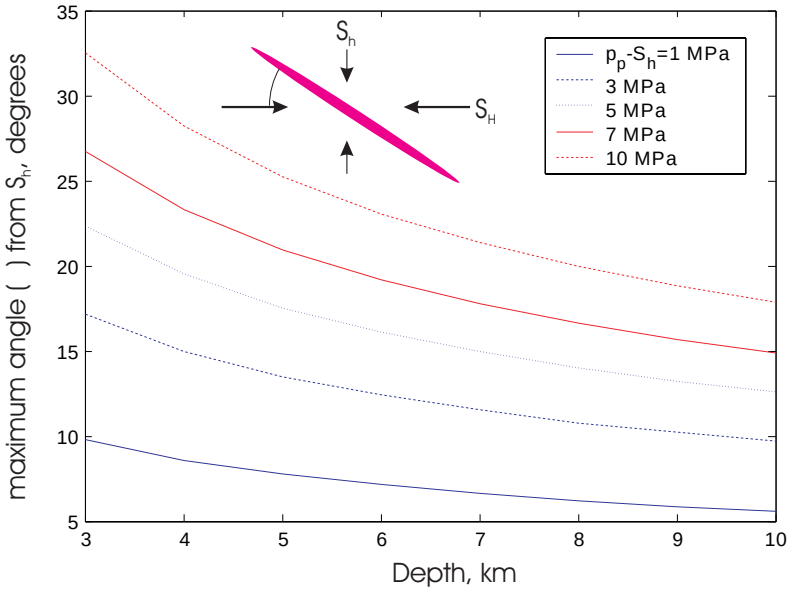

Figure 2-3 ***Maximum angle from S_H at which a dike of a given excess magma pressure can intrude pre-existing fractures as a function of increasing depth (Assumptions regarding the magnitude of S_H, S_h, and pore pressure (p_p) are given in the text.)***

CHAPTER 3 INTERACTION BETWEEN A DIKE AND THE REPOSITORY — THE DOG-LEG SCENARIO

3.1 INTRODUCTION

3.1.1 Dog-Leg Scenario

One possible sequence of igneous events at Yucca Mountain that has been investigated by the Panel is the "dog-leg" scenario. In this scenario, radioactive materials are brought to the surface through a chain of events that involves successively (1) a rising dike intersecting the repository, (2) magma being diverted from the dike and flowing into the drifts, and (3) flow of either magma or pyroclastic material down some drifts over considerable distances and entraining waste material before venting to the surface via a preexisting fracture.

In principle, this particular chain of events cannot be examined in isolation of the sequence of phases that could take place during an eruption, as discussed in Chapter 2. In particular, the bringing of magmatic material to the surface usually involves, according to the geological evidence, the formation of cylindrical conduits where the magmatic flow localizes through a transition from the planar dike flow. Unfortunately, as pointed out in Chapter 1, the mechanisms of flow localization into a conduit are not yet understood; thus, there are presently few mechanistic constraints on the timing of the formation of a conduit in regard to the progression of the dike tip toward the surface, at least for analog (i.e., high water content) basalts, whether involving a dog-leg or not. In view of the lack of this critical link between the two modes of magma transport, and despite the shallow depth of the repository (which implies a small chance that a conduit could even form before the dike intersects the repository), we are forced to examine the mechanics of interaction of a dike with the repository and the succession of events that lead to a dog-leg scenario in complete disconnection with the formation and existence of a volcanic conduits. Yet, it has to be kept in mind, throughout the following detailed examination of the dog-leg scenario that a large part of the total volume of magmatic material erupted is eventually brought to the surface via a cylindrical conduit.

3.1.2 Chapter Organization

Assessing the plausibility of the dog-leg scenario requires several packets of information that are provided sequentially in Sections 3.2 to Section 3.4.

Section 3.2 concerns some aspects of dike propagation in the absence of a repository. It provides information about the factors that control the quantities that are most relevant in regard to the scenario of a dike intersecting the repository — namely, (1) the pressure of the gas and/or vapors that first enter into contact with the drifts before magma starts to fill the repository, (2) the velocity of the magma and the dike aperture at the magma front (loosely defined as separating regions with and without melt), and (3) the nature of the

magma flow at the magma front. The particular conditions that arise at Yucca Mountain invalidate some of the assumptions of laminar incompressible flow on which the dike propagation models found in the literature are based. The section then gives a description of efforts expended by the Panel to modify dike models to account for gas exsolution from the magma and compressibility of the bubbly magma. Despite these efforts, the current lack of any comprehensive models means that one is still not in position to state whether the magma that will first contact the drifts is essentially degassed (lava flow) or gas-rich and, thus, whether it will give rise to pyroclastic flow.

Section 3.3 explores the consequences of the initial interaction between the ascending dike and the repository. On one hand, the thermal stress induced around the repository influences some of the dike characteristics (namely, the length of the tip cavity and the magma pressure gradient beneath the magma front). On the other hand, the drifts act as mass sinks and, in principle, can slow the progression of the dike tip. The discussion in this section distinguishes between the two limiting cases of a slow incompressible lava flow and fast pyroclastic flow.

Section 3.4 analyzes various instances of the dog-leg scenario, concentrating mainly on cases where the magma is diverted from the parent dike to reach the surface via a pre-existing fracture that intersects the repository. A necessary condition for such a scenario to take place is that the pressure of the magma in the drifts must be larger than the normal stress across the pre-existing fracture. Thus, the report focuses on the factors influencing the stress variation across the fractures and the pressure in the drifts, while again distinguishing between the two extreme cases of pyroclastic flow and lava flow. In the case of a lava flow, the dog-leg scenario must overcome the additional obstacle of avoiding thermal death by freezing of the magma during initiation of the secondary dike. In the case of pyroclastic flow, the effect of the large permeability on the Yucca Mountain tuff to limit the gas pressure is considered. The consequences of a plug of frozen magma in the parent dike above the repository are also examined.

A detailed program of recommended modeling tasks is presented in Section 3.5.

3.2 DIKE PROPAGATION PRIOR TO REACHING THE REPOSITORY

3.2.1 Preamble

This section focuses on some important aspects of dike propagation that are most relevant in regard to the scenario of a dike intersecting the repository:

(1) the characteristics (length, width, and pressure) of the “tip cavity” or “magma lag zone” between the dike tip and a well- or poorly-defined magma front; and

(2) the magma pressure gradient and dike thickness behind the magma front.

The importance of these factors is that they control the explosivity of the initial interaction between the dike and the proposed repository. The location of the dike tip when magma first reaches the repository may also affect dike/repository interaction on longer time scales.

First, we summarize basic results that are predicted by classical dike propagation models, which are based on the assumption of an incompressible Newtonian fluid, slow viscous flow, impermeable rock, and constant pressure at the magma front. It is shown that the mechanics of dike propagation requires the existence of a tip cavity filled by exsolved gas and vapors at a pressure less than the dike normal stress. The size of the lag between the magma front and the tip could vary between a few meters to hundreds of meters depending on the difference between the far-field normal stress and the gas pressure. It is shown that the particular conditions at Yucca Mountain entail that the gas pressure in the tip cavity is low (possibly close to atmospheric), with the implication that the conditions at the magma front may be exceedingly complex. Such a situation cannot be analyzed in the context of classic models and we then discuss some of work carried out by the Panel to account for the additional physics of gas leakage from the tip cavity into the host, unsteady flow of compressible magma, flow of gas across the "magma front," nature of the magma flow, and magma fragmentation. Finally, brief mention is made of other factors related to dike propagation that might affect the TSPA, such as the expected lateral extent of vertically propagating dikes.

3.2.2 Mechanics of a Rising Dike (Incompressible Flow)

3.2.2.1 Classical Models

Many aspects of dike ascent from the mantle to the surface are inaccessible to direct observation and must be deduced from continuum mechanical models. These models generally treat the host rock as linear elastic and the magma as incompressible and linear viscous (Lister and Kerr, 1991; Rubin, 1995b). Under these conditions, a Poiseuille flow or lubrication approximation, in which the fluid pressure is taken to be uniform across the dike thickness, is appropriate. A minimum necessary additional ingredient is a rock fracture criterion, which incorporates the energy requirement, largely dissipative, for creating new fracture surfaces. Because of the difficulty of coupling the fluid flow to the solid deformation while simultaneously satisfying a fracture criterion, most models are planar and couple unidirectional (1D) magma flow with equations for two-dimensional (2D) elastic deformation of the crack walls. A comprehensive review of current knowledge about the mechanics of dike propagation is summarized in a supporting document (Rubin, 2003).

Essential ingredients of the dike propagation problem are summarized in Figure 3-1, which shows a sketch of the near-tip region of an ascending dike intruding into host rock with an elastic modulus $E' \equiv E/(1-\nu^2)$, where E is Young's modulus and ν is Poisson's ratio. This near-tip region is characterized by the presence of gas-filled tip cavity of length λ separating the magma front from the dike tip. The dike plane is subjected to an

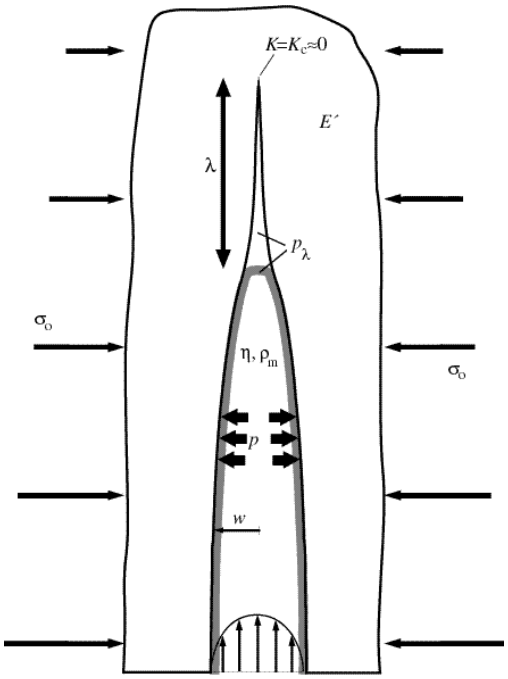

Figure 3-1 Cartoon depiction of a "classical" mechanical model of a vertically-propagating dike

ambient normal stress, σ_o, which generally increases with depth. (Note that, in general, we assume that σ_o corresponds to the minimum horizontal in-situ stress S_h mentioned in Chapter 2, although the value of S_h may differ from that listed in Table 1-2 with the addition of thermal or other stresses.) A pressure, $p_\lambda < \sigma_o$, acts within the tip cavity and is continuous with the magma pressure at the magma front. Within the framework of classical dike models, the tip cavity pressure, p_λ, is constant and either is prescribed using ad hoc considerations or computed using extraneous information.

Magma with viscosity η and density ρ_m is injected with a specified pressure or flux history at depth, which is generally chosen to be slowly varying on the timescale of magma flow from the source to the propagating tip.

It is generally assumed that rock fracture properties can be encapsulated into the toughness, K_c (taken to be a material parameter related to the energy dissipated per unit length of new fracture surfaces), with the corollary that the fracture propagation criterion can be expressed as $K = K_c$, where K is the stress intensity factor due to the stress loading on the dike. However, analysis of dike propagation models suggests that the rock fracture properties may be neglected, even for toughness values more than an order of magnitude larger than those determined in the laboratory. Hence, in largely elastic rock (i.e., where dike propagation is not hindered by large-scale faulting), the propagation criterion can be simplified to $K = 0$.

Given these parameters and within the assumptions outlined above, models of propagating dikes can be used to compute the magma pressure, p, and dike aperture, w, as func

tions of position and time, as well as the location of the magma front and dike tip as functions of time. An example of a dike propagation calculation illustrating the distribution of dike aperture w and excess pressure $\Delta p = p - \sigma_o$ at two different times is shown in Figure 3-2. (w is directly related to the distribution of Δp.) It can be seen that the cavity length increases with ascent of the dike and that most of the drop in Δp near the magma front occurs on a length scale comparable to the cavity length.

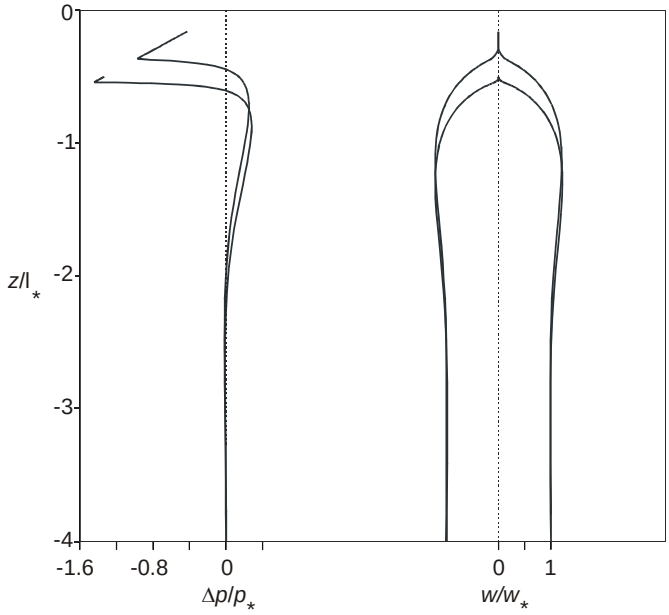

Figure 3-2 ***Example of Dike Propagation Calculation (incompressible flow)***: This figure shows the profile of the dike excess pressure, Δp, and aperture, w, as functions of depth z computed at two different times for a zero tip cavity pressure. The calculations are based on the assumption of plane strain and take into account the influence of the free-surface. The results are expressed in dimensionless form, as all the quantities are scaled by their respective characteristic values, p_*, w_*, and l_*; see Appendix 3.3. (For example, a plausible set for the characteristic quantities are, $p_* \approx 2.6$ MPa, $w_* \approx 0.15$ m, and $l_* \approx 575$ m.) The results shown in this figure pertain to the dike tip located at a depth of 0.5 (288 m) and 0.16 (91 m), with the shallow position corresponding to the onset of unstable propagation. Between the first position shown and the onset of instability, the tip cavity size has grown from 0.042 (24 m) to 0.209 (120 m). Note that the increase of pressure from the zero tip pressure at the magma front to the magnitude of the dike normal stress takes place over a distance comparable to the lag size.

3.2.2.2 Tip Cavity Length

The tip cavity, or magma lag zone at the tip of a dike propagating in largely elastic rock (Figure 3-1), arises as a consequence of the large pressure drop required to force a viscous fluid through a slot of ever-decreasing thickness (Barenblatt, 1962; Lister, 1990; Rubin, 1993; Garagash and Detournay, 2000). This region may be filled at some low pressure by either pore fluids infiltrating from the adjacent host rock or by volatiles exsolving from the magma. Beneath Yucca Mountain, the water table is about 300 m be

low the proposed repository, and the likely magma is H_2O-rich, so we expect the lag zone in the vicinity of the proposed repository to be filled by H_2O vapor. Because the viscosity and density of this vapor is very low, the pressure within the lag zone is (still within the framework of classical models) approximated as constant. For a rock fracture toughness comparable to laboratory values and even up to 1 to 2 orders of magnitude larger, the pressure, p_λ, within the lag zone must be less than the dike-normal stress if the dike tip is to propagate at less than elastic wave speeds (Lister and Kerr, 1991). Furthermore, as is discussed below and in Appendix 3.1, the length, λ, of the tip cavity is of direct relevance to the assessment of the igneous consequences at the proposed YMR. Perhaps most importantly, as is shown below, there exist plausible conditions at Yucca Mountain for which the dike daylights at the ground surface before the magma front reaches the repository depth, thus greatly reducing the possibility of a dog-leg scenario. Solutions of propagating dike models show that the lag length increases as the under-pressure, $\sigma_o - p_\lambda$, within the lag zone decreases in order to satisfy the fracture propagation criterion at the dike tip. With p_λ constant and σ_o increasing with depth, these solutions indicate that the lag length increases with ascent of the dike. For example, under the simplifying assumptions that λ is small compared to other relevant length scales (in particular, so that $\sigma_o - p_\lambda$ does not vary significantly over the cavity height), the rock toughness is negligible, and the effect of the free surface small, λ is given by (Garagash and Detournay, 2000):

$$\lambda \approx \frac{4\eta V E'^2}{\left(\sigma_o - p_\lambda\right)^3} \qquad (3\text{-}1)$$

This expression yields a cavity length of $\lambda \sim 200$ m for $\eta = 10$ Pa s, $E' = 10^4$ MPa, $\sigma_o = 3$ MPa, $p_\lambda = 0$, and a tip ascent velocity $V = 1$ m/s, which are within the range of plausible estimates of the relevant parameters for the proposed YMR site. The dike aperture at the magma front is about 0.15 m for the same parameters. However, for this model, the lag would be reduced to less than 20 m if $\sigma_o = 10$ MPa, a value which reflects the peak horizontal thermal stress in the current design scenario. It is worthwhile to emphasize that the inference that the cavity pressure is essentially atmospheric results in a conservative (i.e., minimum) tip cavity length.

Improved estimates of the cavity length λ can be computed with analytical or numerical models including additional physics. For example, Figure 3-3 shows the evolution with time of the magma front, dike tip and lag, computed with a two-dimensional model that takes into account a linear increase of the horizontal stress with depth and the presence of the free surface. This plot clearly shows that the tip becomes unstable when the tip depth is at about 90 m and the magma depth at about 210 m (corresponding to a cavity length of 120 m) for a length scale $l_* \approx 575$ m. (The length scale l_* is a function of several parameters, among them the magma viscosity and density; see Appendix 3.3). Physically, this length scale corresponds to the vertical distance over which the dike excess pressure is substantially larger than that in the dike "tail" at great depth, or, equivalently, the distance over which the pressure gradient for vertical flow deviates significantly from

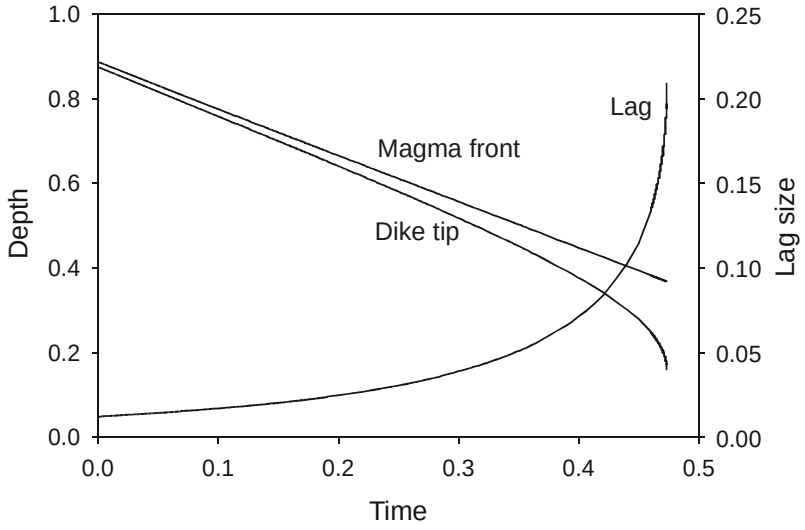

Figure 3-3 ***Example of Dike Propagation Calculation (incompressible flow)***: This figure shows the evolution of the lag size, the depth of the magma front and the depth of the dike tip as a function of time. The calculations are based on the assumption of plane strain and take into account the influence of the free surface. The results are expressed in dimensionless form, with the lag size and depth scaled by the length scale l_*; see Appendix 3.3. (As in Figure 3.2, $l_* \approx 575$ m is a plausible value.) The results show that the velocity of the magma front remains virtually constant and equal to the magma velocity at the source. The calculations stop at the point of instability already discussed in Figures 3.2.

$\Delta\rho g$. This instability is preceded by a gradual increase of the tip velocity compared to the magma front velocity, the latter of which remains virtually constant.

This instability of the crack tip may be rationalized by an approximate analytical solution discussed in Appendix 3.2. This model suggests that the dike tip will become unstable when the under-pressure at the tip is 1/2 that at the magma front. In the context of Yucca Mountain, this implies that the dike tip might become unstable when its depth is ~ 1/2 that of the magma front if the instability takes place when the tip cavity is mainly in the unsaturated rock horizon, as the lag pressure, p_{λ}, is then likely to be near atmospheric. Thus, in the absence of large-scale inelastic deformation, it seems entirely plausible that the dike tip could reach the surface before magma reached drifts at a depth of 200 m to 300 m. (Length scales l_* larger than 575 m, as seem appropriate for analog dikes, yield instability at correspondingly greater depths than shown in Figure 3-3.) If, on the other hand, thermal stresses increased the dike-normal stress at repository depths to 10 MPa, reasonable lag lengths might be only a few meters, according to models where the dike normal stress increases linearly with depth.

Thus, a full spectrum of atmospheric-pressure lag lengths at repository depths, from less than 10 m to hundreds of meters, seems possible. The associated range of apertures at the

magma front varies from < 1% to > 20% of the maximum dike thickness. These ranges should be considered in models of dike/drift interaction.

3.2.2.3 Pressure in the Tip Cavity

The pressure, p_λ, of the vapors in the tip cavity is intimately linked to the cavity length, λ. For example, dike propagation models show that λ is inversely proportional to $(\sigma_o - p_\lambda)^3$ for a given ascent velocity, V, under the restrictive assumptions of a small λ (Garagash and Detournay, 2000). Furthermore, the gap between the tip and the magma front is the first part of the dike to intersect the repository; thus, the magnitude of the tip pressure, p_λ, determines the passivity or the degree of violence of this initial interaction.

In principle, both the lag length and the lag pressure must be computed simultaneously from dike models that have been enriched, compared to the bare-bones model presented earlier, with the minimum additional physics of two-phase flow (gas and melt) in a region below the magma front and bleed-off of gas or vapors to the host rock. Below we outline a simple mass-balance approach to estimating the pressure in the cavity, described more fully in Appendix 3.1, that also serves to motivate the compressible dike flow models described in the following section.

Gas Influx — Because of the no-slip boundary condition at the dike wall, magma at the dike center moves faster than the magma front. This magma is free to supply some or all of its bubble content to the cavity as it reaches the magma front, turns toward the wall, and becomes part of the (partially or fully degassed) "return" flow ("return" in the moving reference frame of the magma front). The gas volume fraction of the magma supplying the tip cavity depends upon the pressure at the magma front. A simple working hypothesis is that, at least under near-equilibrium conditions, this pressure is essentially fixed by the gas volume fraction at which gas escapes into the cavity. Provisionally, we assume that this is the pressure corresponding to a gas volume fraction of ~70% (roughly 10 MPa for 2.5 wt % water), as this is typically assumed to be the gas volume fraction at which magma fragments (Chapter 2).

Gas Outflux — The large intrinsic permeability of the proposed repository host rocks, 10^{-12} m^2 to 10^{-13} m^2, ensures that above the water table at about 600 m depth outgassing of the tip cavity is very efficient. Assuming quasi-steady propagation in which the magma front moves at more-or-less the magma flow velocity behind the magma front, the permeability is too high by orders of magnitude to maintain pressures approaching 10 MPa. This result led to the statement in the Panel's Interim Report that the pressure in the cavity would be near-atmospheric.

The simple imbalance identified in the above two paragraphs (that the pressure allowed by the permeable host rock is far below that at which the magma would fragment) guarantees both that the region of the magma front is exceedingly complex and that classical models of dike propagation are inadequate to assess this complexity. This result motivated the compressible flow models described below.

3.2.3 Mechanics of a Rising Dike (Compressible Flow)

The expected presence of dissolved volatiles (mainly H_2O and CO_2) in the Yucca Mountain magma (see Chapter 2) invalidates some of the assumptions on which classical dike models are based — namely, (1) incompressible flow, and (2) the existence of a "simple" magma front separating a pseudo single-phase fluid from a gas.

Magma (liquid plus gas) compressibility, in principle, can be accommodated in a relatively straightforward manner by modifying the continuity equation and by adding an equation of state that expresses magma density as a function of pressure (Appendix 3.3). Variable viscosity (for example, as functions of both bubble fraction and strain rate; see Chapter 2) adds some complexity, but it can be taken into account as well. Non-equilibrium conditions (e.g., differences between the pressure inside a bubble and the normal stress exerted by the magma on the dike walls) also play a role, but are probably a second-order effect for dike calculations involving basaltic magma.

The primary difficulty in constructing a proper model to account for the presence of dissolved volatiles in the magma stems from the current uncertainty about the exact nature of the magma front. It is usual in eruptive flow calculations to assume that the flow fragments at a fixed bubble fraction (e.g., ~70%), but this fragmentation condition is not by itself sufficient to solve for the flow near the magma front. Based on the mass balance considerations discussed in the preceding section, we envision two scenarios.

1. At considerable depth, where the ambient dike-normal stress far exceeds the pressure corresponding to the assumed bubble fraction at the magma front (e.g., ~10 MPa for 70%), growth of the cavity is slow. Because the host rock is water-saturated and relatively impermeable, this growth can easily be fed by a small gas fraction crossing the magma front into the cavity; and most of the gas remains in the "return flow" (for more details, see Appendix 3.3). Because the pressure in the cavity equals that at the magma front, decompression of the basalt approaching the magma front is not explosive and nearly all the magma joins the return flow. This scenario actually corresponds quite closely to "classical" dike models in that there is a well-defined magma front and a gas-dominated cavity. It differs in that it includes compressible flow, and in that the velocity of the magma front is less than the average flow velocity just behind the magma front (to compensate for gas loss into the cavity).
2. Once the pressure in the tip cavity drops below the fragmentation pressure, either because the dike tip has started to go unstable or because a stable tip approaches the water table and diffusive gas loss is easy, decompression becomes potentially explosive. In more typical conduit-flow calculations, the fragmentation pressure marks the transition from liquid-dominated flow below to gas-dominated flow above. This might be the appropriate model for the case of an unstable dike tip. For a

> stable tip with diffusive gas loss, however, the story is much more complex. Instead of rapidly leaving the system, the magma fragments carried by the gas remain behind to clog the cavity and continue exsolving gases. One could imagine a very complex region in which a separate gas phase downstream of the fragmentation front attempts to tunnel through this magma-clogged region and out through the dike walls, all the while being constrained by the narrow dike thickness that is influenced significantly by the local pressure distribution. Depending on the degree of clogging, the magma fragmentation front might remain at a relatively fixed depth or continue following the tip. In either case the flow velocity behind the fragmentation front greatly exceeds the velocity of the magma front.

Despite the lack of any comprehensive model for dealing with scenario 2 above, it is possible to construct one qualitative image of the different flow regimes that would develop in an ascending dike and thus examine plausible consequences of the presence of dissolved volatiles for the characteristics of the tip cavity, under some simplifying assumptions. Consider the situation when the tip is at a depth below the repository but above the water table, in which outgassing is easy. Four main regions can be identified with decreasing depth; these are described below.

I. An incompressible flow region, below a depth estimated to be greater than 10 km (In this region, the bubble fraction is virtually zero.)

II. A homogeneous compressible flow region characterized by an increasing bubble fraction with decreasing depth and the same (average) velocity for the bubble and the fluid

III. A multiphase compressible flow region below the fragmentation depth. In this region, the gas and the liquid phases ascend at different speeds with the liquid phase still continuous.

IV. A complex flow region between the fragmentation front and the dike tip, where the gas phase becomes continuous.

Regions I-III are also applicable to scenario (1) above, while region IV pertains to (2) alone. Based on the above discussion, some prescriptions that account approximately for the nature of the magma front under scenario (2) are given in Appendix 3.3, and in more detail in a supporting document (Detournay and Savitski, 2003). The two models considered neglect region III (on the assumption that it is very short) and any dynamic flow regime in region IV. One model is based on identifying the magma front with the fragmentation front, at the expense of having a time-varying pressure and critical bubble fraction at the front. Another model is constructed on the assumption that the magma completely degasses in region IV, over a distance small compared to the length of this region, so that the fragmentation front can be viewed as a separating magma at the critical

bubble volume fraction, θ_c, from pure melt (i.e., there is a "magma front" closer to the tip than the "fragmentation front"). Some results obtained with these two models are shown in Figures 3-4 and 3-5.

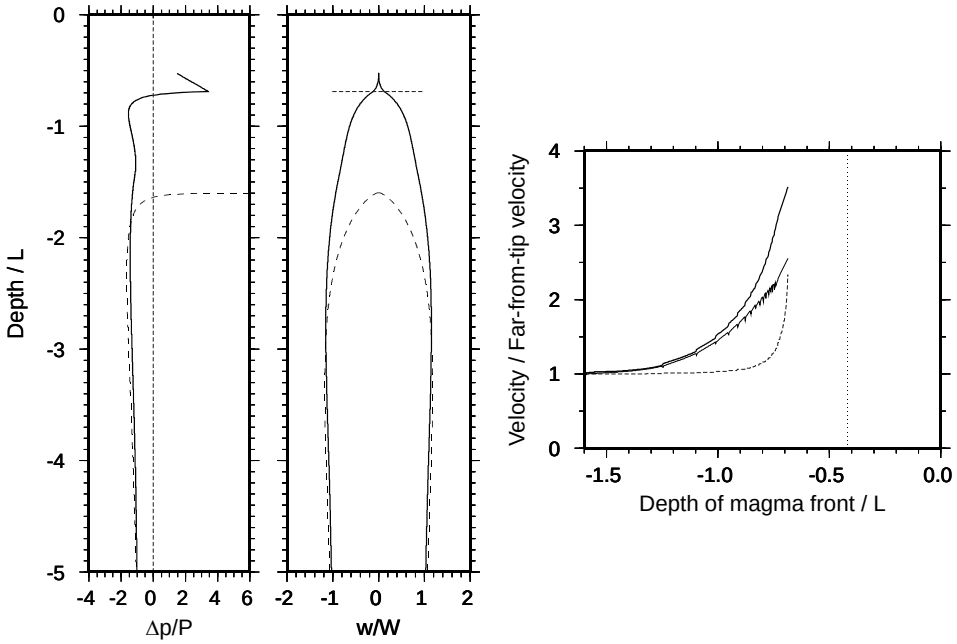

Figure 3-4 ***Example of Dike Propagation Calculation (compressible flow — Model 1)***: In the left panels, the dike excess pressure, Δp, and thickness, w, as functions of depth, are shown at two different times (dimensionless results are shown; to scale to YMR set the length scale L [the dike half-length in horizontal section], to 2 km, and the pressure and thickness scales P and W [the excess pressure and dike half-thickness at great depth] to 2 MPa and ~1 m, respectively. Dashed curves show a deeper dike, such that the tip cavity (length ~ 2 m) is not resolved. Solid curves show the last position of the dike before the tip propagates unstably. In the right panel, the average flow velocity at the magma front (top curve; solid) and the velocity of the magma front (middle curve, solid) are shown as functions of depth. (The curves are "jittery" because the cavity lengthens by discrete 10 m jumps.) The curves become smooth as the tip pressure drops to feed the more rapidly growing cavity (see text for discussion). The bottom curve (dashed) shows the ratio of the underpressure at the magma front to the underpressure at the dike tip, and shows rough agreement with the analytical estimate that the tip should go unstable when this ratio is ~ 2. The vertical dashed line to right shows the depth at which the host rock stress equals the initial magma front pressure of 10 MPa. The mechanical influence of the free surface is neglected. Note that the sign convention for the excess pressure is reversed from that of Figures 3-2 and 3-5.

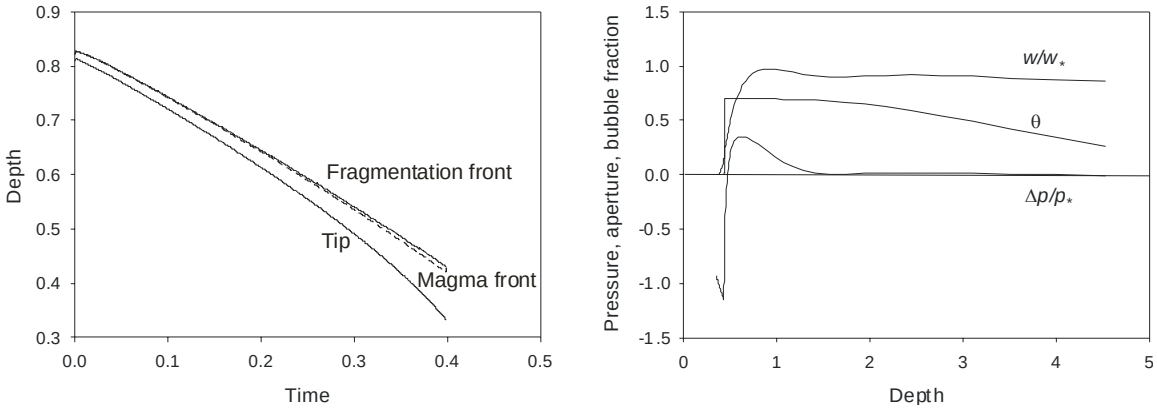

Figure 3-5 ***Example of Dike Propagation Calculation (compressible flow — Model 2)*** : This figure shows, on the left panel, the evolution with time of the depth of the fragmentation front, magma front and dike tip; the right panel shows the profile of the dike excess pressure, Δp, and aperture, w, and bubble volume fraction, θ, at a particular time. The calculations take into account the influence of the free surface and assume the presence of a pure melt region that separates the tip cavity (here at zero pressure) from the fragmentation front. The results are expressed in dimensionless form, as all the quantities are scaled by their respective characteristic values, p_*, w_*, and l_* ; see Appendix 3.3. The left panel shows a gradual increase of the pure melt region, as well as increasing velocity of the magma front and the fragmentation front with time. The right panel shows the jump of the bubble volume fraction, θ, at the fragmentation front from the critical value of 70% to zero in the pure melt region. Also, the bubble fraction progressively decreases with depth. The small pure melt region between the magma front (corresponding to the point of minimum net pressure) and the fragmentation is characterized by a discernible change in the pressure gradient.

In Figure 3.4, distances are scaled by the dike half-length L, which can be taken to be 2 km to scale appropriately to analog dikes. During most of dike ascent the magma front corresponds to a fixed pressure and bubble fraction (10 MPa and 73%, respectively). No gas leak-off into the host rock is assumed, as the tip cavity is located beneath the water table. Eventually, as instability is approached and the cavity volume begins to grow too fast, the pressure at the magma front drops so as to satisfy gas mass balance; this process is assumed to be "nonexplosive" (Appendix 3.3, Section 4.7). The pressure drop occurs over about the last 200 m of ascent of the magma front prior to dike-tip instability. At instability the magma front is at about 1400 m depth and the dike tip at just under 1100 m depth. Note that although the pressure is dropping, it reaches only to 9.7 MPa (the bubble fraction increases only from 73% to 73.9%) before instability occurs. Instability occurs even with a pressure drop because the cavity volume is actually growing quite slowly; in other words, the small pressure drop required to satisfy mass balance is insufficient to suppress the elastic instability. Computing the subsequent evolution of the system would require inertial terms in the fluid flow and possibly elastodynamics in the solid. Most likely, the pressure would drop sufficiently (due to cavity expansion or gas diffusion above the water table) to stabilize the tip before it reached the surface.

Two significant differences between the classical dike models and those portrayed in Figures 3-4 and 3-5 are the substantial increase of the flow velocity at the magma front and the amount by which this exceeds the velocity of the magma front. Both effects in

crease the gas flux into the cavity relative to the flux out, and this will increase the pressure that can be maintained in the cavity. Quasi-steady calculations outlined in Appendix 3.1 suggest that pressures exceeding 1 MPa are achievable under certain conditions. However, these calculations neglect the fact that the drift permeability on the scale of 10 m and at pressures exceeding 1 MPa are likely to be considerably larger than 10^{-12}.

If the permeability is low enough to permit gas pressures of a few MPa under quasi-static conditions, then the process limiting the cavity pressure becomes not only diffusion out through the dike wall but unstable propagation of the tip. The calculations described in this section show that cavity pressures below the dike-normal stress (lower by an amount that exceeds the dike excess pressure, so perhaps a few MPa), the tip becomes unstable. As instability proceeds, the cavity pressure would be expected to drop owing to both (1) the increasing cavity volume and (2) the opening of "fresh" dike walls for gas diffusion.

3.2.4 The Tip Cavity in the Presence of Inelastic Deformation

In the tectonic environment of the proposed YMR, and in the absence of large horizontal thermal stresses, dike intrusion is virtually certain to be accompanied by significant slip along existing faults (see Rubin, 2003). Such fault slip can reduce the tip cavity length in two ways. First, normal fault slip that occurs tens to hundreds of meters from the cavity will increase the horizontal compressive stress acting to close the cavity. These stresses might plausibly reach a few MPa and can be accounted for in existing dike propagation models simply by increasing the ambient stress in the appropriate depth range. Second, fault slip that cuts only one wall of the cavity can "shut down" the cavity at shallower depth, possibly until that piece of the fault is abutted by magma. At this point, propagation could locally halt, or proceed either up along the fault or the continuation of the dike plane.

The outcome of most significance to the TSPA would be that propagation would halt between the repository and the surface, as this could channel more flow into the drifts and increase the probability of a dog-leg eruption. Evaluating the probability that propagation will halt locally is difficult. This is observed quite frequently where dikes cut cinder cones, but this typically happens under conditions of very low confining pressure in incompetent material, and the dike might already be near the limit imposed by its head. At depths of hundreds of meters in eroded drift zones along the coasts of Iceland, where near-vertical exposure of dikes are very common, it has been observed only extremely rarely (Gudmundsson, 1983). Large horizontal thermal stresses will reduce the chance of occurrence at repository depth, but not at somewhat shallower depth. For purposes of the TSPA, this possibility can be added to that short list of scenarios by which flow up the parent dike would halt at a shallower depth than the repository (e.g., in addition to magma freezing after the drifts siphon some of the flow; see Section 3.4).

3.2.5 Magma Freezing

Adding magma freezing to numerical models that couple viscous flow, elastic deformation, and crack propagation during dike intrusion is a difficult proposition that has been carried out only incompletely to date (e.g., Delaney and Pollard, 1980; Bruce and Huppert, 1990; Rubin, 1995b; Lister, 1994; Lister and Dellar, 1996; Fialko and Rubin, 1998). Nonetheless, observations indicate that freezing plays a crucial role in governing the course of the first few hours to days of a dike-fed eruption. In this section, we briefly summarize aspects of this role that are important for assessing potential igneous events at Yucca Mountain. More details are provided in Appendix 3.4 (which also covers topics relevant to other scenarios discussed later in this Chapter).

When dikes in Hawaii, Iceland, or Mt. Etna breach the surface, they produce "curtain-of-fire" eruptions that typically localize to one or a few quasi-cylindrical conduits ("plugs") in a matter of hours to days. This time is generally consistent with the estimated conductive cooling time of dikes with thicknesses of the order of 1 m. The short end of this time range is also small compared to propagation times from the source, indicating that freezing has become important long before eruption begins.

The details of the localization process are poorly understood. Based on observations of eroded dikes and associated plugs on the Colorado Plateau, Delaney and Pollard (1981) inferred that mechanical brecciation and erosion of the dike wall rock is responsible, often initiating at overlapping dike segments with small offsets. Note that brecciation mechanisms might be different for gas-charged basaltic eruptions. As extreme examples, kimberlites and diatremes form plugs apparently in advance of the propagating dike (or at least in advance of the propagating magma front — if not the propagating crack tip). It has also been suggested that thermal instabilities are responsible (Bruce and Huppert, 1990), whereby locally thicker regions of the dike capture more of the flow and become more resistant to freezing. However, preliminary numerical work (summarized in Lister and Dellar, 1996) suggests that this mechanism might be ineffective.

Whatever the source of the instability, it is clear that once the dike locally widens sufficiently, the growing conduit often captures enough of the flow that the increased advective transport of heat first slows and later reverses growth of the chilled margin. Once this meltback occurs, in a practical sense the duration of the eruption is limited not by freezing but by the availability of magma from the source. A recent example of this is the ongoing eruption of the vent Pu'u O'o at Kilauea, which grew from a dike intruded in January 1983.

Relevant lessons from the above include the following. First, because most of the dike shuts down quite quickly, the average eruption rate during the course of an extended eruption can be orders of magnitude less than that might be implied by first glance at a dike propagation calculation of the sort described in this chapter (e.g., a 1 km by 1 m dike flowing at 1 m/s would produce an erupted volume 1 km^3 in 10 days). Second, if the part of the dike that freezes includes the portions that intersected the drifts, there will be no

mass flux between the two after the first hours to days of an eruption. Because dike/drift intersections are regions where mechanical erosion of the host rock may be favored, it is reasonable and conservative to assume that dike/drift intersections become part of the conduit system; however, this is not guaranteed. Third, a mechanism for enhancing freezing that is relevant to a potential igneous event at Yucca Mountain but not (to the same extent) at Hawaii, Iceland, or Etna is the increase in magma solidus temperature upon devolatilization (Chapter 2). While this devolatilization is expected to occur at all depths near the propagating dike tip, it may be more effective in shutting down the dike at shallow depth where low pressures develop over an increasingly large region behind the tip. Because of the inherent variability of volcanic eruptions and the small number of analog (high water content) basaltic eruptions observed, it difficult to assess the full range of behaviors that such freezing might lead to. However, partial freezing of the parent dike prior the eruption of Parícutin might have been instrumental in setting the tone of the onset of that eruption (see Appendix 3.4 for further discussion).

3.2.6 Lateral Extent of Rising Dikes

As is discussed in one of the supplementary documents (Rubin, 2003), no existing model can explain how dikes emanating from a deep crust or mantle source have strike lengths of only 4 km near the surface. Either the approximations used by the models lead to significant error, or phenomena not considered in the models (such as vesiculation or, if the leading edge of the dike has a small enough radius of curvature, a pressure reduction upon eruption) cause the lateral extent to decrease with height near the surface. Limited observations suggest that the lateral extent of mantle-derived dikes does decrease upward in the depth range of 0.5 km to 1.5 km (Delaney and Gartner, 1997). The choice for the TSPA is whether to base the probable distribution of dike lengths on the observed distribution or to use greater lengths that would be more in keeping with existing models. Given that plausible mechanisms exist for limiting the lateral extent near the surface, that this is consistent with observations and that observations have been made at erosional depths of hundreds of meters, it is reasonable to assume a length distribution based on the observations alone. This distribution should not be weighted heavily toward the observed lengths of eruptive fissures or cinder cone arrays, however, as these may be reasonably expected to underestimate the extent of the dike at depths of hundreds of meters.

3.3 INTERACTION BETWEEN THE DIKE AND THE REPOSITORY

3.3.1 Preamble

The presence of drifts at atmospheric pressure can influence dike propagation and the flow of magmatic material in the following ways.

- The drifts can locally increase the ambient compressive stress acting normal to the dike plane (by tunneling or by thermally induced stresses).
- The drifts can locally alter the principal stress directions. For example, thermal stresses might make the least compressive stress vertical and thus promote sill formation. Alternatively, if the drifts and dike are not orthogonal, local rotation of the horizontal principal stresses might cause the dike to break down into overlapping en-echelon segments that intersect a drift a short distance from one another.
- The drifts can act as mass "sinks", spaced about 80 m apart (for an orthogonal dike), that suck off magma or pyroclastic material that otherwise would have been available to pressurize and promote continued propagation of the parent dike.
- The drifts can act as corridors for magma or pyroclastic material that flows down the drifts for hundreds of meters before finding a new pathway to the surface (the "dog-leg" scenario).

Section 3.3 discusses the first three of these potential interactions in turn. We emphasize events and processes that occur shortly before and after intersection, as they are most critical. Discussion of the "dog-leg" scenario is deferred to Section 3.4, and this discussion includes some potential longer-term processes as well.

3.3.2 Influence of the Repository on Dike Propagation

As was discussed in Section 3.2, the length of the dike-tip cavity at the depth of the proposed repository might vary from values of the order of 100 m for a robust dike and stress fields similar to those of today (assuming largely elastic deformation of the host rock) to a few meters for a thinner dike in the presence of thermal stresses near 10 MPa. This difference profoundly affects the initial dike/drift interaction, as will be discussed more fully in Section 3.3.3. Numerical models of time-dependent planar dike propagation could be modified to account for spatial variation in the dike-normal stress with little difficulty.

The implications of a change in the principal stress directions near the repository are significantly more complex than changes in principal stress magnitudes. For discussion purposes, it is convenient to decompose this stress perturbation into a mechanical and a thermomechanical component.

The mechanical perturbation is essentially time-independent (assuming that the rock does not have any "viscosity") and is limited to a cylindrical zone around each drift, having a thickness of about 5 m (i.e., about twice the radius of the tunnel). Assuming that the rock is elastic and the dike orthogonal to the drifts, the stress perturbation perpendicular to the dike plane decays as the inverse of the square of the distance from the tunnel axis from a maximum (minimum) of about 2 MPa at the drift wall. In view of the localized nature of this stress perturbation, and also taking into account that the distance between the axes of two adjacent drifts is about 80 m, we can conclude that propagation of the dike will hardly be affected by the mechanical stress perturbation induced by the repository.

The thermomechanical perturbation is time-dependent, both in magnitude and extent. Calculations of the temperature and stress changes due to thermal loading are summarized by Barr (2000) and by Elsworth (2001). Such predictions are reliable because of the relatively small range of variation of the thermal properties among rocks (expansivity, conductivity, heat capacity, and diffusivity) and the well-defined boundary conditions for this class of problems.

During the first few years following the closure of the repository, the thermal stress induced around each drift is unaffected by the heat generated in the other drifts. The maximum compressive stress change takes place at the tunnel wall and is of the order of a few MPa. The perturbation decays with distance from the drift, and the zone of influence increases with time (initially as the square root of time, and later more slowly). After a period of about 100 years, the temperature between the drifts becomes more uniform, as thermal interaction between the drifts has taken place. The thermal stresses induced around the repository become progressively more consistent with those that would have been generated by a uniformly distributed heat source across the footprint of the repository. In the "hot" design scenario, the thermal perturbation is large enough to cause a rotation of the principal stresses in the repository region over a period of about 2000 years (i.e., the minimum horizontal stresses becomes greater than the vertical stress and could reach nearly 10 MPa, an increase of about 6 MPa over the initial value). After this period, the repository will progressively cool down, with the thermal stresses essentially vanishing after about 100,000 years.

The stress barrier that develops around a hot repository during the intermediate period spanning the first 2000 years could cause the dike to be deflected so as to avoid crossing of the repository, promote the creation of a sill, or halt propagation of the tip approaching the repository if the dike is centered a few kilometers north or south. Such protection is time-limited, however; it is therefore conservative to assume that the dike would propagate vertically under all circumstances and would intersect the repository. The major impact of the thermal perturbation would be to reduce significantly the size of the tip cavity ahead of the magma front and perhaps to increase the magma pressure gradient behind the magma front.

3.3.3 Mass Flux into the Repository

Once the dike intersects the drifts, magmatic material will flow into them. This flow can take the form of pyroclastic material and/or magma. Evaluating the detailed evolution of such flows would require complex models, necessarily highly idealized, that couple elastic widening and narrowing of the dike, propagation of the dike tip, flow (possibly dynamic) of a compressible liquid/gas mixture in both the dike and drift, gas diffusion from the drifts into the host rock, and the possible mechanical erosion of rock near the dike/drift intersection. We present here a simplified view of the processes that are likely to occur as a prelude to suggestions for calculations that appear to be feasible on a short to medium term.

3.3.3.1 Progression of Dike Tip

As was discussed in Section 3.2, a cavity filled with gas or a gas/particulate mixture exists at the tip of the dike. At repository depths, this cavity is expected to be at low (perhaps near-atmospheric) pressure because of the large permeability of the host rock. If a near-atmospheric cavity is tens of meters long or more, the drifts will be nearly invisible to the dike; until magma intersects the drifts, the dike tip will continue propagating as if the drifts were not present. If, on the other hand, the tip cavity is a few meters or less in length (e.g., due to large thermal stresses), magma that just moments earlier was at a pressure of a few MPa may approach the drifts before the dike tip propagates beyond the drifts. Mass flux into the drifts then might prevent the dike tip near the drifts from propagating for some time (although the tip might continue to ascend between adjacent drifts).

If the tip cavity pressure is modestly in excess of atmospheric, the story changes only slightly. Once the cavity intersects a drift, the pressure quickly drops to atmospheric (at least locally) while leaving the drift pressure essentially unchanged (because the drift volume greatly exceeds the cavity volume). A uniform pressure reduction within the cavity would cause the cavity to thin elastically and the dike walls near the tip to close. An initial move in this direction, however, would restrict further gas flow into the drift and prevent an "instantaneous" pressure drop (one that traveled at the gas/particulate sound speed). The result is that the tip would approximately stabilize as the moving magma front reduced the cavity length to its atmospheric-pressure value, at which point the tip would continue propagating in the manner outlined in the above paragraph.

3.3.3.2 Pyroclastic Flow

Because the drifts are initially at atmospheric pressure, magmatic material is likely to first enter the drifts as a pyroclastic flow as a result of gas exsolution and expansion. One version of this scenario was considered by Woods et al. (2002), who investigated the consequences of an explosive decompression of magma leading to significant shock waves when the dike reaches the drift. The development of a shock wave, however, is critically

dependent on the assumed initial and boundary conditions. In Woods et al. (2002), the magma erupts into the drift by suddenly depressurizing from an initial pressure of 10 MPa and is fed by a dike 1 m wide; however, these initial and boundary conditions are deemed to be completely unrealistic.

The first portion of the dike to intersect the drifts is the tip cavity, which is expected to be at low pressure for reasons detailed before. However, as this pressure is below the fragmentation pressure of the magma, the gas and particle velocities in this region may be quite large. The subsequent rate of increase of the pressure near the dike/drift intersection will be, in large measure, controlled by the magnitude of the horizontal stresses at the repository depth, as can be seen from considering two limiting cases.

- In the presence of large (10 MPa) thermal stresses, the tip cavity is expected to be of the order of meters, the dike aperture at the magma front of order of centimeters, and the magma pressure behind the magma front to increase to the horizontal in-situ stress level over a distance of an order of meters. Under these conditions, the drift may be approached within seconds by magma that quite recently was at pressures exceeding 10 MPa; eruption into the drift may quickly become violent, but will be hampered by the small aperture of the dike.
- If the horizontal stress is a comparable to the present in-situ values of only a few MPa, pressurization of the drift will be slow, as the length of the tip cavity may be of order 100 m.

Some recommendations for the numerical simulations of pyroclastic flows into the drift using computational fluid-mechanics codes are discussed in Section 3.5.

3.3.3.3 Flow of Degassed Magma

The common observation of surface lava flows at analog eruption sites, and poorly vesiculated dikes at repository depths in the surrounding region, makes it virtually certain that, unless the drifts have filled previously with pyroclastic material, magma will at some point enter the drifts as a coherent lava flow. This flow may take the form of partially degassed magma that enters either as gas-accelerated spatter from the dike/drift intersection or by the viscous flow of already degassed magma up the dike. The alternative scenario, whereby the flow takes the form of largely undegassed magma at high pressure following an initial pyroclastic flow, is deemed unlikely in view of the more gradual initial pressurization of the drifts than in the calculation of Woods et al. (2002) and the permeable nature of the repository rocks (see Section 3.4.3.2).

In Appendix 3.5, we examine the case of incompressible magma flowing up a rigid vertical slot (representing the dike), into which are drilled horizontal holes with diameter and spacing appropriate for the drifts. The goal is to obtain a simple analytical estimate of how far above the repository the magma front in the dike might be at the time the drifts fill (height H). The calculations are deficient in that they neglect (1) the changes in dike aperture that would be associated with flow into the drifts (lower pressure and hence re

duced thickness at the dike/drift intersection), (2) magma compressibility, and (3) the full time-dependence of the flow. For this reason these calculations should be superseded by more rigorous 3-D calculations described in Section 3.5. Below, we emphasize what we believe are the most robust conclusions of this simplified analysis.

As might be expected, *H* is very sensitive to the dike thickness. For sufficiently narrow dikes, estimated to be somewhat thinner than 1 m, the magma front is only a small fraction of the distance to the surface by the time the drifts fill. For dikes thicker than about 2 m, however, the magma front might be most of the way or all of the way to the surface by the time the drifts fill. The significance of these results is that once the dike tip breaches the surface the likelihood of a "dog-leg" is greatly reduced, and owing to the tip instability mechanism discussed above, the shallower the magma front the harder it is for the dike tip to remain subsurface. These preliminary results suggest that it is likely that the dike has breached the surface by the time the drifts fill, even if it has not done so by the time the drifts are intersected. For the given dike thicknesses the magma front will extend even higher once elastic narrowing of the dike in the vicinity of the dike/drift intersection is accounted for, but the effect of full time-dependence is more difficult to estimate.

3.4 THE DOG-LEG SCENARIO

3.4.1 Preamble

A scenario of considerable concern involves either magma or pyroclastic material flowing down one or more drifts for considerable distances and entraining waste material before venting to the surface. Owing to the large number of fractures in natural settings, it is reasonable (and conservative) to assume that the last leg of the dog-leg is up an existing fracture.

In order for magmatic material to erupt through a secondary fracture distant from the parent dike, some conditions must be met. First, the pressure must be large enough to overcome the normal stress acting across that fracture. If the flowing material is magma, additional considerations come into play — for example, the secondary dike must be "jump-started" in some way and propagate fast enough to prevent freezing of the magma and, thus, arrest of the crack.

In the following, we limit ourselves to a discussion of the factors controlling the stress state around the drifts, the orientation of secondary dike, the pressure within the drifts and the freezing of the magma in the secondary dike. There are enough arguments arising from this discussion to suggest that a dog-leg scenario is unlikely. The question for the TSPA is whether the product of this small probability and the larger number of waste canisters a dog-leg would impact is small enough, relative to the "standard" scenario, to have only a slight or modest impact.

3.4.2 Stress Considerations

The stress state around the drifts controls not only the magma pressure required to open pre-existing cracks or initiate and propagate fractures from the drift walls, but also the most likely orientation of these fractures. In fractured rock, the magma pressure has to be slightly larger than the stress normal to the crack, and the most likely fracture orientations are those nearly perpendicular to the minimum normal stress. In intact rock, the stress perturbation required to initiate a fracture must exceed the minimum normal stress by an amount equal to the tensile strength of the material.

The factors influencing the stress around the drifts relative to the expected virgin stress at that depth are topography, inherent variability, the geometry of the drifts, thermal loading, the primary dike, dike-induced fault slip, and dike-induced tensile fracturing (see Appendix 3.6 for further details). However, with the exception of thermal stresses, these factors introduce stress variations of 1 MPa to 2 MPa at most. Appendix 3.6 also examines several stress scenarios and their implications for the orientation of the reopened or induced fractures.

3.4.3 Pressure in the Drifts

3.4.3.1 General Considerations

In the typical case that magmatic material in the dike is ascending rather than descending, the pressure within the drift distant from the dike can be no larger than that at the dike/drift intersection. The pressure at the dike/drift intersection, and the pressure drop from that location to a potential dog-leg fracture down drift, depend upon several factors, including whether the parent dike has breached the surface, whether the flow in the drift is a magma flow or a pyroclastic flow, and additional factors that follow from these. These factors are discussed in the following sections.

3.4.3.2 Pyroclastic Flows

Pressure at the Dike-Drift Intersection —

- During dike propagation and before the dike breaches the surface, the pressure in the dike tip cavity must be less than the dike-normal stress (at least a few MPa less in largely elastic rock, based on the calculations presented in Chapter 3, Sections 3.2.2 and 3.2.3) or the tip will propagate unstably (elastodynamically) to the surface. (This statement is independent of any assumption about the permeability of the tip cavity walls; the intrinsic host-rock permeability may ensure pressures much closer to atmospheric). Once this instability begins, it is very doubtful that gas exsolution can maintain pressures approaching the dike-normal stress, because the cavity volume (not to mention the additional volume represented by the drifts) grows so quickly. Thus, such high pressures are expected to be of short duration (less than 1 s).

- After the dike breaches the surface, mass fluxes appropriate for pyroclastic eruptions are such that the flow most likely is choked — that is, the velocity at some constriction is limited by the sound speed at the constriction (Wilson and Head, 1981). Numerical models (e.g., Wilson and Head, 1981; Mastin, 2002) show that pressures upstream of the choked point in such eruptions depend upon the conduit geometry, the frictional pressure loss (related to viscosity) and the density of the erupting mixture. Using Mastin's (2002) model for mass fluxes of 10^5 to 10^6 kg/s, pressures of a few MPa (typically no more than 5 MPa) can be reached at 300 m depth. Above the choke point, the pressure is close to atmospheric, so another relevant concern for the TSPA is the depth of the choke point relative to the repository. This is most sensitive to the conduit geometry and is difficult to estimate; it is conservative to assume that the choke point lies above the repository.
- If the dike or conduit becomes "blocked" at a level above the repository (e.g., by normal faulting into the cavity or by freezing of an earlier batch of magma), pressures exceeding the dike-normal stress are possible (Vulcanian explosions are frequently attributed to formation of such solidified plugs, with gas accumulation below them; Self et al., 1979). In such cases, the relevant question is whether pressures that are large enough to open a potential dog-leg fracture are associated with pressures in the parent dike that are sufficient to "unblock" the obstruction. Such considerations involve several levels of "what ifs" that are discussed more fully in Appendix 3.7. In summary, the Panel considers it most likely that, as the pressure at the dike/drift intersection increases, the obstruction will fail before the dog-leg will open.

Pressure Drop Down Drift — If the drifts are permeable to gas, the pressure at the site of a potential dog-leg fracture distant from the parent dike will be less than that at the dike/drift intersection. In view of the unsaturated conditions of the tuff at the repository level and the large intrinsic permeability of the rock (10^{-12} to 10^{-13} m^2 at the meter scale and presumably larger at the drift scale), only modest pressures are required for gas to diffuse out of the drift as fast as even quite vigorous eruptions into the drift could supply it. Numerical calculations (see Appendix 3.8) of 1-D (radial) isothermal gas diffusion from the drifts into the host rock, using a host permeability of 10^{-12} m^2 and porosity of 10% and assuming 4 weight percent water in the magma, show that the drift pressure reaches less than 2 MPa even for a mass flux into the drift of 10^5 kg/s (at this mass flux the drift fills with pyroclastic material in a few hundred seconds, and in this time the pore pressure has diffused only a small fraction of the drift spacing). Pressures approaching 5 MPa would be reached for mass fluxes of 10^6 kg/s, but at these rates the drift would fill with pyroclastic material in tens of seconds, and this seems a very short time for such a vigorous eruption to develop. In addition, because the permeability is dominated to several orders by a fracture permeability that is very sensitive to gas pressure, at pressures of a few MPa the permeability at the drift scale is likely to be considerably larger than measured in field tests.

A question that could be raised is whether gas escape may be hindered significantly by a decrease in permeability caused by fine pyroclastic material that has entered the host rock

with the diffusing gas. Again, however, because the permeability is dominated by a fracture permeability, this mechanism for "clogging" the host rock is not deemed to be realistic. Condensation of water vapor as it cools in the host rock does not appear to be an effective mechanism for reducing the diffusive mass flux because, at pressures of a few MPa, the increase in viscosity is more than offset by the increase in density. These assertions can presumably be checked by additional calculations, but such computations were not undertaken by the Panel.

3.4.3.3 Magma Flows

Pressure at the Dike/Drift Intersection — The comments here are similar to those above, except that, for flowing magma, there is no equivalent of the choked condition for pyroclastic flows. Prior to venting at the surface, the pressure is limited by roughly the larger of the dike-normal stress or the weight of the overlying column of magma. After venting, the pressure at repository depths is close to the weight of the overlying column. If the vent becomes blocked then higher pressures at the dike/drift intersection are possible, but it seems likely that the blockage would rupture prior to a dog-leg fracture being initiated (Appendix 3.7).

For TSPA purposes, it is necessary to specify the magma volatile content as well as pressure, and the two are in some ways linked. The pressure at the repository level could reach 8 MPa if a column of bubble-free magma extended to the surface, but the gas fraction of such magma must be exceedingly low, implying the same for the magma in the drift if the two batches are similar. On the other hand, if it is assumed that the magma column is at the critical bubble fraction of ~ 70%, then the pressure at the repository level is only ~ 2 MPa, and the equilibrium mass fraction of dissolved volatiles remaining in the magma is only ~ 0.3%. In both cases, the resulting eruption (up the main dike or a dog-leg, if one occurred) would not be highly explosive. More explosive eruptions could ensue if the gas content of the magma below the repository were much higher than that above (e.g., if a fresh batch were somehow to arrive from the source); however, if the vent is open, then the ensuing eruption is much more likely to use that than initiate a dog-leg. A more likely dog-leg scenario involving magma at both high pressure and high volatile content within the drift would be for the main dike or vent to be plugged, but, again, the chance that, as the pressure rises, the plug breaches before a dog-leg forms (Appendix 3.7) seems high.

Pressure Drop Down Drift — Once the drifts fill to the ceiling at the dike/drift intersection, the drift flow may be divided into a filled section and a sloping flow-front section. The results of the simplified calculations in Appendix 3.5 suggest that, except for the thinnest parent dikes, the filled section comprises the bulk of the flow in the drift once the flow has traveled a substantial fraction of the drift. Over the filled section of the drift there is a more-or-less linear drop in pressure from the dike/drift intersection to the (likely to be low) pressure at the flow front. Once the drift fills (on either side of the parent dike), the pressure to that end of the drift quickly equilibrates to essentially that at the dike/drift intersection.

3.4.4 Flux Partitioning Between Primary and Secondary Dike

The sustained propagation of a secondary dike requires considerations beyond the simple condition that the magma pressure in the drift has to exceed the normal stress across the fracture. The supply of magma into the drifts and up to the primary dike above the repository is best characterized as flux-limited. In other words, a constant-supply flow rate (from the primary dike) is partitioned into a component flowing up the primary dike and another one flowing into the secondary dike (once the drift is fully filled). Even with the conservative assumption that the pressure drop along the drift is negligible, it can be argued, using hydrodynamic considerations, that the great majority of magma would flow in the fracture with the widest opening — i.e., generally along the pre-existing dike.

3.4.5 Secondary Dike Initiation and Thermal Death

An important consideration relevant to magmatic dog-legs is that it is very difficult to start a dike in cold rock. In order for a dike to escape an early thermal death, it must widen elastically (due to propagation of the tip) faster than it freezes shut. Flow of hot liquid through a cold channel can be divided into a thermal entrance region, where most of the heat still resides in the liquid, and a downstream region, where most of this heat has been lost to the surroundings. The thermal entrance length is proportional to the product of the flow velocity and the cooling time, where the latter is proportional to the channel thickness squared. For a dike driven by a constant-pressure source, both the flow velocity and dike thickness are proportional to length. Thus, the thermal entrance length is proportional to the dike length cubed, and sufficiently short dikes are always longer than the thermal entrance length and near the temperature of the host rock (Rubin, 1995a). In Appendix 3.4, we estimate that basaltic dikes in cold rock would not widen elastically faster than they freeze shut until the dike length was tens of meters and the thickness several centimeters. As a concrete example, a typical dike thickness:length aspect ratio is ~ 1:1000, and a typical propagation velocity for a km-scale dike is 1 m/s. A reasonable estimate is that a 1-m long dike is ~ 1-mm wide, propagates at ~ 1 mm/s, and widens at $\sim 10^{-3}$ mm/s. The chilled margin in the same dike would reach 1 mm (the dike thickness) in ~ 1 s. Such a dike could not grow. This is not an argument that dikes cannot form — clearly, they do. However, those that survive thermally must satisfy conditions (discussed in Appendix 3.4) that cannot easily be met by dikes initiating from a drift.

3.4.6 Dog-Leg via Sill Formation

At Paiute Ridge, dikes are observed to follow normal faults and to feed sills locally in the hanging wall. Because the ambient stress is expected to impose a component of (hanging wall down) shear stress on the fault and, during dilation by a dike, this shear stress is relaxed to near zero, a component of normal fault slip is expected should a dike intrude one of the faults cutting the proposed repository. In the vicinity of the dike tip, this gives rise to a tensile stress along horizontal surfaces on the hanging wall side of the fault and the

possibility of sill formation (Ziv et al., 2000). Dikes do not always follow the faults that they cross and, when they do, they do not produce sills within each bedding plane of the hanging wall. The probability that a dike will both (1) intrude along one of Yucca Mountain's faults and (2) form a sill along a horizon that cuts through the proposed repository must be viewed as small, even though the thermal stresses increase the chance that sill formation will occur at the repository depth rather than along some deeper or shallower horizon.

Which horizon is favored depends upon the dip of both the fault and the strata and perhaps the detailed nature of the thermal stresses. Should a sill form, it may cut as many drifts as the parent dike. A pyroclastic sill seems exceedingly unlikely because of the permeability of the host rock and the fact that the vertical stress is so large. The number of canisters directly impacted (in the path of magma flowing in the sill) depends upon the strike of the drifts relative to that of the bedding. If the sill grows to a large enough size, it may vent to the surface away from the parent dike/fault (a "sill dog-leg"), in much the same way that large laccoliths sometimes do (although venting up the parent dike seems more likely).

The worst-case scenario would involve magma rising above the drifts along a dike or fault within the repository footprint near its western margin, turning into a sill along an east-dipping bedding plane that again cuts the drifts (most notably between the Lower Lithophysal unit and the Middle Nonlithophysal unit), and then rising again to the surface some distance to the east (along either an existing fault or a vertical magma-induced fracture outside the region of large thermal stresses). This would create magma pathways up the parent dike, through multiple drifts for perhaps hundreds of meters (bypassing much of the sill), and then up to the surface. The chance of such an occurrence seems difficult to estimate but small; again the probability is increased somewhat by large thermal stresses. Most of the hazard could be avoided by engineering the drifts in such a way that they are not cut by the Lower Lithophysal/Middle Nonlithophysal contact, if this is deemed feasible.

3.4.7 Eruption via a Shaft

Finally, we consider the possibility of an eruption through one of the exhaust or intake airshafts. This scenario would seem plausible only in the 200 or so years prior to the permanent closure and sealing of the repository. If the seals on these shafts are engineered and constructed with the possibility of an eruption in mind, their strength should exceed that of the surrounding rock, ensuring that any intrusion proceeds elsewhere. If an intrusion were to take place in the first 200 years of the repository, the magma must either (1) be diverted through the intake air shaft to the surface, or (2) flow downward from the drifts into the exhaust main, then along the exhaust main and upward through the exhaust air shaft.

3.4.8 Plausibility of a Dog-Leg Scenario

Despite the many situations that could be envisioned by the multiple combinations of possible stress states, magma flows and magma pressures, the above considerations suggest that a dog-leg scenario is quite improbable. The main arguments are given in Section 3.4 and Appendix 3.4 to 3.8. The best chance for a dog-leg to occur apparently requires that the following conditions be met.

Magmatic Dog-Leg

- The main dike or vent must be blocked (e.g., by inelastic deformation or magma freezing) and must not be unblocked at pressures large enough to initiate a dog-leg.
- The secondary dike must avoid an early thermal death.

Pyroclastic Dog-Leg

- The main dike or vent must be blocked (e.g., by inelastic deformation or magma freezing) and must not be unblocked at pressures large enough to initiate a dog-leg, or the pressure due to choked flow in the main vent must be larger than the normal stress acting across potential dog-leg fractures.
- In order for large pressures at the dike/drift intersection to persist down drift, the permeability of the drift walls must be greatly reduced from its intrinsic value before the drifts fill with coarse pyroclastic material.

For a discussion of the difficulty meeting these requirements, see Section 3.4 and related appendices.

3.4.9 Considerations for Alternative Design

The Panel's Interim Report noted that the explosivity of the initial interaction between a dike and one or more drifts would be reduced if waste-generated thermal stresses were kept to a minimum. The reason is that the magma pressure a short distance behind the magma front is closely tied to the dike-normal stress. However, for the reasons discussed in this Chapter it is currently our opinion that the risks arising form this initial interaction are minimal, and that a more important concern is reducing the possibility of a dog-leg magma pathway after the drifts fill with magma. Once the dike tip breaches the surface, as outlined in Section 3.4.3, the magma pressure at the dike/drift intersection is tied more closely to the weight of the overlying column of magma than to the dike-normal stress. Under these conditions, large thermal stresses help minimize the risk by increasing the compressive stress around potential secondary dogleg fractures and acting to contain the magma within the drifts. For these reasons, a "hot design" for the repository seems desirable. The one disadvantage of a hot design is that the chances of sill formation within the level of the repository are increased.

If additional measures need to be taken to eliminate the risk of a dog-leg scenario, then design changes, such as backfilling the drifts (either fully or partially), or constructing bulkheads at select intervals to isolate sections of the repository, should be considered. In addition, the possibility of engineering the drifts so as to remain entirely within a single stratigraphic unit should be considered, so as to reduce or eliminate the hazards of sill formation. More extreme measures, such as excavating diversion drifts beneath the repository, could also be envisioned.

3.5 CONCLUSIONS AND RECOMMENDATIONS FOR FURTHER STUDY

3.5.1 Dike Propagation Models with Compressible Flow

As was pointed out above, models of dike propagation available in the literature do not account for some of the processes that are likely to take place during ascent of a dike at Yucca Mountain and that are thought to be critical for the sequence of events following the intersection of a dike with the repository. These processes include gas exsolution from the magma with decrease of the pressure, fragmentation of the magma, gas bleed-off into the country rock and, perhaps, pyroclastic flow above the fragmentation front. To assess the implication of these processes, the Panel has expended some effort into formulating mathematical models that account in some approximate way for these processes and in writing software dealing with propagation of dikes to quantify their effects. This work is preliminary and needs to be extended by removing some of the simplifying assumptions and by including additional physics. The Panel is of the opinion that it is possible in the short- to medium-term to expand on the work presented in this report by including computation of the gas bleed-off from the tip cavity into the host rock and of dynamic gas flow in some region above the fragmentation front.

These enhanced dike propagation models should then be used to carry out a parametric analysis to scan the range of plausible conditions at Yucca mountain (including varying thermal stresses and magma composition), with the objective of placing tighter bounds on the tip cavity length and pressure, melt and gas velocity, magma front velocity, pressure increase behind the magma front, and the critical depth at which dike tip instability takes place. In particular, these calculations should verify the adequacy of the statements pertaining to the cavity length in the presence of large thermal stresses (as the implication of a non-monotonic variation of horizontal stress with depth has not yet been assessed) and should include situations before and after the magma front reaches the repository.

3.5.2 Dike Propagation Once Magma Reaches the Repository

The position of the dike tip when magma reaches the repository and when it fills the drift system is an important factor affecting the likelihood of the dog-leg scenario. The dominant role of thermal stresses in controlling the position of the tip with respect to the position of the magma front (i.e., the length of the tip cavity), as well as the tip run-away

instability as it comes close to the free surface, was discussed earlier in this chapter. On the basis of this discussion, we have concluded that it is very likely that the dike breaches the free surface if the horizontal stresses at the repository depth and above are not significantly larger than those measured today. Under much larger horizontal in-situ stress conditions than contemporary ones, the tip is at distance of order of 10 m or less beyond the magma front, and progression of the tip will be hindered once magma flows into the repository.

The qualitative analysis of the magma flow splitting into a fraction moving up the dike and a fraction filling the drift system should be complemented by a series of numerical simulations using a 2D dike-propagation model in which the magma loss into the repository is simulated as a point (line) sink in the model. Several degrees of approximation for the magma sink could be envisioned, ranging from a constant rate to a time-varying rate accounting for the progressive filling of the drifts. The main objective of this analysis would be to ascertain whether it is likely that the repository could be filled before the dike breaks at the surface.

3.5.3 Nature of the Magma Flow Erupting into the Drift

The consequences of a gas-rich and a gas-poor magma flowing into the drifts have been discussed in this report. Improved dike models that take into account gas bleed-off into the host rock, above the fragmentation front, could provide improved limits on the gas content of the magma entering the drift as a function of time. However, it is not clear at this point in time what the precise additional ingredients are that would have to be considered in the dike models and, thus, what efforts would be needed to carry out such exercise. Nonetheless, any knowledge that would be gained from such modeling exercises would further limit the nature of flow during filling of the repository.

3.5.4 Magma Flow into the Repository and the Dog-Leg Scenario

3.5.4.1 Pyroclastic Flow

Evaluating the consequences of the pyroclastic eruption of a gas-rich magma into the drifts will require carrying out numerical simulations, using a 2D (axisymmetric) computational fluid-mechanics code, that include magma compressibility and gas exsolution in the calculations.

Instead of the uniform dike pressure/thickness initial condition adopted by Woods et al. (2002), these new simulations should be performed using dike pressure/thickness profiles that are generally consistent with those predicted from 2D dike propagation models. One approach would be to couple the two computational models (dike propagation and pyroclastic flow into a drift) in such a way that there is continuity of the pressure and flux from the dike into the drift at the drift/dike intersection (while recognizing the need for some “patching” in view of the different 2D natures of the two models). A simpler ap

proach would be to advect past the drift opening, at the dike propagation velocity, the thickness/pressure profile of the dike computed in the absence of a repository. More complete numerical calculations can be conducted to capture the 2D nature of the flow field in the dike as the drifts fill. The consequence of implementing more realistic initial/boundary conditions at the dike/drift intersection would be a much more gradual pressurization of the drift than in the calculations of Woods et al. (2002), because of the low pressure and the narrow aperture near the dike tip. Other processes that should be included, relative to the Woods et al. (2002) calculations, are (1) gas loss by diffusion out of the drift and (2) the disruptive effect of the canisters and other material in the drift on an idealized "shock tube" geometry. Thought should be given to the possibility of laboratory or numerical experiments designed to assess whether the intrinsic permeability of the host rock can be greatly reduced by infiltration of fine pyroclastic debris.

This series of computations would be directed at predicting the evolution of the pressure field in the drifts, as part of the information needed to evaluate the possibility of a surface eruption via a secondary dike. (Another objective of the calculations is to compute the hydrodynamic forces acting on the canisters, as discussed in Chapter 4.)

More calculations of choked flow during violent Strombolian eruptions can be carried out to determine if pressures at 300 m are large enough to exceed even modest additions of thermal stress.

3.5.4.2 Incompressible Flow Calculation

The conclusions about the apparent implausibility of a dog-leg scenario along a pre-existing fracture by a largely degassed magma if the primary dike has reached the ground surface depend partially on the assumption that the stress variation at the repository is small (1 or 2 MPa). Numerical simulations with 3D computational geomechanics codes, having the capability of modeling the flow of an incompressible viscous fluid along deformable planar fractures and cylindrical drifts, could be used to test the robustness of this conclusion.

The main objective of this analysis would be to confirm the preliminary conclusions that the magma flow is almost entirely along the primary dike (assumed to break to the surface), rather than along favorably oriented pre-existing fractures (also assumed to connect the repository to the surface), taking into account a realistic state of stress in the rock mass with variations due to thermal loading, topography, the drift system and the presence of the primary dike. Particular attention should be paid to the thermal and mechanical stresses near the drift ends.

CHAPTER 4 ERUPTIONS AND WASTE ENTRAINMENT

This chapter considers the effects of a volcanic eruption on radioactive waste release at the YMR. In the first part of this chapter, we review some of the primary characteristics of basaltic eruptions that relate to potential hazards at Yucca Mountain and then use those known characteristics to critique assumptions used in the TSPA-SR to assess radioactive dosage resulting from such eruptions. In so doing, we attempt to translate the rather "reductionist" approach of Chapter 3 into qualitative estimates of probabilities that are significant for the TSPA. This process is necessarily subjective, as it involves the merging of imperfect models with limited and imperfectly understood observations.

4.1 CHARACTERISTICS OF BASALTIC ERUPTIONS

In contrast to the intrusion of dikes, eruptions can be observed directly, and vivid accounts of violent basaltic eruptions have existed since at least the first mention of Stromboli in classical Roman times. Descriptions usable to scientists are primarily limited to the last century, but, even within that short window of time, numerous detailed records from Kilauea Volcano, Mount Etna, Stromboli, and several other shield or composite volcanoes are available. To date, however, only a handful of descriptions exist for alkali-basalt cinder-cone eruptions of the type anticipated at Yucca Mountain. The best-documented of these are cited in Chapter 2 and Appendix 2. Alkali basalts are notable for their high gas content (a few weight percent versus < ~ 0.5 wt % for Kilauean tholeiites), which increases explosivity by gas expansion and also by degassing-induced crystallization, which increases viscosity and may clog the vent at shallow depth.

Basaltic fissure eruptions are usually preceded by seismic swarms, lasting hours to weeks, that migrate toward the surface with the dike front. Though few seismic data have been recorded above vertically propagating dikes, seismicity ahead of laterally propagating dikes migrates at a large fraction of a meter per second, or about a kilometer per hour (e.g., Brandsdottir and Einarsson, 1979). The weeks-long duration of precursory seismicity for alkali basalts such as Parícutin, however, implies a much slower average ascent rate. Hours or less before the appearance of magma, surface fissures some tens to hundreds of meters long develop at the site of the future vent (Parícutin, Tolbachik, Kilauea), followed sometimes (e.g., Parícutin) by loud subterranean noises and by escaping gas that may drive jets of dust or eject blocks meters from the vent. In some cases [e.g., Parícutin (Luhr and Simkin, 1993, p. 57)], vents develop along the fissure due to slumping and enlargement prior to the arrival of magma.

Once magma arrives at the surface, the eruptive character varies with fluidity of the magma. Tholeiitic basalts (Kilauea) and some alkali basalts (Tolbachik) erupt as curtains of fire along the full length of the fissure. Less fluid basalts (Parícutin, Lonquimay) eject cinders and scoria from the outset through one or a few vents. In both cases, ejection height increases over minutes from meters to tens of meters or more, and ejection velocity from less than a meter per second (estimated from ejection height) to tens of meters

per second. Eruptions that begin as curtains of fire generally localize within hours to fountaining at several vents along the fissure, then at a few vents, and eventually (within a few days at Kilauea) to a single vent.

In general, mass flow rates are highest early in the eruptive sequence and drop gradually with time (e.g., Parícutin, Heimaey, Laki). Most alkali basalt eruptions form cinder cones early in the eruptive sequence by normal Strombolian activity, with mass flow rates of the order of tens of cubic meters per second (~ 10^5 kg/s; Parícutin, Lonquimay). With some exceptions (Tolbachik), eruptive sequences tend to produce more tephra near the beginning and more effusive lava toward the end (e.g., Heimaey, Lonquimay, Laki). Violent Strombolian phases (e.g., Cerro Negro, 1995) may occur throughout the eruptive sequence, though they persist only for a period of hours. Violent Strombolian phases emit several hundred cubic meters per second of magma (~ 10^6 kg/s) at velocities over a hundred meters per second and disperse tephra over hundreds of square kilometers. Hydromagmatic phases may occur early in the sequence, late (Tolbachik), or at some intermediate stage (e.g., Lathrop Wells).

A key element in the early eruptive history is the transition from flow in dikes to conduits. In low-viscosity basalts, the transition from dike to conduit flow is thought to result largely from freezing in narrow parts of the dike, followed by thermal and mechanical erosion of wider dike sections as flow is diverted into them (e.g., Delaney and Pollard, 1981, 1982, Appendix 3.4). In more viscous, gas-rich magmas, conduits may develop by piping of gas above stalled, shallow magma bodies. In either case, conduits are assumed to widen during an eruption by erosion and slumping (followed by ejection) of conduit walls.

4.2 CONCEPTUAL MODEL USED IN THE TSPA-SR

The Igneous Consequences Peer Review Panel was asked to review both the conceptual model on which calculations of eruptive consequences are based and the adequacy of investigative methods used to reduce uncertainty. The conceptual model of DOE and NRC assumes that future Yucca Mountain igneous activity would resemble late Cenozoic monogenetic alkali basalt eruptions in nearby Crater Flat. Such eruptions are assumed to: (1) reach the surface as fissures but quickly focus to a small number cylindrical conduits; (2) erupt cinder cones, lava flows, and tephra sheets; (3) range in duration from days to years, with the greater eruptive volumes (> ~ 10^{-1} km^3) lasting a few years; (4) erupt a few thousandths to a few tenths of a cubic kilometer in a given sequence; and (5) disperse tephra over a few hundred square kilometers during the most violent eruptive phases, which are assumed to be violent Strombolian.

With a minor caveat, we consider this model to be appropriate for Yucca Mountain based on the eruptive history of the area. The caveat is that violent Strombolian phases do not occur during all monogenetic basalt cinder cone eruptions, and their occurrence (or lack thereof) at these sites has been the subject of some debate. At Crater Flat, it cannot be determined whether vents older than the Lathrop Wells cinder cone produced tephra

sheets, as these vents are too old for such deposits to be preserved. At Lathrop Wells, erosional remnants of a violent Strombolian tephra sheet have been recognized, though its areal extent and volume are poorly constrained. Overall, we accept the DOE and NRC assumption that a future event will involve violent Strombolian phases as conservative and probably realistic.

4.2.1 Waste Transport and Factors That Affect It

Given this conceptual model, the transport of waste to inhabited areas could occur by three paths: (1) atmospheric entrainment in tephra plumes; (2) wind-borne or water-borne reworking of tephra or lava; and (3) groundwater transport of material leached from surface deposits or subsurface drifts containing damaged canisters. Here, we primarily shall review waste released only by path (1). Factors that affect waste transport by surface water or groundwater are outside the expertise of the Panel, though volcanic damage to canisters, which affects access to the groundwater system, is within our purview. Apropos this point, we comment briefly on TSPA analysis of canister damage in Section 4.4.

Along path (1), the amount of waste that enters the biosphere in nearby populated areas depends primarily on four factors: (1) the number of waste canisters entrained in erupting magma; (2) the fraction of waste that escapes each canister; (3) the grain size distribution of waste (which influences its mode of transport and ingestion); and (4) the transport distance of eruptive debris. Factors (1) and (4) are affected primarily by volcanic processes; (2) and (3) are affected by both volcanic and non-volcanic processes, the latter of which includes material strength of canisters, integrity of waste pellets, etc. In the following sections, we examine each of these factors.

4.3 AMOUNT OF WASTE ENTRAINED

TSPA-SR calculations assume that the number of waste canisters entrained in the eruption equals the number directly intersected by conduits at repository level, plus a few waste canisters on either side. The number of entrained canisters ranges up to a few dozen depending on the number of conduits that intersect drifts and their diameter. Canisters might also be entrained when magma drains from drifts back into the conduit or if magma is diverted through one or more repository drifts en route to the surface (the dog-leg scenario). The dog-leg scenario, considered the more serious of these, could add up to 230 canisters per drift assuming a maximum drift length of 1400 m (from Fig. 4-1) and 5.5-m long canisters arranged 0.1 m apart (hot scenario). As described below, drainback is unlikely to add substantially to the total number of entrained canisters, and a dog-leg diversion, though more serious, is thought to be much less likely than eruption up the parent dike (or a vent that grew in the plane of that dike).

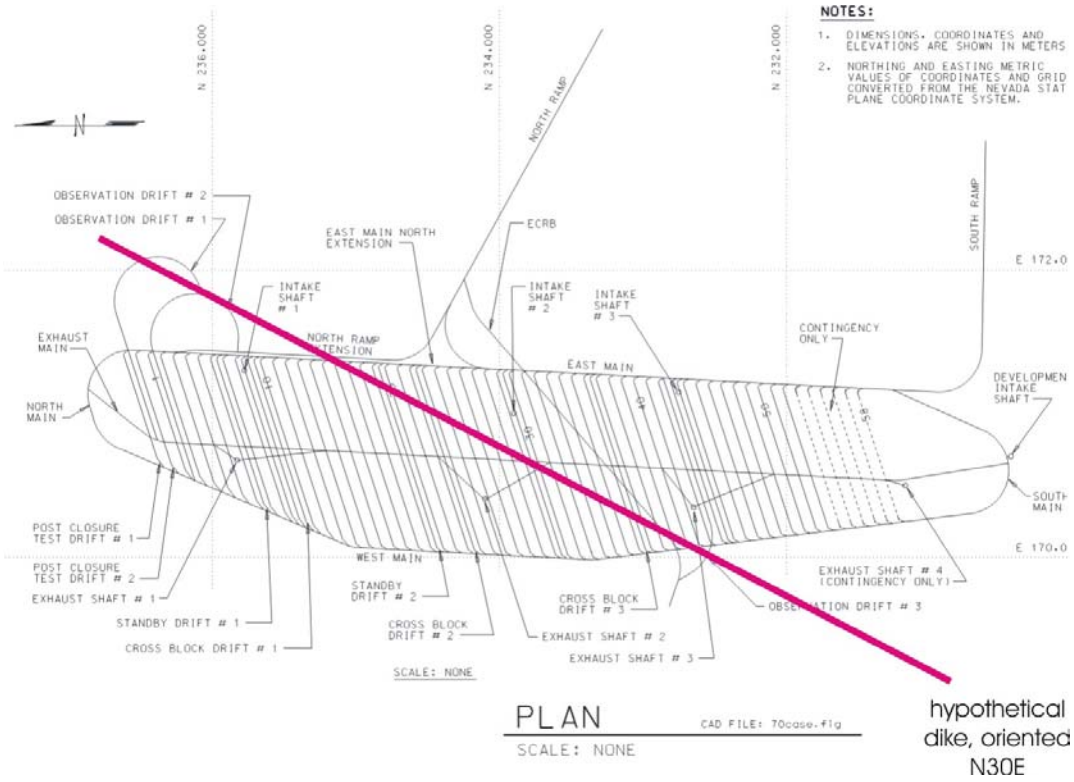

Figure 4-1 ***Preliminary map of the Yucca Mountain Repository showing a dike oriented parallel to the most compressive horizontal stress (N25-30E; Stock et al., 1985; N25-30E) (This is nearly equal to the dike orientation assumed most likely to intersect the repository (CRWMS M&O, 1996, p. 102)***

4.3.1 Waste Entrained by Engulfment within Conduits

Conduit Diameter — The TSPA-SR assumes conduit diameters range from 15 m to 150 m (mode = 50) and conservatively assumes that each conduit will be centered along a drift (CRWMS M&O 2001, p. 41). This range of diameters is based on sparse observations of ancient, eroded basaltic conduits (e.g., WoldeGabriel et al., 1999) and xenolith studies of historical eruptive deposits (Doubik and Hill, 1999). **We encourage more field observations of eroded conduits that can constrain diameter.** Numerical models (Table 4-1) suggest that mass flow rates commensurate with violent Strombolian activity (10^5 kg/s to 10^6 kg/s) can be delivered through a conduit 1 m to 6 m in diameter. The fact that many basaltic conduits observed in the field have greater diameters suggests that only a small fraction of the cross-sectional area may be active during such eruptive phases. Large conduits likely grow by repetitive episodes of erosion, collapse and repeated expulsion of wall rock, and magma freezing, perhaps during prolonged eruptions.

Table 4-1 Modeling results of mass flux (kg/s) versus conduit diameter for three initial dissolved water contents

	Mass Flux (kg/s)		
conduit diameter (m)	***1 wt % H_2O***	***2 wt %***	***4 wt %***
1	9.4E+03	1.5E+04	2.2E+04
2	7.1E+04	1.0E+05	1.3E+05
3	2.2E+05	3.1E+05	3.5E+05
4	4.8E+05	6.5E+05	6.9E+05
5	*2.1E+05*	*4.3E+05*	*4.5E+05*
5	**5.0E+05**	**8.0E+05**	**8.9E+05**
5	8.6E+05	1.1E+06	1.2E+06
6	1.4E+06	1.8E+06	1.8E+06
7	2.0E+06	2.6E+06	2.5E+06
8	2.7E+06	3.5E+06	3.4E+06
9	3.6E+06	4.6E+06	4.4E+06
10	*1.0E+06*	*1.9E+06*	*2.1E+06*
10	**2.6E+06**	**4.0E+06**	**4.2E+06**
10	4.6E+06	5.9E+06	5.6E+06

These values were calculated using a public, open-source conduit-modeling program (Mastin and Ghiorso, 2000) that uses a magma with the same composition as Lathrop Wells basalt (Appendix 2, Table 2A) at 1120 ^{o}C with 15% crystals by volume in a conduit extending from the surface to 1 km depth. Results in plain (non-bold, non-italic) text are for a pressure of 27 MPa at the base of the conduit; results in **bold** are for a basal pressure of 20 MPa; and results in *italics* are for a basal pressure of 10 MPa.

4.3.2 Waste Entrainment by Drainback

During nearly all basaltic eruptions that have persisted for months or longer, the level of lava at the eruptive vent has varied by tens or sometimes hundreds of meters. Eruptions at Parícutin, Tolbachik, Lanquimay and elsewhere constructed cinder cones more than 100 m high whose flanks collapsed under pressure of internal lava (Appendix 2). During cone construction, levels of lava in the vent increased by hundreds of meters over days or weeks, then dropped by tens of meters during flank collapses that took place over a period of hours (e.g., June 9, 1943 at Parícutin; Luhr and Simkin, 1993, p. 81). In a poorly vesicular magma column, elevation changes of this magnitude imply pressure fluctuations of a few MPa (assuming a cone height of 100 m to 200 m and magma density of ~ 2000 kg/m^3).

More rapid pressure fluctuations may occur during hydromagmatic phases, which are commonly triggered when the magma level in the conduit drops below the water table.

At Yucca Mountain, hydromagmatic phases of this type would require a drawdown of more than 600 m and a pressure drop at repository level from ~ 10 MPa (the pressure of a static, unvesiculated magma column at a depth of 300 m to 400 m) to 1 atmosphere. During hydromagmatic explosions, large pressure fluctuations could occur over periods of minutes, though the pressure drop associated with magma drawdown that precedes such explosions might take much longer.

Rapid conduit pressure decreases at repository depth could drive magma, gas and waste from drifts back into the conduit, where it is expelled in the next eruptive pulse. If the drifts were not filled completely, liquid magma would be driven into the conduit only by the small head gradient associated with variation in magma surface elevation. In a filled drift, magma at high pressure could expand into the conduit if its gas content (and hence expansivity) were high. Drainback would carry waste into the conduit only if hydrodynamic drag were sufficient to transport whole canisters or if canister damage were extensive enough that most waste had already escaped. Drift cooling calculations (e.g., CRWMS M&O, 2000a) suggest that magma would solidify in 70 to 82 days after intrusion. It likely would crystallize enough to inhibit flow in a much shorter time, though this should be verified by calculation.

If one assumes that drainback entrains canisters within one radial distance of each active conduit, drainback could affect about five canisters on either side of a 50-m diameter conduit. However, three canisters on either side are already assumed engulfed in the TSPA-SR. The number of additional canisters seems small compared with the overall uncertainty already inherent in the TSPA calculations. If it is decided that the potential increase in the number of waste canisters entrained by this mechanism is sufficient to warrant further study, much of the problem could be addressed by numerical modeling. **Aspects of the problem that are numerically tractable include calculating the temperature and crystallinity of magma in the drift versus time, and the hydrodynamics of flow in the drift for observationally calibrated rates of pressure drop in the conduit.**

4.3.3 Waste Entrainment Along a Dog-Leg

The diversion of magma through one or more drifts and up a pre-existing shaft or a new dike has been considered in some studies (Woods et al., 2002; NRC, 1999, pp. 78-81). In our view, such a diversion, termed the dog-leg, is the only plausible scenario that may release substantially more waste than a standard scenario that involves intersection of drifts by vertical conduits. The amount of waste entrained in a dog-leg eruption would depend primarily on three factors: (1) the number of drifts involved; (2) the flow distance in each drift; and (3) the characteristics (e.g., duration, velocity, pyroclastic versus magma) of the flow. In this section, we examine the first two of these.

Number of Drifts Intersected — As with vertical conduits, we consider it most likely that flow will concentrate along one drift at the expense of others. In a standard scenario, the TSPA-SR gives 86% probability that the eruption will focus to a single vertical conduit,

98% for two or fewer conduits, 99.8% for three or fewer, and so on, up to five (CRWMS M&O 2001, p. 62). The probability that a dog-leg will involve only one drift would seem to be similarly large (80% to 90%) given that a 5.5-m diameter drift can accommodate nearly the full range of mass flow rates of these eruptions (Table 4-1). On the other hand, the total number of drifts that may serve as conduits may be greater than five, as drifts already exist, whereas conduits must develop by increasing flow localization. The exponential tail to the probability function might extend to dozens of drifts. We assume that access drifts, which connect the main drifts, are backfilled.

Dog-Leg Length — Once magma enters a drift, potential points of exit include (1) pre-existing fractures; (2) dike-parallel fractures created by the intrusion; and (3) drift ends. Pre-existing and dike-created fractures near the dike are opened more easily than more distant ones**,** at least while the magma front in the dike does not extend far above the drifts, because under these conditions tensile stress increases toward the dike. In addition, drift pressure is likely to be highest near the dike, especially immediately after intersection. On the other hand, drift ends may underlie the flanks of the mountain and be subject to a lower ambient stress field that is more conducive to dike initiation. In the absence of better predictive powers, the simplest probability distribution for dog-leg length would be a flat one (equal probability for all lengths ranging from zero to ~ 1400 m). This would imply entrainment of up to 230 entrained canisters per drift under the hot scenario (5.6 m/canister), or 186 under the cold scenario (7.5 m/canister). Mean values would be 115 (hot) or 93 (cold).

Thus a "mean" dog-leg scenario would involve one drift of about 700-m length and entrain about 100 canisters — an order of magnitude more than in a typical standard scenario (1 vertical conduit, 10 canisters per conduit). If the development of a dog-leg is judged to be at least an order of magnitude less probable than a standard vertical eruption, its consequences, on a probability-weighted basis, would not greatly affect the mean eruption-related dosage calculated in the TSPA-SR. Based on mechanical considerations outlined in Chapter 3, Section 3.4, we are inclined to believe that this is the case — i.e., a dog-leg scenario is at least an order of magnitude less probable than a standard eruption scenario. However, we recommend further work, as described in Chapter 3, Section 3.5, to increase our confidence in this assessment.

4.3.3.1 Movement of Canisters

In a dog-leg scenario, waste canisters will be erupted only if they can be moved by the horizontally flowing magma. In our preliminary report and in Woods et al. (2002), simple calculations of drag force were used to suggest that canisters could be moved by a gas-tephra mixture flowing at tens of meters per second.. The conclusion must be revised, however, if the containers are separated by a distance (s) less than about five times their radius (r); in such a case, the drag coefficient (C_D) should be nearly zero for all canisters after the first in a long train, or slightly negative for the second in a pair (Hoerner, 1965, p. 8-1). The proposed s/r is 0.12 (hot scenario) or 2.4 (cold scenario), placing each canister well within the slipstream of the upstream one. We therefore expect canisters to be

moved only if forces other than steady-state hydrodynamic drag were involved, such as impact by upstream canisters or other objects. In a *vertical* conduit, the upward force required to lift a canister can almost certainly be supplied under certain circumstances (e.g., lifting of debris en masse during an explosion). **These calculations should be verified by more exacting numerical analysis.**

If a dog-leg were to persist for weeks or longer, continuous flow could thermally erode the drift floor and undercut ground supports beneath containers. In lava tubes in Hawaii, sustained flow rates of a few meters per second cause tube floors to erode thermally by centimeters per day (Kauahikaua et al., 1998; Kerr, 2001). Drift floors at Yucca Mountain may erode more quickly, as they are composed of silicic pyroclastic debris whose melting temperature is lower than basalt. Thermal erosion may also remove the rock support from semicircular steel supports, wire screens, and longitudinal steel support beams that line the drift.

Aside from the dog-leg scenario, these considerations are also relevant when drifts fill with magma after intersection by the dike. In that circumstance, canisters may be submerged in a laminar-flowing sublayer rather than a turbulent gas-driven mixture. On the other hand, if a dog-leg were to become established, a violent Strombolian phase were to take place through the drift and the fragmentation point lay within or upstream of the drift segment, fully turbulent flow with velocities of tens of meters per second in the drift are possible.

4.4 AMOUNT OF WASTE THAT ESCAPES FROM CANISTERS

The TSPA assessment of eruption-related dosage depends heavily on the percentage of nuclear waste in each waste package that separates from its container and is directly incorporated into the erupting magma. The TSPA-SR assumes that all waste packages in the direct path of the eruption are sufficiently damaged that they provide no further protection. This conservative assumption is based in part on lack of data on the performance of Alloy 22 under magmatic temperature (Reamer, 1999).

Waste packages have a variety of forms depending on the type and source of waste. Waste from spent commercial nuclear plants, for example, is contained in 6-mm to 12- mm diameter sealed cylindrical rods, typically of zirconium metal, bundled in arrays of ~ 200 with spacer grids of stainless steel (e.g., Fig. 3-6 of CRWMS, 2001b). Approximately 20 to 40 such arrays are contained in a single waste package (Fig. 3-5 of CRWMS, 2001b). The escape of all waste requires that the end caps be removed, that the zirconium rod cladding be broken, and that the fuel pellets be pushed out of each ~ 5-m long, 6-mm to 12-mm diameter tube.

The few observations of volcanic damage to metal containers come primarily from metallic objects entrained in lava or pyroclastic flows. At Mount St. Helens, the lateral blast on May 18, 1980 damaged vehicles primarily by melting or breaking of glass, plastic and upholstery, and by battering and abrasion from flying objects (e.g., Waitt, 1981, p. 454).

Steel gas canisters and water tanks entrained in pyroclastic flows at Montserrat also are battered but intact (e.g. Fig. 12a of Loughlin et al., 2002). At Kilauea volcano, lava flows generally burn away non-metallic components of vehicles with relatively less dismemberment to the metallic shell (Thornber, 2003). At Yucca Mountain, waste canisters could be subjected to hotter temperatures for longer periods of time than vehicles at Mount St. Helens, and to higher flow rates and greater agitation than in typical lava flows at Kilauea. Similarly, canisters within drifts will encounter higher pressure than those in surface flows and are more likely to suffer pressure-induced damage to welds that open pathways for groundwater to enter. For evaluating groundwater waste transport, the TSPA-SR assumes that all canisters in drifts intersected by a dike (zone 2) suffer damage that makes waste available to leaching, and that canisters within three canister-lengths of the dike-drift intersection (zone 1) are completely destroyed. These assumptions strike us as reasonable given our experience with volcanic phenomena; but observations that can be used to calibrate our judgment on this subject are extremely sparse.

Our understanding of the effects of magma on waste canisters would be greatly improved by experimental data. For example, experiments might address (1) the conditions of heat and corrosive gas exposure required to cause the canister welds and casing to completely fail, and (2) the degree of physical disruption required to completely remove all waste from canisters and fuel rod casings.

4.4.1 Grain Size of Waste

The degree of disaggregation of nuclear waste pellets has been considered in other studies (e.g., CRWMS M&O, 2000b, Table 8) and is mostly outside this Panel's field of expertise. On this topic, we note only that, in studies of wallrock incorporated into eruptions (e.g., Mastin, 1991), the moderately- to well-cemented elastic rocks such as sandstone generally are not broken down in any thorough manner to the grain-size of their component materials. The degree of disaggregation depends, of course, on the degree of cementation, as well as on the amount of disturbance to which these materials are subjected. Experimental incorporation of UO_8 pellets into dusty gas jets may provide some insight into the degree to which these materials might be disaggregated.

4.5 EFFECTS OF HYDROMAGMATISM.

TSPA assessments to date have ignored effects of water-magma mixing, although the presence of some hydromagmatic beds at the Lathrop Wells cinder cone (G. Heiken, LANL, personal communication, 2002) make it relevant to ask how explosive water-magma mixing might affect the consequences of an eruption. Hydromagmatic eruptions result when magma mixes explosively with ground or surface water; they differ from dry magmatic eruptions in that they (1) tend to produce more discrete explosions, (2) expel more country rock per mass of juvenile magma, and (3) fragment the magma by a combination of quench granulation and thermal fracturing. The median grain size of juvenile hydromagmatic pyroclasts (< ~ 1 mm) is typically much finer than that from dry mag

matic eruptions (Fisher and Schmincke, 1984, Chapter 9; Wohletz and Heiken, 1992, p. 24). Thus, hydromagmatic eruptions could potentially (1) engulf more waste canisters as conduit walls erode, and (2) disperse waste widely during discrete explosions.

Hydromagmatic wall-rock erosion is already implicitly included in TSPA assumptions of conduit diameter, which are based, in part, on xenolith volumes ejected during hydromagmatic phases of the 1975-76 Tolbachik eruption (Doubik and Hill, 1999). Conduit diameter estimates in Doubik and Hill (1999) were in the range of tens of meters, similar to xenolith studies at phreatic craters (e.g., Mastin, 1991) but smaller than at some purely magmatic vents (WoldeGabriel et al., 1999). Whether conduits that are initially large (> 100 m diameter) enlarge further during hydromagmatic phases is not well known.

Regarding tephra dispersal, areal distribution during large hydromagmatic eruptions is likely similar to that from violent Strombolian activity. Surtseyan hydromagmatism (the kind normally produced in small basaltic eruptions) typically disperses tephra over several tens of square kilometers or less (Fisher and Schmincke, 1984, p. 61). On the other hand, the hydromagmatic White Ash 1 event at Tolbachik deposited > 1 cm ash of ash over ~ 100 km^2 (Doubik and Hill, 1999, Fig. 2) and likely covered hundreds of square kilometers to a thickness > ~ 1mm.

In brief, violent hydromagmatic eruptions could erode conduits to a similar diameter as that assumed in TSPA calculations and deposit material over about as large an area as violent Strombolian eruptions. It is not clear that hydromagmatic activity would increase substantially the amount of waste entrained or its dispersal.

4.6 DISPERSAL OF ERUPTED WASTE

The amount of waste that is transported to nearby populated areas depends both on the fraction of erupted waste that is entrained in violent Strombolian phases and on the areal distribution of tephra during those phases.

The TSPA-SR conservatively assumes that all waste is ejected during violent Strombolian phases, though at Parícutin (Segerstrom, 1950), Tolbachik (Budnikov et al., 1983) and Heimaey (Self et al., 1974), among others, widespread tephra sheets compose only about half the total erupted volume. At still larger eruptions (e.g., Laki, Iceland, 1790; Thordarson and Self, 1993) tephra sheet volume/total volume is even smaller, because activity evolved from initially pyroclastic to prolonged lava effusion. The assumption that all waste is entrained in violent Strombolian eruptions could be reduced realistically by a factor of two based on erupted volume ratios from these eruptions.

4.6.1 Volcanic Plumes and Strombolian Eruption Columns

Tephra (ash, lapilli, bombs and blocks) dispersal associated with an explosive eruption depends on many factors. The most determinative include the height of the eruption col

umn, the particle size distribution and the structure of the winds aloft (wind speed and direction as a function of height, including temporal and spatial wind variability). Eruption column heights range from hundreds of meters for low-intensity spatter eruptions to ~ 50 km for eruptions with mass flow rates of ~ 10^9 kg/s. Eruption column height, or plume height, scales according to $H \approx 0.24\ M^{1/4}$, where M is the mass flow rate [units: kg/s], and H is the plume height [units: km]. Particle size distributions depend on the volcanological parameters (e.g., volatile content of magma, melt viscosity, melt surface energy, temperature and composition) discussed in Chapter 2. Meteorological factors govern the structure of winds aloft. Forecasts of winds aloft on climate-variation time scales (e.g., 5000 years from today) cannot be made reliably. Even with deterministic models for ash dispersal at hand, the dispersal of ash is a highly stochastic process and is treated that way in the current TSPA.

Strombolian eruptive activity, the type most relevant to disruptive magmatism at the YMR, is characterized by explosive bursts of congealed and partly congealed tephra that includes ash (< 2 mm), lapilli (2mm to 64 mm), and blocks and bombs (> 6 cm). Within the conduit, jets of melt, accelerated by vapor exsolution, break up into clusters of pyroclasts. Although most particles are lapilli-size, larger blocks and aerodynamically streamlined bombs are also ejected and follow ballistic trajectories. Bombs can be hurled several kilometers during energetic Strombolian eruptions, although most of the tephra is deposited close to the vent and piles up to form cinder or scoria cones. Strombolian eruptions are characterized by mass flow rates in the range 10^4 kg/s to 10^6 kg/s, with consequent eruption column heights in the range 1 km to 10 km. It is critical to note that eruption intensity is rarely constant during a Strombolian eruption. As noted in Chapter 2, most eruptions are described by a sequence of phases, each characterized by a unique set of parameters. Normal Strombolian eruptions are best represented as single detonations or as a series of short duration explosions. These eruptions do not produce sustained eruption columns; hence, distal transport of ash is limited. *Models used to predict ash dispersal are based on the assumption of energetic steady-state activity producing a sustained eruption column of fixed height, H. This type of activity is termed violent Strombolian behavior. The models of ash dispersal discussed below refer specifically to violent Strombolian (sustained) eruptions.*

4.6.2 Pyroclast Dispersal in Violent Strombolian Eruption near the YMR

During a violent Strombolian eruption through the YMR, tephra dispersal would be the most rapid and effective means of transporting HLW to inhabited areas and increasing dose rates. Remnants of tephra blankets from the Lathrop Wells eruption are widespread enough to not allow discounting a priori the possibility of violent Strombolian phases at the YMR in the future. A sustained violent Strombolian eruption at rate 10^6 kg/s would produce the entire eruptive mass of the Lathrop Wells volcano (~ 0.1 km^3) in about one day and produce eruption column heights around 10 km. Although sustained violent Strombolian eruptions are perhaps unlikely, intermittent violent Strombolian activity interspersed with periods of normal Strombolian activity and emission of mildly effusive lava flows is a possibility. The age and lack of preservation of older basaltic centers in

the region make it impossible to know if violent Strombolian activity took place during earlier Quaternary or Pliocene eruptions from the CFVZ. It is conservatively assumed in the TSPA that future eruptions through the repository are capable of violent Strombolian activity with widespread tephra blanks. One wishes to be able to predict the surface density (i.e., kg m^{-2}) and tephra size-distribution as a function of distance from the vent for a given set of meteorological and eruption parameters.

4.6.3 Current Dispersal Model

The current TSPA estimates the amount of tephra dispersed to the nearest inhabited area, 20 km south of Yucca Mountain, using the numerical model ASHPLUME (Jarzemba, 1997). ASHPLUME is based on the model of Suzuki (1983) and calculates tephra dispersal for a fixed-wind vector (speed and direction) using particle-settling velocities, a conservative assumption of northerly wind direction and wind speed data derived from measurements in the region. Other parameters include: (1) plume height derived from mass eruption rate ($H \approx 0.24\ M^{1/4}$); (2) total eruptive mass; (3) fraction of ash of different sizes; (4) Stokes particle fall time; and (5) constant horizontal particle diffusivity. Important factors that are not considered include particle aggregation, thermal disequilibrium, condensation, rainfall, spatial and temporal variations of wind velocity, effects of tephra fallout on plume density and effects of short-lived buoyant thermals. ASHPLUME and other tephra models are validated by comparing their results with tephra dispersal patterns from mapped deposits. Thus, one can check the TSPA estimates of ash thickness at this distance by comparing them with deposits from other violent Strombolian eruptions. Isopach maps from such deposits suggest that, at 20 km from the vent, ash thickness within 30^o to 40^o of the axis of dispersal is of the order of centimeters. Outside of this sector, little or no ashfall is recorded. Ash thickness of the order of centimeters agree with ~ 30% of TSPA-SR realizations that assume a northerly wind direction. TSPA realizations that produce lesser thicknesses presumably are associated with scenarios in which mass flux is lower.

4.6.4 Other Ash Dispersal Models

Since the Jarzemba (1997) study, there has been continued study of methods to forecast ash transport and fallout with application to recent eruptions. In particular, ash dispersal following three volcanic eruptions in 1995 and 1996 of Ruapehu volcano in New Zealand has been studied in considerable detail using the model ASHFALL (Hurst, 1994; Hurst and Turner, 1999). These eruptions raised ash to heights ~ 10 km above sea level. When the forecast wind direction was correct, predictions from ASHFALL proved accurate within a factor of two of measured ash surface loadings. More recently, Turner and Hurst (2001) discussed what is perhaps the most sophisticated algorithm for determination of ash dispersal — the RAMS/HYPACT algorithm.

In order to evaluate accuracy of ASHPLUME isopachs, a study should be made comparing predictions of ASHPLUME, ASHFALL and RAMS/HYPACT for a

fixed set of eruption and meteorological parameters. This would provide an independent measure of the accuracy of ASHPLUME, which is currently used in the TSPA.

4.7 SUMMARY AND RECOMMENDATIONS

We view the conceptual model used to assess the consequences of igneous intrusion into Yucca Mountain to be, in general, realistic. Numerical values used of eruptive parameters used in the TSPA-SR appear to be realistic or conservative. Conduit diameters of ~ 15 m to 150 m, for example, appear realistic — or perhaps conservative. An areal extent of a few hundred square kilometers for violent Strombolian tephra sheets, which is used indirectly in the TSPA calculations, appears realistic, though recent field studies (F. Perry, 2002, personal communication) suggest that conduits >100 m in diameter may be more common than currently assumed. The assumption that all entrained waste is erupted in a violent Strombolian phase is conservative by probably a factor of two, based on the percentage of erupted debris expelled in violent Strombolian phases in historical eruptions.

The only scenario we envision that may result in significantly more waste release than predicted in most TSPA-SR estimates would involve a dog-leg diversion of magma through one or more repository drifts. A dog-leg scenario involving a single drift potentially could release an order of magnitude more waste than the typical standard scenario. However if, as we are currently inclined to believe, a dog-leg is at least an order of magnitude less likely than a standard vertical intrusion, its effect on TSPA assessment may fall within the range of uncertainties due to other factors. This view should be further evaluated following the recommendations provided in Section 3.5.

The objective of further work should be to reduce the uncertainty. As a guide for further work, we offer our own estimates of the order of magnitude uncertainty in some key numerical parameters (Table 4-2). Observations of conduit diameter, ash dispersal, and the fraction of violent Strombolian products ejected in cinder-cone eruptions constrain the uncertainty in the second, fifth, and sixth parameters in this table to an order of magnitude or less. Regarding the first parameter, we accept the conservative assumption that an intrusion that reaches the repository will have a >10% probability of erupting. Ironically, the two parameters that appear most poorly constrained are those that we feel least qualified to evaluate: the fraction of waste that escapes from entrained canisters, and the average grain size of erupted waste. The former conceivably could be two orders of magnitude less than the 100% assumed in the TSPA-SR. The latter could also be two orders of magnitude larger than the TSPA median value of ~ 10^{-5} m. (The size of waste pellets is about 10^{-2} m.) **The uncertainty in these parameters is likely to be reduced only by experiments that are carefully designed by both volcanologists and engineers familiar with waste canister and waste form materials.**

Table 4-2 Order of magnitude estimate of uncertainty in numerical values used in the TSPA-SR to calculate dosage to nearby residents following a volcanic eruption through the waste repository

Factor	*Uncertainty*[*]
Probability that a dike will erupt once it reaches the repository	10^0
Number of waste packages entrained in a conduit	10^1
Fraction of waste in each package that is entrained into erupted material	10^2
Grain size of entrained waste	10^2
Fraction of erupted waste that is entrained in a violent Strombolian phase	10^0
Areal distribution of tephra sheet(s)	10^1

[*] An uncertainty of 10^2 implies that we can predict the value of a parameter to within about two orders of magnitude.

CHAPTER 5 CONCLUSIONS AND RECOMMENDATIONS

We have used the questions asked in Table 1-1 as a guide and have borne in mind those that the TSPA has to answer, in presenting our conclusions and recommendations.

1. The overall conceptual model (namely, that of a rising dike intersecting several drifts into which magma flows, followed by localization into a pyroclastic Strombolian eruption along a conduit) is both adequate and reasonable. No fully satisfactory mechanistic explanation of the localization process is currently available, and separation of the hazards into additive components, on the one hand, for damage done to canisters by magma flowing from a dike into drifts and, on the other, for that done by pyroclastic conduit flows past canisters is justified. It would be unreasonable to expect major advances in understanding of the localization process within the next three years, and we do not recommend any alteration to the present overall model.
2. As far as the range of quantitative characteristics of the igneous event considered is concerned, we have reviewed all the literature available and conclude that the approach adopted so far — namely, that the analog evidence from recent (< 5 Ma) igneous events that have occurred close to (Crater Flats, Lathrop Wells) be given more weight than earlier events or those further afield — is entirely reasonable. We recommend that further high-resolution geochronological work be performed to better constrain the ages of exposed Pliocene and Quaternary basalts in Crater Flat as well as possible basaltic volcanic rocks identified by aeromagnetic studies. (More detailed proposals on this are given at the end of Sections 2.6.1, 2.6.2 and 2.6.3 above.)
3. Quantitative assessment of the rate and type of magma flow into drifts from a rising dike has not been as carefully analyzed in the past as it could be. Chapter 3 and its appendices provide a structured approach to tackling the problem, and we recommend that this be pursued as a high priority activity. Particular attention should be paid to

    (a) modeling the region near the magma front in a rising dike to account for gas/vapor evolution, and embedding this in global planar dike propagation models,

    (b) estimating the length of the gas/vapor cavity behind the dike tip in (a) for various scenarios,

    (c) developing coupled 3D models for unsteady dyke/drift flow when a planar vertical dike intersects drifts, acting as regularly spaced sinks (this would be relevant both to refining arguments about the probability of dog-legs arising and to calculating the impact of drift flows on canisters within the drifts affected), and

    (d) modeling the effect of infiltrating tephra and variable gas pressure on the loss of gas through permeable dike and drift walls.

4. "Hand calculations" will not suffice for obtaining useful quantitative results from the models recommended in 3 (a-d) above. Suitable CFD and geotechnical software, using either commercially available codes or special-purpose codes (available to consultants or at National Laboratories) could be customized to quantify these models within a year. We note that a degree of idealization is always required when converting a general mathematical model into a well-posed numerical problem using particular algorithms. Therefore, we recommend that such work be planned under a single manager to ensure close collaboration between modelers, numerical experts and Earth scientists.

5. Significant large-scale dispersal of tephra will be dominated by violent Strombolian phases of the eruption. The key issues are the number of canisters affected by the erupting mixture, the extent to which these canisters are disrupted and the consequential distribution of particle size of the high-level waste that is then dispersed aerially. Although this problem involves engineering topics outside our specialty, our knowledge of volcanic processes incline us to believe that the assumptions made in the published TSPA (namely, that the contents of all canisters within or closer than 3 canister lengths to conduits will be converted to small particles and widely dispersed) is overly conservative. The probability that a violent erupting mixture could follow dog-leg conduits, thus potentially entraining a larger number of canisters, is, in our opinion, small and is more than offset by the level of conservatism built into the existing estimates.

6. The Panel has not been able to quantify the probability of a dog-leg conduit in any rigorous fashion, nor its effect on canisters. The opinion expressed in 5 above was arrived at by combining our separate independent views of where the upper limits would lie. We recommend that any results obtained by following recommendations 3(a)–(d) and 4 be applied to obtaining time-dependent material and pressure fields within invaded drifts with the aim of reducing the uncertainties we now face.

7. Experimental studies could play a role in resolving various uncertainties. These would have to refer to laboratory-scale processes or to processes where scaling laws could be relied upon. Candidates for consideration are:

   (a) the transition region from bubbly magma to a gas-filled cavity near a magma front in a dike flow or near the corresponding nose in a drift flow; and

   (b) the chemical and mechanical effects of basaltic magma on canisters in drift and conduit flows.

   We recommend that (b) be carried out as a priority, because of its direct impact on TSPA estimates, but that (a) be restricted to accelerating existing work or commissioning new work at those centers that are already carrying out related work on model systems easily handled in a laboratory.

8. Repository design and operation play a significant and possibly critical roles in determining the extent and effects of igneous intrusion into the repository drifts containing canisters. Although such considerations were not part of our original brief, we suggest that the following design elements be considered or reconsidered in light of our findings:

    (a) orientation of drifts to minimize the number statistically intersected by rising dikes;

    (b) diameter and spacing of drifts to increase the chance of continued rise of planar dikes to surface;

    (c) separation and fixing (to one another as well as to the floor) of canisters to reduce the chance of movement when magma flows into drifts and, hence, of damage to them;

    (d) introduction of bulkheads suitably spaced along drifts to minimize magma flow into drifts and reduce the length of possible dog-legs;

    (e) backfilling of drifts after the cooling-off period to further minimize magma-canister interactions; and

    (f) the possible redesign of canister exteriors to make them more resistant to damage by flowing magma, if such can be accomplished without otherwise sacrificing their integrity.

REFERENCES

Barenblatt, G. I., The mathematical theory of equilibrium cracks in brittle fracture, *Adv. Appl. Mech.*, *7*, 55-129, 1962.

Barr, G. E., *Dike Propagation Near Drifts,* ANL-WIS-MD-000015 REV00, ICN1, 2000.

Barr, G. E., *Modeling of Propagation of a Dike in a Non-Uniform Stress Field, BSC/SAIC LLC,* 2002.

Blakeley, R. J., V. E. Langenheim, D. A. Ponce, and G. L. Dixon, *Aeromagnetic Survey of the Amargosa Desert, Nevada and California: A tool for Understanding Near-Surface Geology and Hydrology, U.S. Geological Survey,* Open-File Report 00-188, 2000.

Brace, W. F., and D. L. Kohlstedt, Limits on lithospheric stress imposed by laboratory experiments, *J. Geophys. Res.*, *85*(B11), 6248-6252, 1980.

Brandsdottir, B., and P. Einarsson, Seismic activity associated with the September 1977 deflation of the Krafla central volcano in northeastern Iceland, *J. Volcanol. Geotherm. Res.*, *6*(3-4), 197-212, 1979.

Bruce, P. M., and H. E. Huppert, Solidification and melting along dikes by the laminar flow of basaltic magma, in *Magma Transport and Storage*, edited by M. P. Ryan, pp. 87-101, Wiley, Chichester, England, 1990.

Budnikov, V. A., K. Ye, A. Markhinin, and A. A. Ovsyannikov, The quantity, distribution, and petrochemical features of pyroclastics of the Great Tolbachik Fissure Eruption, in *The Great Tolbachik Fissure Eruption*, edited by S. A. Fedotov, and Y. K. Markhinin, pp. 41-56, Cambridge University Press, Cambridge, 1983.

Buttner, R., B. Zimanowski, C. Lenk, A. . Koopmann, and others, Determination of thermal conductivity of natural silicate melts, *Appl. Phys. Lett.*, *77*, 1810-1812, 2000.

Carr, W. J., *Summary of Tectonic and Structural Evidence for Stress Orientation at the Nevada Test Site, U.S. Geological Survey,* Open-File Report 74-176, 1974.

Coppersmith, K. J., and R. R. Youngs, *Probability of Occurrence: Overview of PVHA and Application of Results, Bechtel SAIC LLC,* 2002.

Crowe, B. M., and F. V. Perry, Volcanic probability calculations for the Yucca Mountain site: Estimation of volcanic rates, in *Proceedings Nuclear Waste Isolation in the Unsaturated Zone, Focus '89,* American Nuclear Society, La Grange Park, IL, 1989.

Crump, T., *Igneous Activity Regulatory Requirements, Bechtel SAIC LLC,* 2002.

CRWMS M&O, *Probabilistic Volcanic Hazard Analysis for Yucca Mountain, Nevada, BA0000000-01717-2200-00082 REV 0,* ACC: MOL.19971201.0221, Las Vegas, Nevada, 1996.

CRWMS M&O, *Dike Propagation Near Drifts, ANL-WIS-MD-000015 REV 00*, ACC: MOL.20000523.0157, Las Vegas, Nevada, 2000a.

CRWMS M&O, *Miscellaneous Waste-Form FEPs, ANL-WIS-MD-000009 REV 00*, ACC: MOL.20000526.0339, Las Vegas, Nevada, 2000b.

CRWMS M&O, *Igneous Consequence Modeling for TSPA-SR, ANL-WIS-MD-000017 REV 00*, ACC: MOL.20000501.0225, Las Vegas, Nevada, 2001a.

CRWMS M&O, *Yucca Mountain Science and Engineering Report, U.S. Department of Energy, DOE/RW-0539, 2001b*

Delaney, P. T., and A. E. Gartner, Physical processes of shallow mafic dike emplacement near the San Raphael Swell, Utah, *Geol. Soc. Am. Bull., 109*, 1177-1192, 1997.

Delaney, P. T., and D. D. Pollard, *Deformation of Host Rocks and Flow of Magma During Growth of Minette Dikes and Breccia-Bearing Intrusions Near Ship Rock, New Mexico, U. S. Geological Survey Professional Paper*, p. 61, 1981.

Delaney, P. T., and D. D. Pollard, Solidification of basaltic magma during flow in a dike, *Am. J. Sci., 282*, 856-885, 1982.

Delaney, P. T., D. D. Pollard, J. I. Ziony, and E. H. McKee, Field relations between dikes and joints: Emplacement processes and paleostress analysis, *J. Geophys. Res.*, *91*(B5), 4920-4938, 1986.

Department of Energy/Nuclear Regulatory Commission, *Summary Highlights of DOE/NRC Technical Exchange and Management Meeting on Igneous Activity*, September 5, 2001.

Detournay, E., and A. Savitski. *Mathematical Model of Dike Propagation with Compressible Flow*, to be submitted to Bechtel SAIC, 2003.

Doubik, P., and B. E. Hill, Magmatic and hydromagmatic conduit development during the 1975 Tolbachik eruption, Kamchatka, with implications for hazards assessment at Yucca Mountain, NV, *J. Volcanol. Geotherm. Res., 91*, 43-64, 1999.

Elsworth, D., *The Consequences of Igneous Intrusion at Yucca Mountain - Some Rock Mechanics Aspects of Dike-Repository Interaction*, Summary Report to NWTRB, Nov. 12, 2001.

Fedotov, S. A., G. N. KKovalev, Y. E. K. Markhinin, Y. B. Slezin, A. I. Tsyurupa, N. A. Gusev, V. I. Andreyev, V. L. Leonov, and A. A. Ovsyannikov, Chronology and features of the Southern Breakthrough of the Great Tolbachik Fissure Eruption, 1975-1976, in *The Great Tolbachik Fissure Eruption*, edited by S. A. Fedotov, and Y. Markhinin, pp. 11-25, Cambridge University Press, Cambridge, 1983.

Fedotov, S. A., and Y. E. K. Markhinin, editors, *The Great Tolbachik Fissure Eruption*, Cambridge University Press, Cambridge, 1983.

Fialko, Y. A., and A. M. Rubin, Thermodynamics of lateral dike propagation: Implications for crustal accretion at slow spreading mid-ocean ridges, *J. Geophys. Res., 103*, 2501-2514, 1998.

Fisher, R. V., and H.-U. Schmincke, *Pyroclastic Rocks*, Springer-Verlag, Berlin, 1984.

Frizzell, V., and M. L. Zoback, Stress orientation determined from Fault Slip Data in the Hampel Wash Area, Nevada, and its relation to Contemporary Regional Stress Field, *Tectonics*, *6*(2), 89-98, 1987.

Gaffney, E. S., *Modelling of Magma/Gas-Drift Interactions, BSC/SAIC LLC*, 2002.

Garagash, D., and E. Detournay, The tip region of a fluid-driven fracture in an elastic medium, *J. Appl. Mech., 67*, 183-192, 2000.

Gudmundsson, A., Form and dimensions of dikes in eastern Iceland, *Tectonophysics*, *95*, 295-307, 1983.

Harmsen, S. C., and A. M. Rogers, Inferences about the local stress field from focal mechanisms: Applications to earthquakes in the southern Great Basin of Nevada, *Bull. Seism. Soc. America, 76*, 1560-1572, 1986.

Hill, B. E., C. B. Connor, M. S. Jarzemba, P. C. La Femina, W. Navarro, and W. Strauch, 1995 eruptions of Cerro Negro volcano, Nicaragua, and risk assessment for future eruptions, *Geolog. Soc. Am. Bull., 10*, 1231-1241, 1998.

Hill, B., *Update on Igneous Activity: Magma-Repository Interactions and Tephra-Fall Remobilization, ACNW Meeting, Rockville*, July, 2001.

Hill, B., *NRC Perspective on Magma-Repository Interactions, CNWRA*, 2002.

Hoerner, S. F., *Fluid Dynamic Drag*, The Author, Vancouver, WA., 1965.

Hurst, A. W., *ASHFALL — A Computer Program for Estimating Volcanic Ash Fallout: Report and Users Guide., Institute of Geological & Nuclear Sciences*, Report 94/23, p. 22, 1994.

Hurst, T., and R. Turner, Performance of the program ASHFALL for forecasting ashfall during the 1995 and 1996 eruptions of Ruapehu Volcano, *New Zealand J. Geol. Geophys.*, *42*, 615-622, 1999.

Jarzemba, M. S., Stochastic Radionuclide Distributions after basaltic eruption for performance assessments of Yucca Mountain, *Nucl. Tech.*, *118*, 132-142, 1997.

Kauahikaua, J. P., K. V. Cashman, T. N. Mattox, C. C. Heliker, K. A. Hon, M. T. Mangan, and C. R. Thornber, Observations on basaltic lava streams in tubes from Kilauea Volcanic, Island of Hawai'i, *J. Geophys. Res., B, Solid Earth Planets*, *103*(11), 27, 303-27, 323, 1998.

Kerr, R. C., Thermal erosion by laminar lava flows, *J. Geophys. Res., B, Solid Earth Planets*, *106*(11), 26, 453-26, 465, 2001.

Loughlin, S. C., P. J. Baxter, W. P. Aspinall, B. Daroux, C. S. Harford, and A. D. Miller, Eyewitness accounts of the 25 June 1997 pyroclastic flows and surges at Soufrière Hills Volcano, Montserrat, and implications for disaster mitigation, in *The Eruption of Soufrière Hills Volcano, Montserrat from 1995 to 1999, Geological Society Memoirs 21*, edited by T. H. Druitt and B. P. Kokelaar, pp. 211-230, Geological Society of London, 2002.

Lister, J. R., Buoyancy-driven fluid fracture: The effects of material toughness and of low-viscosity precursors, *J. Fluid Mech., 217*, 263-280, 1990b.

Lister, J. R., The solidification of buoyancy-driven flow in a flexible-walled channel. Part 1. Constant-volume release, *J. Fluid Mech., 272*, 21-44, 1994.

Lister, J. R., and P. J. Dellar, Solidification of pressure-driven flow in a finite rigid channel with application to volcanic eruptions, *J. Fluid Mech., 323*, 267-283, 1996.

Lister, J. R., and R. C. Kerr, Fluid-mechanical models of dike propagation and their application to magma transport in dykes, *J. Geophys. Res., 96*, 10,049-10,077, 1991.

Luhr, J. F., and T. Simkin, *Parícutin: The Volcano Born in a Mexican Cornfield*, Geoscience Press, Phoenix, AZ, 1993.

Mastin, L. G., The roles of magma and groundwater in the phreatic eruptions at Inyo Craters, Long Valley Caldera, *Bull. Volcanol., 53*, 579-596, 1991.

Mastin, L. G., Insights into volcanic conduit flow from an open-source numerical model, *Geochem. Geophys. Geosys., 3*(7), 10.1029, 2002.

Mastin, L. G., and M. S. Ghiorso, *A Numerical Program for Steady-State Flow of Magma-Gas Mixtures Through Vertical Eruptive Conduits, U.S. Geological Survey*, Open-File Report 00-209, 2000.

Mastin, L. G., and M. S. Ghiorso, Adiabatic temperature changes of magma-gas mixtures during ascent and eruption, Contributions to *Mineralogy & Petrology, 141*(3), 307-321, 2001.

Melson, W. G., *Responses to Questions Resulting from the November 8, 2001, Meeting at NWTRB Headquarters Concerning Igneous Intrusion Consequences, Memo to L. Reiter, NWTRB, Nov. 21*, 2001.

Morrisey, M. M., *Review of Shock Wave Models and Igneous Activity, year unknown*.

National Regulatory Commission, *Issue Resolution Status Report (Key Technical Issue: Igneous Activity, Rev 2*, July, 1999.

Nuclear Regulatory Commission, *Issue Resolution Status Report, Key Technical Issue: Igneous Activity, Rev. 2*, 1999.

OCRWM, *Dike Propagation Near Drifts*, OCRWM AMR ANL-WIS-MD-000015 REV00, ICN1, November, 2000.

OCRWM, *Characterize Eruptive Processes at Yucca Mountain*, OCRWM AMR ANL-MGR-GS-000002, REV00, ICN 01, December, 2001.

O'Leary, D. W., E. A. Mankinen, R. J. Bailey, V. E. Langenheim, and D. A. Ponce, *Aeromagnetic Expression of Buried Basaltic Volcanoes Near Yucca Mountain, Nevada, U.S. Geological Survey*, Open-File Report 02-020, 2002.

Papale, P., Modeling of the solubility of a two-component H2O + CO2 fluid in silicate liquids, *Am. Mineralog., 84*, 447-492, 1999.

Perry, F. V., *Overview of Volcanism in the Yucca Mountain Region: The Geologic Basis for Probability Estimates, Bechtel SAIC LLC*, 2002.

Perry, F. V., B. M. Crowe, G. A. Valentine, and L. M. Bowker, editors, *Volcanism Studies: Final Report for Yucca Mountain Project, Los Alamos National Laboratories*, LA-13478, Tables 1.2, 2.A and 2.B, December 1998.

Pollard, D. D., Elementary fracture mechanics applied to the structural interpretation of dykes, in *Mafic Dyke Swarms; a Collection of Papers Based on the Proceedings of an International Conference*, edited by H. C. Halls, and W. F. Fahrig, pp. 5-24, Geological Association of Canada, Toronto, 1987.

Reamer, C. W., *U.S. NRC Memorandum MOL 1999-810.0639 Concerning IRSR-KTI Igneous Activity, Revision 2*, July 16, 1999.

Rogers, A. M., S. S. Harmsen, W. J. Carr, and W. Spence, *Southern Great Basin Seismological Data Report for 1981 and Preliminary Data Analysis, U.S. Geological Survey*, Open-File Report 83-699, 1983.

Rubin, A. M., Tensile fracture of rock at high confining pressure: Implications for dike propagation, *J. Geophys. Res.*, *98*, 15,919-15,935, 1993.

Rubin, A. M., On the thermal viability of dikes leaving magma chambers, *Geophys. Res. Lett.*, *20*, 257-260, 1993a.

Rubin, A. M., Tensile fracture of rock at high confining pressure: Implications for dike propagation, *J. Geophys. Res.*, *98*, 15,919-15,935, 1993b.

Rubin, A. M., Propagation of magma-filled cracks, *Ann. Rev. Earth Planet. Sci.*, *23*, 287-336, 1995a.

Rubin, A. M., Getting granite dikes out of the source region, *J. Geophys. Res.*, *100*, 5911-5929, 1995b.

Rubin, A. M. Background report on dike propagation, report to Bechtel SAIC, 2003.

Rubin, A. M., and D. Gillard, Dike-induced earthquakes: Theoretical considerations, *J. Geophys. Res.*, *103*, 10,017-10,030, 1998.

Sandia National Laboratories, *Hydraulic Fracturing Stress Measurements in the Test Hole ESF-AOD-HDFR#1, Thermal Test Facility, Exploratory Studies Facility at Yucca Mountain*, WA-0065, SNL TIC: 237818, 1997.

Segerstrom, K., *Erosion Studies at Parícutin Volcano, State of Michoacán, Mexico, U.S. Geological Survey Bulletin 965A*, 1950.

Self, S., R. S. J. Sparks, B. Booth, and G. P. L. Walker, The 1973 Heimaey Strombolian scoria deposit, Iceland, *Geolog. Mag.*, *111*, 539-548, 1974.

Self, S., L. Wilson, and I. A. Nairn, Vulcanian eruption mechanisms, *Nature*, *277*, 440-443, 1979.

Snyder, D., E. Gier, and I. Carmichael, Experimental determination of the thermal conductivity of molten $CaMgSi_2O_6$, and the transport of heat through magmas, *J. Geophys. Res.*, *99*, 15503-15516, 1994.

Spera, F. J., Physical properties of magma, in *Encyclopedia of Volcanoes, H*, 2000.

Springer, J. E., R. K. Thorpe, and H. L. McKague, *Borehole Elongation and Its Relation to Tectonic Stress at the Nevada Test Site, Lawrence Livermore National Laboratory*, Report UCRL-53528, 1984.

Stewart, J. H., Tectonics of the Walker Lane Belt, western Great Basin — Mesozoic and Cenozoic deformation in a zone of shear, in *Metamorphism and Crustal Evolution of the Western United States, Rubey Vol. VII*, pp. 683-713, Prentice-Hall, Englewood Cliffs, NJ, 1988.

Stock, J. M., and J. H. Healy, Stress Field at Yucca Mountain, Nevada, *U.S. Geological Survey*, Bulletin 1790, 87-93, 1988.

Stock, J. M., J. H. Healy, S. H. Hickman, and M. D. Zoback, Hydraulic fracturing stress measurements at Yucca Mountain, Nevada, and relationship to the regional stress field, *J. Geophys. Res.*, *90*(B10), 8691-8706, 1985.

Suzuki, T., A theoretical model for the dispersion of tephra, in *Arc Volcanism, Physics and Tectonics*, edited by D. Shimozuru, and I. Yokiyama, pp. 95-113, Terra Scientific Publishing, Tokyo, 1983.

Swift, P., *Modeling Igneous Disruption in Yucca Mountain Total System Performance Assessment*, *Bechtel SAIC LLC*, 2002.

Thorarinsson, S., *Surtsey — The New Island in the North Atlantic*, Viking Press, New York, 1967.

Thordarson, T., and S. Self, The Laki (Skaftár Fires) and Grímsvötn eruptions, *Bull. Volcanol.*, *55*, 233-263, 1993.

Turner, R., and T. Hurst, Factors influencing volcanic ash dispersal from the 1995 and 1996 eruptions of Mount Ruapehu, New Zealand, *J. Appl. Meteorol.*, *40*, 56-69, 2001.

Valentine, G., *Overview of YMR Volcanology, Bechtel SAIC LLC*, 2002.

Valentine, G., *Summary of Proposed Studies on Consequences, Bechtel SAIC LLC*, 2002.

Viramonte, J. G., and L. DiScala, Summary of the 1968 eruption of Cerro Negro, Nicaragua, *Bull. Volcanol.*, *34*, 347-351, 1970.

Waitt, R. B., Devastating pyroclastic density flow and attendant air fall of May 18-stratigraphy and sedimentology of deposits, in *The 1980 Eruptions of Mount St. Helens, U.S. Geological Survey*, Professional Paper 1250, edited by P. Lipman, and D. R. Mullineaux, pp. 439-460, 1981.

Warren, W. E., and C. W. Smith, In situ stress estimates from hydraulic fracturing and direct observation of crack orientation, *J. Geophys. Res.*, *90*, 6829-6839, 1985.

Williams, R. S., and J. G. Moore, *Man Against Volcano: The 1973 Eruption onHaemaey, Vestmannaeyjar, Iceland, U.S. Geological Survey*, 1983; http://pubs.usgs.gov/gip/heimaey/heimaey.pdf

Wilson, L., and J. W. I. Head, Ascent and eruption of basaltic magma on the earth and moon, *J. Geophys. Res.*, *86*(B4), 2971-3001, 1981.

Wohletz, K. H., and G. Heiken, *Volcanology and Geothermal Energy*, University of California Press, Berkeley, 1992.

WoldeGabriel, G., G. N. Keating, and G. A. Valentine, Effects of shallow basaltic intrusion into pyroclastic deposits, Grants Ridge, New Mexico, USA, *J. Volcanol. Geotherm. Res.*, *92*, 389-411, 1999.

Woods, A. W., S. Sparks, O. Bokhove, A.-M. LeJeune, C. B. Connor, and B. E. Hill, Modeling magma-drift interaction at the proposed high-level radioactive waste repository at Yucca Mountain, Nevada, USA, *Geophys. Res. Lett.*, *29*(13), 10.1029, 2002.

Younker, J., *Overview of Igneous Consequences Peer Review*, *Bechtel SAIC LLC*, 2002.

Ziv, A., A. M. Rubin, and A. Agnon, Stability of dike intrusion along preexisting fractures, *J. Geophys. Res.*, *105*, 5947-5961, 2000.

Zoback, M. D., and J. H. Healy, Friction, faulting, and in situ stress, *Annalen der Geophysik*, *2*, 689-698, 1984.

Zoback, M. L., State of stress and modern deformation of the northern Basin and Range Province, *J. Geophys. Res.*, *94*(B6), 7105-7128, 1989.